The role of the South Atlantic in the upper branch of the global thermohaline circulation

Het belang van de Zuid-Atlantische Oceaan voor de lichte tak van de globale thermohaliene circulatie.

(met een samenvatting in het Nederlands)

PROEFSCHRIFT

ter verkrijging van de graad van doctor aan de Universiteit Utrecht
op gezag van de Rector Magnificus Prof. dr. W.H. Gispen
ingevolge het besluit van het College voor Promoties
in het openbaar te verdedigen op
12 januari 2005 des ochtends te 10.30 uur

door

John Donners

geboren op 15 februari 1977, te Ransdaal

promotor: Prof. Dr. W.P.M. de Ruijter
Faculteit Natuur- en Sterrenkunde,
Instituut voor Marien en Atmosferisch Onderzoek,
Universiteit Utrecht
co-promotor: Dr. S.S. Drijfhout
Koninklijk Nederlands Meteorologisch Instituut (KNMI),
De Bilt

These investigations were supported by the Netherlands Council for Earth and Life Sciences (ALW) with financial aid from the Netherlands Organisation for Scientific Research (NWO). This study was part of the MARE project 'Mixing of Agulhas Rings', which forms part of the NWO theme Climate Variability. This study was carried out at the Royal Netherlands Meteorological Institute (KNMI) in De Bilt, the Netherlands.

Roll on, thou deep and dark blue Ocean – roll!
Ten thousand fleets sweep over thee in vain;
Man marks the earth with ruin – his control
Stops with the shore.

Childe Harold's Pilgrimage (1812–1818)
canto 4, strophe 179

Contents

Chapter 1

Introduction

1.1 Global thermohaline circulation

The earth is forced externally by solar radiation. Insolation is strongest in the tropics and diminishes polewards. The earth radiates the same amount of energy back into space, but the distribution is well spread over the globe. This leaves a net surplus of heat in the tropics, and a deficit near the poles. The global circulation of the atmosphere and the oceans transports heat polewards to bridge the spatial imbalance between the in- and outflux of radiation.

The ocean circulation in the South Atlantic basin is unique in being the only major ocean basin in which the meridional flux of heat is equatorward at mid-latitudes. An extensive survey of the Atlantic Ocean by Wüst in 1935 showed this phenomenon for the first time, but he found such a result too strong a violation of his intuition to mention it in his discussion. The first study to comment on the anomalous heat transport implied by the oceanographic observations was that of Model (1950), 15 years later. Although several studies, using a variety of methods, have confirmed that the meridional flux of heat in the South Atlantic is equatorward, estimates of its magnitude vary over a wide range. Wüst (1935) partitioned the meridional circulation into four core layers (see Fig. 1.1): surface and intermediate waters, both moving northwards; North Atlantic Deep Water (NADW), flowing southward; and a layer of cold and fresh Antarctic Bottom Water (AABW) also moving northwards. His picture has survived intact to the present day.

The equatorward heat transport in the South Atlantic basin can be attributed to the thermohaline circulation (THC), popularised as the Ocean's conveyor belt (see Fig. 1.2, Broecker, 1991). Broecker's picture was based on a paper by Gordon (1986), describing how the warm waters in adjacent ocean basins communicate. In these papers a circulation is sketched where warm and salty water in the North Atlantic is transported further northwards by the Gulf Stream. In winter, cold and dry air from the North-American continent flows across the Irminger and Greenland-Iceland-Norwegian seas and extracts large

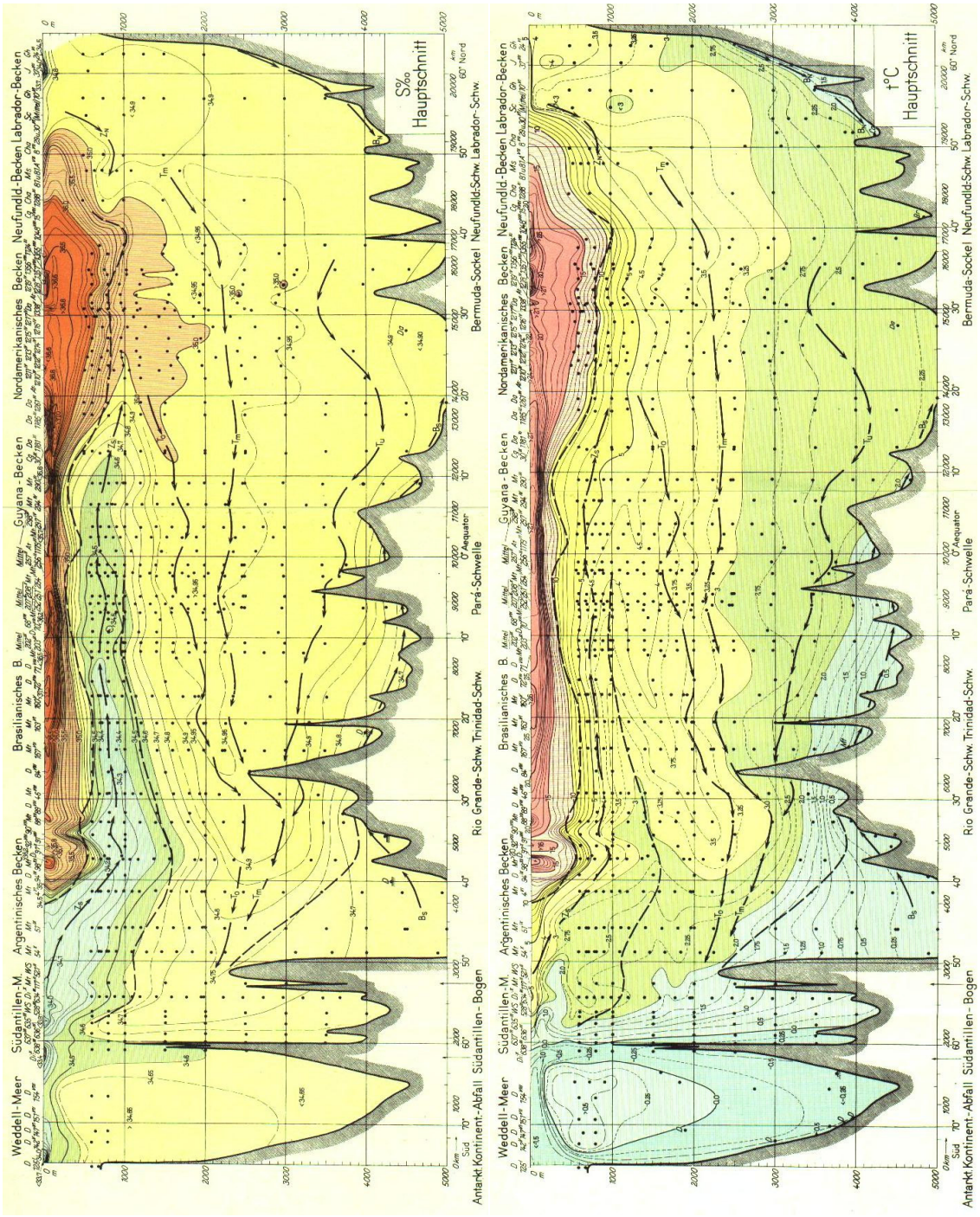
S‰
Hauptschnitt
Weddell-Meer
Südantillen-M.
Argentinisches Becken
Brasilianisches B.
Guyana-Becken
Nordamerikanisches Becken
Neufundld-Becken
Labrador-Becken
Antarkt. Kontinent.-Abfall
Südantillen-Bogen
Rio Grande-Schw.
Trinidad-Schw.
Pará-Schwelle
Bermuda-Sockel
Neufundld-Schw.
Labrador-Schw.
Süd
Nord
0° Aequator
60° Nord
t°C
Hauptschnitt

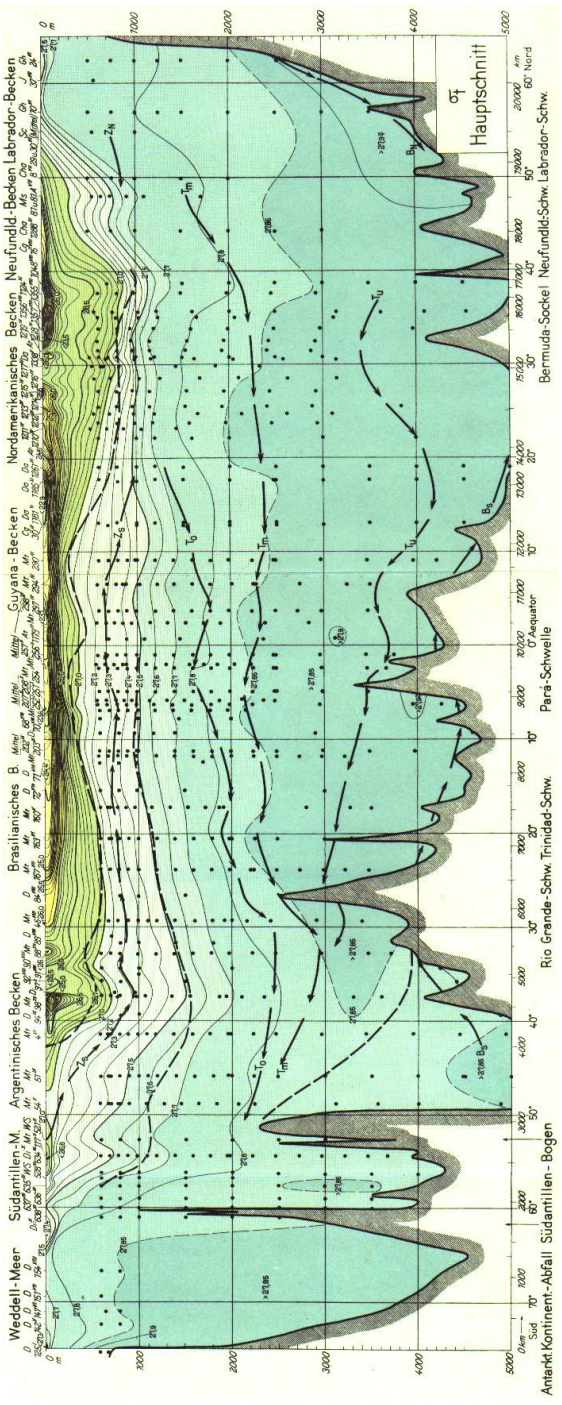

Figure 1.1: *Maps of temperature and salinity in the western Atlantic (by Wüst 1935). The figures give respectively salinity, temperature and potential density along this section. The currents in this meridional section, denoted by the black arrows, are based on the propagation of the different watermasses, characterized by their temperature and salinity. The temperature and salinity intrusions, or tongues, can only exist due to advection by a current. The thermocline water near the surface can be recognized by its warm and salty signature. The Antarctic Intermediate Water (AAIW) is clearly seen as the salinity minimum tongue that reaches the surface at 50° S and penetrates the Atlantic basin below the thermocline water as far as 10° N. The North Atlantic Deep Water (NADW) is characterized by its high salinity and fills up most of the Atlantic basin below 1500 m. The cold Antarctic Bottom Water (AABW) is formed near the Antarctic continent and fills the bottom of the South Atlantic basin where topography permits throughflow.*

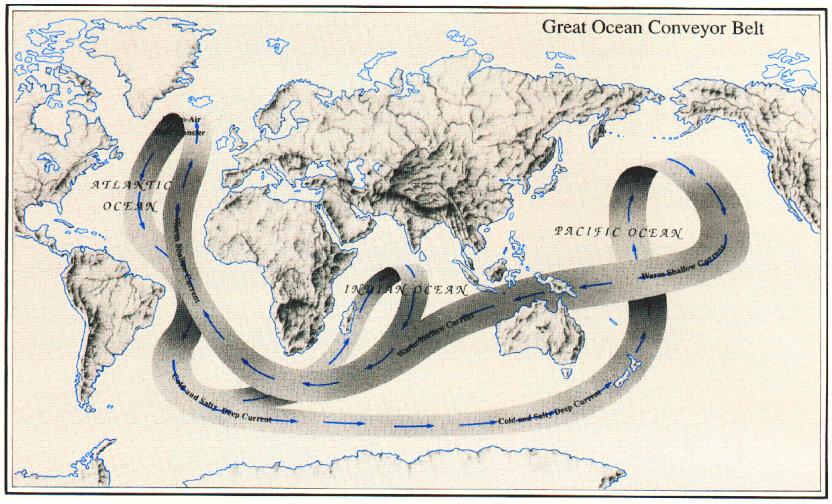

Figure 1.2: *The great ocean conveyor logo (Broecker, 1987). (Copyright by Joe Le Monnier, Natural History Magazine)*

amounts of heat from the ocean. The ocean is cooled and deep convection results in a well-mixed, dense water column. The atmospheric heat gain moderates the climate of northwestern Europe. The newly formed North Atlantic Deep Water (NADW) flows southward and is efficiently spread globally by the Antarctic Circumpolar Current (ACC), forming part of the lower branch of the THC. Internal mixing processes slowly diffuse heat downwards and the NADW upwells. The light water passes through the Indonesian Archipelago and rounds South Africa on its return to the North Atlantic, known as the upper branch of the THC. The turnaround timescale of the THC is approximately 1000 years.

The atmospheric freshwater export from the Atlantic basin is an important forcing factor for the THC. Consequently, the sea surface salinity (SSS) in the Atlantic is higher than in the other basins. The high SSS in the Atlantic facilitates deep convection; the strong halocline assures that, when cooling sets in, the water column gets unstable. The weak halocline in the North Pacific prevents deep water from being formed there.

The cartoon in Fig. 1.2 suggests that the upwelling is concentrated at specific locations in the Pacific and Indian Oceans. In reality this upwelling is widely spread with a large amount taking place in the Southern Ocean. A recent model study supports the notion that NADW is upwelled along the isopycnals in the Southern Ocean and then driven northwards by the westerlies (Döös and Coward, 1997). The logo in Fig. 1.2 also suggests that the major route for return flow to the North Atlantic is through the Indonesian Archipelago and around the tip of Africa. Other studies have updated the oversimplified picture of the conveyor belt logo with different pathways for the THC. The imported water that feeds the upper branch could also be provided by Antarctic surface waters

passing through the Drake Passage. Rintoul (1991) argued that this route would represent a significant part of the return flow. Imposing a net inflow of warm water from the Indian Ocean as a boundary condition, rendered an unrealistic circulation pattern in his model. Using chlorofluorocarbon measurements, Gordon et al. (1992) favored the transport of thermocline water from the Indian to the Atlantic Ocean through so-called Agulhas leakage. Agulhas leakage is the transport of warm and salty water by means of large eddies, or Agulhas rings, that are shed off the Agulhas Current and move into the South Atlantic basin. The flows through the Indonesian Archipelago and Drake Passage both contributed to the upper branch. A significant part of the flow from Drake Passage crossed the Atlantic Ocean, passed into the subtropical Indian Ocean and re-entered the Atlantic basin by Agulhas leakage. The import of high-salinity water from the Indian Ocean preconditions water for deep convection in the northern Atlantic. The picture of the THC was changed once more by Speich et al. (2001). A Lagrangian trajectory analysis of a global ocean model showed a third route, 'Tasman leakage'. Transport of water south of Australia from the Pacific to the Indian Ocean contributed 3.1 Sv (about 20%) of the THC. In a follow-up study (Speich et al., 2002) the Tasman leakage was substantiated with observational evidence and it was shown that the three subtropical gyres of the southern hemisphere were intimately connected. A more accurate and up-to-date depiction of the conveyor belt has been drawn in Fig. 1.3.

1.2 South Atlantic Ocean

The debate on the pathways of the thermohaline circulation still focuses on the interocean exchange between the Atlantic and neighbouring oceans (de Ruijter et al., 1999). Peterson and Stramma (1991) summarized knowledge of the mean circulation in the South Atlantic before the intensive World Ocean Circulation Experiment (WOCE) ship surveys began. However, the circulation of the South Atlantic shows some depth dependence, unresolved in their flow schematic. Stramma and England (1999) discussed flow fields for three layers of the upper ocean, based on WOCE data. The upper and lower layers, representing the surface and intermediate water, are indicated in Figs. 1.4 and 1.5. The subtropical gyre of the South Atlantic consists of the eastward flowing South Atlantic Current, the Benguela Current that feeds the southern South Equatorial Current (SSEC), and is closed by the Brazil Current along the South American coast. Part of the SSEC enters the North Brazil Current towards the North Atlantic or the complicated system of equatorial currents and the cyclonic Angola gyre. The northern boundary of the subtropical gyre is located further southward for deeper levels.

The meridional extent of the subtropical gyre is determined by the latitudes of the zero wind-stress curl. The wind-stress curl vanishes at the Subtropical Convergence Zone, approximately 45° S. The African continent extends only until 35° S. De Ruijter (1982) showed that the application of Sverdrup theory alone would result in an Indian-Atlantic 'supergyre', and the Agulhas Current

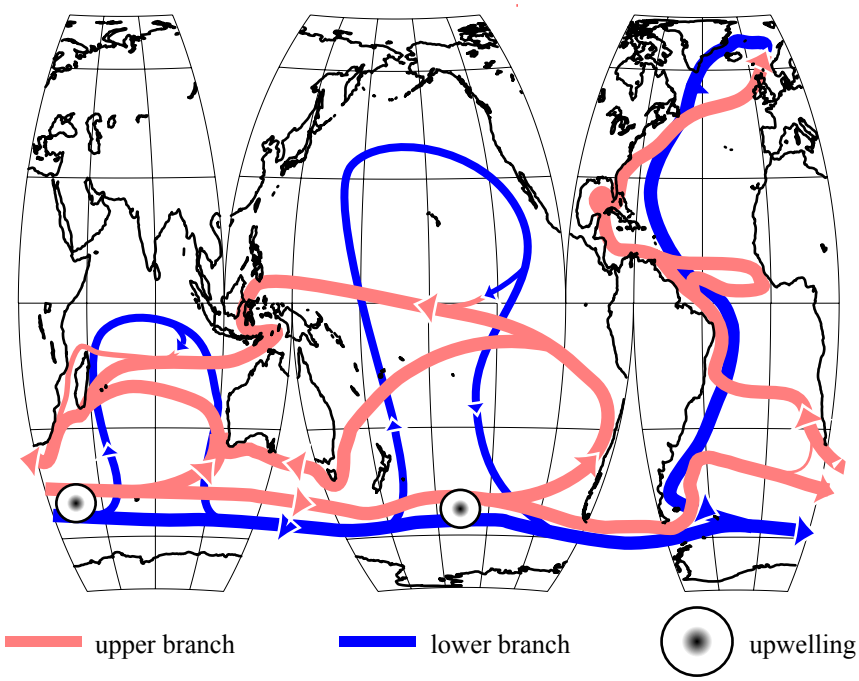

Figure 1.3: *The ocean conveyor belt, based on Schmitz (1995) and further included the Tasman leakage route.*

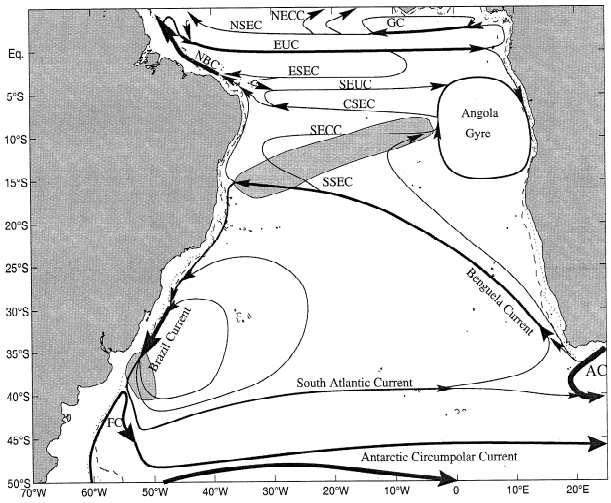

Figure 1.4: *Schematic representation of the large-scale, upper 100-m geostrophic current for southern autumn. The shaded areas denote different mode water formation regions (see also section 1.4. The abbreviated ocean currents are: FC = Falkland Current or Malvinas Current, AC = Agulhas Current, SSEC = southern South Equatorial Current, NBC = North Brazil Current, EUC = Equatorial Under Current. After Stramma and England (1999).*

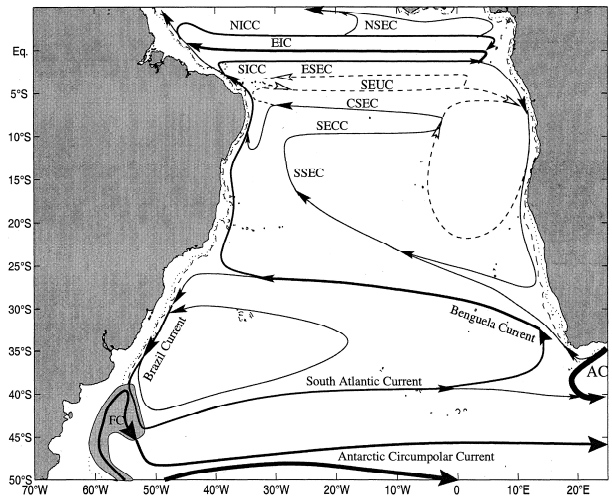

Figure 1.5: *Schematic representation of the large-scale, AAIW layer (between 500 to 1200 m) geostrophic currents. After Stramma 1999.*

(AC) would flow freely into the Atlantic basin. On the contrary, observations show that only a small part of the AC transport leaks intermittently into the South Atlantic as large eddies or Agulhas rings, while most retroflects back into the Indian Ocean as the Agulhas Return Current. A dynamical interplay between inertial overshoot, advection of planetary vorticity, bottom topography and continental geometry bridges the 'gap' between the African continent and the region of zero wind stress curl. Because of the complicated physics involved it is difficult to model and to observe how much of the Agulhas Current (AC) retroflects back into the Indian Ocean, and how much flows into the South Atlantic.

The amount of cold water from the Pacific that enters the South Atlantic (SA) is more easy to estimate, but most of it leaves the South Atlantic at the eastern side, carried by the ACC (see Figs. 1.4 and 1.5). To escape northward, exchange of water between the ACC and the South Atlantic Current (SAC), has to take place. Part of the SAC feeds into the Benguela Current, which carries water further northward. Most of the exchange between the ACC and the South Atlantic subtropical gyre is likely to take place in the Brazil-Malvinas Confluence (BMC), where the ACC and the subtropical gyre almost merge. Again, this exchange is difficult to model and to observe. It is likely that water mass transformation due to air-sea interaction and small-scale mixing determine this exchange.

1.3 Inverse box modelling

The most common oceanographic observations consist of sections of temperature and salinity, from which the density can be calculated. Direct velocity measurements are difficult to interpret, and rather rare. As a result, transport estimates are made in an indirect way. The density distribution determines the vertical velocity shear, or thermal wind, to a very good approximation. Wunsch (1978) addressed the classical problem of physical oceanography: determination of the reference level velocity, which must be added to the thermal wind velocity to give the absolute velocity. Hydrographic sections and land boundaries enclose an ocean "box". The hydrographic sections are boundary conditions to the ocean circulation within the box volume. Conservation of mass, salinity, and other properties results in a linear system of equations with the reference velocities as unknowns. However, this set of equations is often underdetermined. A particular solution is usually selected by a priori assumptions about the circulation. The total error of the conservation equations is then minimized, e.g. with a least squares technique. The method has a high degree of flexibility: any prior knowledge can be used as a constraint and the method can estimate a variety of properties of the ocean circulation. As a result, inverse box models have been successfully used to quantitatively describe many aspects of the global ocean circulation.

However, the accuracy of a inverse box model applied to real data can be difficult to assess. The results are influenced by the assumptions, e.g. many

inverse box model studies neglect the exchange of properties between different density layers. Numerical models provide an opportunity to test the inverse method. McIntosh and Rintoul (1997) showed that inverse box models do work, provided that they include interfacial fluxes as unknowns and that these are weighted appropriately. However, the model will not generally reproduce the detailed structure of the reference level velocities. Ganachaud (2000) calculated a detailed error budget of inverse box models and concluded that linear inverse models can consistently combine different sections as long as the mean Ekman transport is used for all sections; the baroclinic shear is relatively stable on large scales, although the error implied by baroclinic variations is not negligible (up to 2 Sv in shallow density layers); noise is dominated by internal waves and induces errors in the depth-integrated transports of 3 Sv at mid-latitudes. Due to the small Coriolis parameter, the noise increases close to the equator. Variability increases at shallower depths and closer to the equator (Ganachaud, 2003). Ganachaud (2000) estimated the total northward flow in the South Atlantic in the range of 14 to 20 Sv, compatible with previous inverse box model estimates (Macdonald, 1998).

Inverse box models are less suited to estimate the strength of boundary currents, because of small scale baroclinic variability, the intense eddy field in western boundary regions and sensitivity to the choice of integration boundaries. The North Brazil Current increases downstream, from 18 Sv at 11° S to 44 Sv at 4.5° S (Ganachaud, 2003). Although Speer et al. (1996) estimated a similar volume flux of 25 Sv from the same hydrographic section, Macdonald (1998) obtained 40 Sv across 11° S from earlier data. Further away from the equator, the errors decrease, resulting in a range of 14 to 22 Sv southward across 30° S. The strength of the Benguela Current is estimated between 14 and 26 Sv.

1.4 Water mass transformation

Most water recirculates in wind-driven currents. A net transport between different ocean basins involves exchange between different current systems and such exchange often implies a transformation of the interacting water masses. The waters from the Indian and Pacific Oceans that enters the South Atlantic basin, will be modified by air-sea interaction and mixing, and the extent of modification is likely to be a controlling factor for the exchange rate.

The surface cooling of the ocean in winter causes turbulent convective mixing and the surface layer is vertically homogenized by this process. The process that water resides at the surface and interacts with the atmosphere is called ventilation. In summer time the cooling is less intense or absent, and consequently the surface layer restratifies and vertically well-mixed water is left behind below the surface. The volume of homogeneous water is also called mode water. In the summer, the circulation may carry the mode water column away from its formation zone. The mode water will reside in the thermocline if the mixed layer reaches less deep in the next winter. The process that transfers newly-formed water masses into the interior ocean is called subduction (Cushman-

Roisin, 1987). The transfer of these subducted water masses may control atmospheric climate variability remotely (Gu and Philander, 1997). The importance of propagation of subsurface heat anomalies for Atlantic climate variability has been suggested by Sutton and Allen (1997).

Poole and Tomczak (1999) used the objective multi-parameter analysis to distinguish different water masses that make up the South Atlantic Central Water (SACW). The SACW penetrates the North Atlantic as far as 15° N. The boundary between the NACW and SACW is a density-compensated thermohaline front, called the Cape Verde Frontal Zone. The frontal zone is sufficiently far north of the equatorial current system for the majority of South Atlantic waters mixed at the front to become part of the subtropical gyre in the northern hemisphere. The temperature-salinity (T-S) properties of the tropical Atlantic indicate that the source is mainly eastern SACW (ESACW). The ESACW is essentially central water formed in the Indian Ocean, that entered the Atlantic basin through Agulhas leakage. The western SACW is formed locally in the BMC and recirculates within the South Atlantic subtropical gyre but does not penetrate further northward. Provost et al. (1999) analyzed the South Atlantic Subtropical Mode Water (SASTMW), a subclass of the SACW. Colder mode water (12° to 14° C), found to the east of 30° W, corresponded to Agulhas ring water. SASTMW to the west of 30° W could be formed in the Brazil Current recirculation region due to air-sea interaction. The Antarctic Intermediate Water (AAIW) found in the South Atlantic is mostly formed in the southeastern Pacific (Talley, 1996). It can be recognized by the low salinity tongue that stretches below the surface from the Antarctic northwards (see Fig. 1.1). The conversion of AAIW in the Atlantic occurs with limited direct atmospheric contact. The water in the Agulhas basin does not contain an AAIW oxygen maximum, and the SSEC has a high potential vorticity, which indicates that it has not been ventilated recently. This suggests that the AAIW is imported from the Indian Ocean rather than being local.

1.5 Agulhas rings

Agulhas rings are shed from the Agulhas retroflection loop irregularly and move into the South Atlantic Ocean in a north-westerly direction (Lutjeharms and Ballegooyen, 1988). Present estimates are that roughly six Agulhas rings are being generated each year. These rings move mainly because of their intrinsic drift and stay south of 20° S. They can persist for several years and penetrate the interior of the South Atlantic subtropical gyre; their water may thus conceivably recirculate back into the Indian Ocean. An immediate contribution to the global THC is expected to result predominantly from their initial decay while crossing the Benguela Current. Schouten et al. (2000) followed these rings with satellite measurements of sea surface height (SSH). During the first five months after the shedding of Agulhas rings the decay of the SSH is strongest.

Even during summer Agulhas rings loose heat to the atmosphere, mainly due to the large mean turbulent flux of latent heat (van Aken et al., 2003). Although

the water mass characteristics of the trapped Subtropical Indian Ocean water do not deviate substantially from the characteristics of subtropical Atlantic water, strong evaporation in the retroflection region boosts the salinity within the rings. The heat loss drives convective mixing in the mixed layer, which is accordingly very homogeneous. Schmid et al. (2003) released drifters in Agulhas rings and observed that they were expelled after two revolutions or less, while at other times drifters were re-captured. Agulhas rings interacted strongly with the surrounding regime that consisted of numerous cyclones and anticyclones Boebel et al. (2003); Schouten et al. (2000).

To be able to estimate the amount of Agulhas leakage that contributes directly to the upper branch of the THC, it is necessary to identify the decay processes of Agulhas rings. Dewar (1987) calculated the restructuring of an idealized warm ring using a two-layer model. Estimates of energy release during adjustment suggest that a significant amount of energy is converted into internal wave energy. Drijfhout et al. (2003b) showed that the strong decay is associated with a mixed barotropic/baroclinic instability. In most cases this instability leads to split-up of the ring. De Steur et al. (2004) modeled an Agulhas ring and found a strong leakage of anomalous ring water below 600 m. These studies are useful to identify decay mechanisms of separate Agulhas rings, but ignore the importance of interaction with the background flow and other eddies. Although several studies analyzed Agulhas rings in global or regional eddy-permitting ocean models (Matano and Beier, 2003; Reason et al., 2003; Treguier et al., 2003), they concentrated on the quantification of Agulhas ring decay in the Benguela basin. The processes that cause the decay in these ocean models, are less well understood.

1.6 Central questions

In this thesis the ocean circulation and transformation of water masses in the South Atlantic is studied, with an emphasis on the upper branch of the THC. Different studies based on observational datasets give clearly opposite views of the pathways of the upper branch of the thermohaline circulation and the Indian-Atlantic interocean exchange. While most inverse box models do not seem to indicate a very strong link between the Indian and Atlantic basins, studies based on chemical tracers and quantitative water mass analysis suggest otherwise. The contrasting T-S properties of water provided by different routes profoundly affects the heat and salt balance of the Atlantic. Water mass properties, however, are not invariable within the South Atlantic basin. Newly-formed water masses can subduct, and create teleconnections with other regions by re-emergence.

The impact of Agulhas rings on the THC depends on its initial decay, while it traverses the Benguela Current. The mechanism of the decay processes is important to estimate the timing, speed and amount of leakage of Agulhas rings. Although much attention has been paid to the quantification of Agulhas leakage in eddy-permitting ocean models, less is known about the processes that

generate the decay in these models.

The problem that is addressed in this thesis can be formulated in the following question:

What are the sources for the upper branch of the South Atlantic THC and how and how and by what processes is it further modified in the South Atlantic basin?

This question is divided into different items which are described in separate chapters:

- What methods can be used to identify different routes of the upper branch of the THC from observations?
- How does air-sea interaction and mixing in the South Atlantic basin form new water masses and how will the subducted mode water circulate once it is closed off from the atmosphere? How do the properties of the upper branch of the THC change while traversing the South Atlantic?
- What are the processes responsible for the decay of Agulhas rings in ocean models?

The data from an eddy-permitting ocean model have been used as the main tool to address the issues raised in this thesis. The model is described in detail in chapter 2. For the analysis of the decay mechanisms of Agulhas rings, an eddy-resolving version of the ocean model has been used. With a Lagrangian particle-following technique, described in the next chapter, pathways of the THC and the subducted water masses were estimated. The upper branch of the THC in the ocean model has been analyzed in chapter 3. To test whether inverse box model studies can distinguish pathways, section-averaged water mass transports from the ocean general circulation model and from different inverse box model studies were compared. The water mass transformations induced by the air-sea interaction have been analyzed with the framework of Walin (1982). The sparsity of observations of air-sea fluxes in the South Atlantic results in large deviations between different datasets (Sterl and Hazeleger, 2002), and their induced water mass transformations are compared in chapter 4. The total buoyancy balance of the South Atlantic mixed layer has been analyzed in a slightly modified framework of Marshall et al. (1999). The relative importance of air-sea transformation, subduction, mixing, interocean exchange and trend is clearly shown. The differing properties of newly-formed Atlantic AAIW and the tropical Atlantic AAIW suggests that the circulation of intermediate water involves Indian-Atlantic interocean exchange. Chapter 6 discusses the origin of equatorial Atlantic AAIW and the fate of the newly-formed Atlantic AAIW. In chapter 5 the exchange of three Agulhas rings with the environment is analyzed. The Lagrangian trajectory analyses clearly indicate enhanced near-surface leakage and the responsible process is identified.

Chapter 2

Model description and method

2.1 Introduction

The depth-averaged ocean circulation can be described concisely by a streamfunction, a scalar field. The water moves on average along the streamfunction contours. The contours give therefore a clear picture of the stream patterns in the ocean. However, the two-dimensional nature of a streamfunction neglects the inherent three-dimensionality of the ocean circulation. With the transport-conserving Lagrangian trajectories we can combine the concept of streamfunctions with the three-dimensional ocean circulation. The water transport is equally large at every point along the trajectory. However, trajectories should not be seen as real 'molecules' or 'water particles', in the sense of real entities. It is a numerical, finite approximation of a three-dimensional streamline. Choosing a smaller water transport per trajectory would better approximate the continuous streamlines. If all streamlines are added together, the streamfunction of the total ocean circulation would result. The strength of the method, although, is that only those streamlines are filtered out that pertain to specific conditions. These can either be sections that the trajectory crosses with its density within a specific interval, that they start or end at the mixed layer base, or that their travelling time is more than one year.

The trajectory is a purely advective pathway, so the diffusion still acts on the properties of the trajectory. The temperature and salinity are therefore not constant along its path. This has a twofold advantage: first of all, the trajectory shows the advective pathway between locations and it can indicate possible teleconnections between these regions. Second, the change of the properties of the particles along its pathway indicates the regions where the ocean circulation is not adiabatic; i.e. regions with strong and weak mixing can be identified.

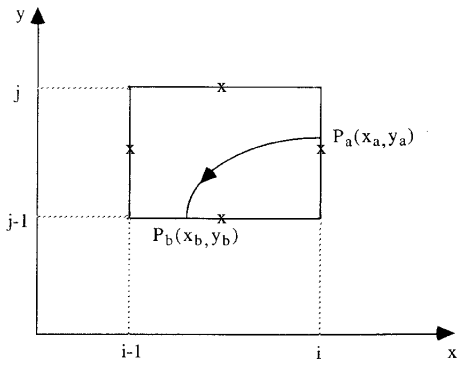

Figure 2.1: *Illustration of the trajectory path through one grid box, where the model velocities are at the four sides of the box.*

2.2 Lagrangian trajectories

The Lagrangian trajectory analysis developed by Döös (1995) and Blanke and Raynaud (1997) is used to track water masses to their destinations or origins. This technique calculates the three-dimensional path of a water particle off-line from the model data. A very efficient implementation of the algorithm enables us to calculate large quantities of trajectories. The method therefore quantifies the importance of different routes taken by the various water masses. The Lagrangian trajectory analysis calculates the advective path of a particle. Diffusion only acts on the properties of the particles, but has no influence on their path.

First, the sections are defined where the trajectory starts and stops. The number of trajectories that starts at the sidewall of a gridbox is proportional to the transport through that sidewall. The starting positions of the particles are equally distributed over the sidewall, and the path of each particle can be calculated. Every particle trajectory is a well-defined streamfunction and different trajectories can be added together. The diapycnal transports of different water masses are determined from the number of particles that cross a certain isopycnal. With this method particles can be followed forward as well as backward in time. The trajectory stops if one of the predefined end sections has been reached. The fate of subducted water masses is found by tracing trajectories forward after they enter the interior through the base of the mixed layer. The end section is here defined as the base of the mixed layer.

The path followed by the particle within one gridbox can be calculated as follows. The velocity through each sidewall of a gridbox is known. Within the gridbox the velocity component is assumed to change only in the direction of the velocity component, e.g. $u(x)$ and $w(z)$. The velocity is interpolated linearly in the position within the gridbox:

$$u(x) = u_{i-1} + \frac{x - x_{i-1}}{\Delta x}(u_i - u_{i-1}) \tag{2.1}$$

With the subscripts $i-1$ and i indicating the locations at either side of the gridbox and $\Delta x = x_i - x_{i-1}$ (see Fig. 2.1). Using the identity $u(x) = \mathrm{d}x/\mathrm{d}t$, follows:

$$\frac{\mathrm{d}x}{\mathrm{d}t} + \alpha x + \beta = 0 \tag{2.2}$$

where

$$\alpha = \frac{u_{i-1} - u_i}{\Delta x} \tag{2.3}$$

$$\beta = x_0 \frac{u_i - u_{i-1}}{\Delta x} - u_{i-1} \tag{2.4}$$

with this condition the location of the particle can be calculated independently for all three directions, giving $x(t)$ and $z(t)$. With the boundary condition $x(t_a) = x_a$, the trajectory is fully determined within the gridbox:

$$x_b = (x_a + \frac{\beta}{\alpha}) \exp[-\alpha(t_b - t_a)] - \frac{\beta}{\alpha} \tag{2.5}$$

or

$$t_b = t_a - \frac{1}{\alpha} \log \left[\frac{x_b + \beta/\alpha}{x_a + \beta/\alpha} \right] \tag{2.6}$$

The calculation is repeated similarly for the meridional and vertical velocities. The lowest of the three passage times t_b defines which side of the box is attended by the particle. This time is used to calculate the new three-dimensional position of the particle when it leaves the gridbox. The procedure is then repeated for the next gridbox.

The transit time of the trajectory through the gridbox can be calculated exactly if the velocity field is stationary. De Vries and Döös (2001) developed an analytical expression for the trajectory inside a grid box with a time dependent velocity field, but the transit time of the trajectory needs to be calculated numerically. Figure 2.2 shows three typical trajectories that have been calculated for chapter 5.

In all calculations with the Lagrangian technique, particles were used that are associated with a transport of 0.01 Sv or less. The error of the calculation was estimated by comparing two runs, where ten times more particles were used for the second run, each particle carrying now at most 0.001 Sv. A second check involved the comparison of tracing particles forward and backward between the same two sections. From both comparisons it follows that the error of the Lagrangian technique is less than 0.2 Sv for a total transport of 15 Sv, or approximately 1% of the transport estimates.

2.3 OCCAM

The Ocean Circulation and Climate Modelling (OCCAM) project is a high-resolution global ocean modelling effort at the Southampton Oceanography Centre. It is aimed at the development of global ocean models that are suitable for

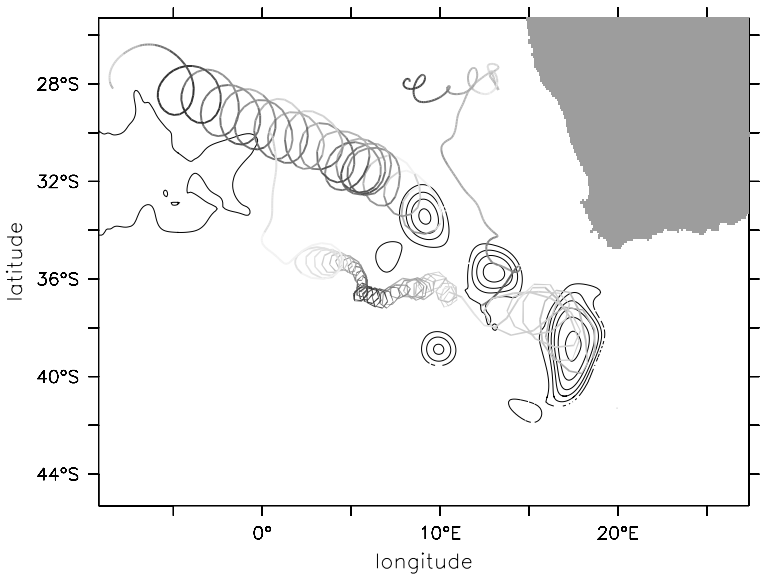

Figure 2.2: *Three Lagrangian trajectories that are initialized within Agulhas rings and calculated with time-dependent velocity fields. Shading of the trajectory indicates its depth (light grey=shallow; dark grey=deep). The contours indicate the SSH anomalies of the Agulhas rings at the moment that the trajectories were initialized.*

studying climate. The OCCAM model is a modified version of the Bryan-Cox-Semtner code (Webb et al., 1998). The model uses an Arakawa-B grid and has an eddy-permitting resolution of $1/4^\circ \times 1/4^\circ$. The model has a free surface and 36 vertical levels at fixed depths, with 16 layers in the upper kilometer. A Laplacian horizontal diffusion and friction is used. The horizontal diffusion coefficient for tracers is $100\,\mathrm{m^2\,s^{-1}}$ and for the velocity the horizontal viscosity coefficient is $200\,\mathrm{m^2\,s^{-1}}$. The Pacanowski and Philander (1981) scheme is used for the vertical mixing of tracers. Away from regions with strong shears this gives diffusivities of $0.5\,\mathrm{cm^2\,s^{-1}}$. A Laplacian vertical mixing is applied to the velocity fields with a diffusion coefficient of $1\,\mathrm{cm^2\,s^{-1}}$. The model has been run for 12 years, with a spin up of 9 years with monthly mean winds and wind stresses from the European Centre for Medium-Range Weather Forecasts (ECMWF) (Gibson et al., 1997). In the last 3 years six-hourly ECMWF winds and wind stresses have been used.

The model employs the Modified Split QUICK scheme to solve the advection-diffusion equation for tracers. The dispersive properties of an ordinary advection scheme would quickly result in very noisy solutions. Instead of linear interpolation, the Modified Split QUICK (MSQ) scheme uses a combination of linear interpolation and quadratic upstream interpolation. This reduces the magnitude of the leading-order error by a factor of 4 and it also introduces a biharmonic diffusion. The QUICK scheme produces less dispersion of the long wavelengths and as a result, the tracer advection is much improved. At the same time the short wavelength components are damped out by the biharmonic diffusion.

The Lagrangian trajectory method requires the data to be defined on an Arakawa C-grid. Since OCCAM uses a B-grid, the data has been regridded. The horizontal velocity points in the C-grid have been averaged over the two nearest points in the B-grid. Vertical velocities have been calculated with the continuity equation.

Recent studies (Griffies et al., 2000; Roberts and Marshall, 1998) have shown that, in high resolution z-coordinate models, the advection scheme and the explicit diffusion used to parameterize sub-grid scale processes may drive unrealistically high rates of diapycnal mixing. This effect has been diagnosed for OCCAM by Lee et al. (2001). They concluded that the impact of spurious diapycnal diffusion is the main cause for model drift and that errors in the surface buoyancy forcing play a lesser role. The high-frequency wind forcing results in internal waves with large, oscillating vertical velocities. The resultant "heaving" of density surfaces is found to give enhanced diffusive fluxes as a result of the biharmonic diffusion within the MSQ scheme acting on vertical advection. Lee et al. (2001) showed that deep and bottom water drift away from the Levitus climatology, due to the unrealistic diapycnal mixing, but that the THC still looks plausible. In particular, deep water formation in the North Atlantic rapidly declines and the overturning suggests deep water formation at subtropical latitudes. Further away from the North Atlantic deep water formation sites, that is, south of the Atlantic equator and in the other ocean basins, the THC is much less affected by drift.

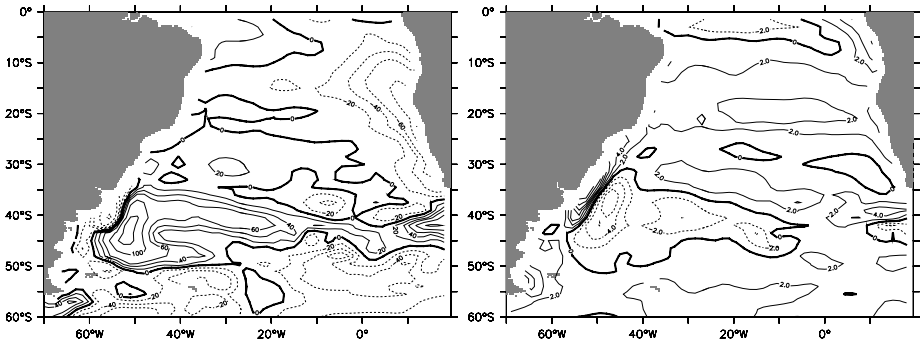

(a) Heat flux ($\mathrm{W\,m^{-2}}$) (b) Freshwater flux ($\mathrm{mm\,day^{-1}}$)

Figure 2.3: *Surface flux difference between OCCAM and the ERA 40 reanalysis dataset. Positive values denote that OCCAM overestimates the flux.*

2.4 Air-sea fluxes

The air-sea fluxes of heat and freshwater are derived from relaxation of sea surface temperature (SST) and salinity. For the heat flux the SST dataset of Reynolds and Smith (1994) for the years 1993 to 1995 has been used. For the freshwater flux the SSS is relaxed to the Levitus et al. (1994) dataset. This ensures that the surface temperature and salinity cannot deviate too much from the observed values. However, the relaxation time scale of 30 days produces only a weak surface forcing and does not guarantee realistic water mass transformations (Fox and Haines, 2003). The differences in heat and freshwater forcing between the ERA 40 reanalysis and the OCCAM model have been plotted in figure 2.3. The surface forcing can be divided into a part that is dependent on the temperature difference between the ocean and the atmosphere (Q_{diff}) and a part that is independent of the temperature difference (Q_{abs}). The heat flux Q_{diff} is linearly dependent on the temperature difference with climatological SST in OCCAM, while in reality this is a complex function determined by atmospheric boundary layer processes and the difference between SST and air temperature. The heat flux component Q_{abs} is not included in the OCCAM model. This will generate biases in the ocean surface temperature and the surface temperature relaxation in OCCAM cannot fully correct for this. Also, the model physics differ from real ocean physics due to subgridscale processes which generate model biases. Consequently, air-sea fluxes can be too large where the model has large biases, for instance the location of the Brazil-Malvinas Confluence zone and other oceanic fronts (Fox et al., 2000). But in general, relaxation to climatological SST will cause the heat fluxes to be too small as Q_{abs} is absent and Q_{diff} is smaller when the air temperature is replaced by climatological SST.

Also, it is likely that a coarser model with larger mixing coefficients will constrain SST and SSS more and yield smaller fluxes. A higher resolution, more complete eddy-permitting model will have more variability and subsequently larger fluxes. Due to the relaxational forcing, the model underestimates the amplitude of SST variability and contains a lag of about one month in the seasonal cycle of SST (Fox et al., 2000). Figure 2.3 clearly shows that the forcing in OCCAM is not in agreement with the atmospheric reanalysis dataset ERA 40 for the same time period, especially along the frontal zones that separate the South Atlantic subtropical gyre and the ACC. Although the surface forcing at this location generates water masses with erroneous T-S properties, the opposing effects on density of the overestimated heat gain and evaporation largely cancel (see chapter 4.

2.5 Bolus transport

Water masses are transported mainly along isopycnals. This implies that to properly describe the Lagrangian flow of water masses, transports should be analyzed along isopycnal surfaces, within isopycnal layers. An isopycnal layer is defined as a layer between two isopycnal surfaces. As the thickness of isopycnal layers is subject to temporal variability, it is important to take into account the correlation of velocity and thickness fluctuations, which defines the 'bolus transport'.

Time averages are usually taken over several annual cycles giving annual mean data. In the present study a model climatology constructed from 219 archived five-day averages was used, comprising three annual cycles. One mostly considers mean transports that are defined on constant z levels, neglecting the bolus velocity. The mean transport $\overline{\mathbf{U}}(z)$ is then defined by

$$\overline{\mathbf{U}}(z) = \overline{\mathbf{u}}(z)\Delta z \Delta x, \tag{2.7}$$

where the bar denotes the time-averaging procedure, z is the cartesian vertical coordinate, Δx and Δz are the horizontal and vertical extent of the gridbox, and $\mathbf{u}(z) = (u, v)$. To include the effect of the bolus transport the five-day averaged velocities have been transformed from a depth coordinate z to a density coordinate σ. From the 219 fields the time-averaged isopycnal mass transport was established. The time-mean mass transport within one density layer can be written as

$$\overline{\mathbf{U}}(\sigma) = \Delta x \left[\overline{\mathbf{u}(\sigma)h(\sigma)}\right] = \Delta x \left[\overline{\mathbf{u}}(\sigma)\overline{h}(\sigma) + \overline{\mathbf{u}'(\sigma)h'(\sigma)}\right] \tag{2.8}$$

with $\mathbf{u}(\sigma)$ the velocity and $h(\sigma)$ the thickness of the isopycnal layer. The primes denote departure from the time average, that is, $\mathbf{u}'(\sigma) = \mathbf{u}(\sigma) - \overline{\mathbf{u}}(\sigma)$, $\overline{\mathbf{u}'}(\sigma) = 0$, and $\overline{\mathbf{u}}(\sigma) = (\overline{u}(\sigma), \overline{v}(\sigma))$. The first term on the right-hand side is equal to equation 2.7, only now defined on a σ-coordinate. This is the transport by the annual mean flow. The second term represents the bolus transport. The bolus transport is not only due to explicit eddies (e.g. Agulhas rings), but due

to all time variability between 5 days and 3 years that induces extra isopycnal transports. This also includes seasonal variations. The bolus velocity does not influence the total, vertically integrated transport, but is merely a vertical redistribution of the fluxes. Ultimately, at every point the averaged isopycnal transport is transformed back to a transport on z levels using the averaged layer thickness. The latter also determines the bolus mean density of each grid box McDougall (1998).

Chapter 3

The Lagrangian view of interocean exchange compared with inverse model results

The interocean exchange of thermocline and intermediate waters in the South Atlantic Ocean has been investigated. To resolve the pathways between different ocean basins a Lagrangian particle following technique has been used. The results have been compared with various inverse models and observational studies addressing the interocean exchange in the South Atlantic Ocean. To facilitate the comparison, section-integrated transports in the same density classes and at the same locations as used in the observational studies have been calculated for OCCAM. The flow toward the North Atlantic, excluding the Antarctic Bottom Water, is made up for more than 50% of thermocline water. The exact ratio of thermocline to intermediate transport depends on the definition of the water masses. Transport of intermediate water plays a less important role. More than 90% of the flow toward the North Atlantic originates from the Indian Ocean via leakage from the Agulhas Current system. Agulhas leakage into the South Atlantic occurs to 2000 m depth, but transport below 1200 m recirculates within the subtropical gyre and flows back into the Indian Ocean. Several observational studies have indicated a dominant role in the transport toward the North Atlantic for intermediate water or for the direct inflow from Drake Passage. The section averaged water mass transports in OCCAM are largely in agreement with these observational estimates. Also in OCCAM, the section-integrated transports suggest a minor contribution from Agulhas leakage to the upper branch of interocean exchange in the South Atlantic, in apparent contradiction with the Lagrangian path that was calculated explicitly. The reason for this discrepancy is that at the

Published as Donners and Drijfhout (2004)

eastern side of the South Atlantic the net mass flux consists of opposing, and in the thermocline layer nearly compensating, east- and westward flows. In the thermocline layer, part of the westward flow connects with the cross-equatorial flow in the Atlantic, while the eastward flow is partly derived from upwelled intermediate and thermocline water that originates from Drake Passage. The detailed Lagrangian analysis suggests that it is arguable to draw conclusions about the flow pathways from integrated mass fluxes across ocean sections, especially when these contain opposing flows in the same density classes.

3.1 Introduction

The upper branch of the THC in the South Atlantic is defined here as the flow within density layers that are lighter than $\sigma_1 = 32.16\,\mathrm{kg\,m^{-3}}$ from the Indian and Pacific Oceans towards the North Atlantic. The upper branch of the THC in the South Atlantic is supplied by two different pathways. Warm and salty thermocline water enters the South Atlantic via Agulhas leakage (Gordon, 1986), known as the warm water route. Cold and fresh intermediate water enters the South Atlantic via Drake Passage (Rintoul, 1991), known as the cold water route. Due to their contrasting properties the ratio of contributions of the warm and cold routes is closely coupled to the heat and freshwater fluxes in the South Atlantic (Gordon, 1997), and subsequently has a strong impact on the heat and freshwater budget of the whole Atlantic. These routes are not mutually exclusive, neither need their relative contributions be constant in time. It is still not clear which of these two routes into the Atlantic basin is on average the most important (Gordon, 1997).

Gordon (1986) used the heat and mass fluxes across 30°S in the South Atlantic to estimate the temperature of the supply of water from the Indian and Pacific Oceans. He concluded that the warm water route accounted for at least 80% of the South Atlantic upper branch of the THC. Rintoul (1991) used an inverse model of the South Atlantic and concluded that the cold water route was the most important source for the South Atlantic upper branch. Intermediate water from Drake Passage was warmed while it crossed the Atlantic sector of the Southern Ocean. This warmed intermediate water directly flowed into the South Atlantic due to the northward Ekman transport. At 32.5°S the South Atlantic mainly transported water in the thermocline layer northward. The model showed an unrealistic circulation when a net Agulhas inflow was prescribed. Gordon et al. (1992) used chlorofluoromethane (CFM) ratios to conclude that the input of the Benguela Current, which is thought to carry the northward flowing upper branch of the THC, consisted for 50%-65% of Agulhas leakage from the Indian Ocean and for 35%-50% of water recirculating in the South Atlantic subtropical gyre. Thermocline water was partially converted to intermediate water in the South Atlantic subtropical gyre. They concluded that the South Atlantic mainly contributed intermediate water to the North Atlantic. The direct inflow of intermediate water from Drake Passage did not play an important role, but could contribute to the South Atlantic upper branch of the

THC, after recirculating in the southwest Indian Ocean subgyre, and flowing back into the South Atlantic via Agulhas leakage.

In the following years a number of inverse model studies were performed with a global hydrographic dataset (Ganachaud, 2000; Macdonald and Wunsch, 1996; Sloyan and Rintoul, 2001a). All studies were based on the inverse model of Wunsch (1978). Macdonald and Wunsch (1996) found that the South Atlantic upper branch of the THC was supplied by both the cold and warm water routes, which suggested that both routes were important. However, the uncertainties were large and both routes could be dominant at different times. In an extension of that study, Macdonald (1998) showed that the South Atlantic mainly contributed thermocline water to the North Atlantic. Drake Passage was thought to be the most consistent source for the South Atlantic upper branch of the THC. The intermittency of Agulhas leakage posed a problem to quantify the flow from the Indian to the South Atlantic Ocean via the warm water route. Ganachaud (2000) used data from the World Ocean Circulation Experiment (WOCE) and found an equipartition between intermediate and thermocline water in the South Atlantic upper branch of the THC. Because of the enhanced eddy field in the Benguela region he did not attempt to distinguish the sources of the South Atlantic upper branch of the THC. Sloyan and Rintoul (2001a) added air-sea fluxes to the original inverse model (Wunsch, 1978). They found that the major source of the South Atlantic upper branch of the THC was intermediate water coming directly from Drake Passage. A minor amount of intermediate water from Drake Passage made a sojourn in the southwest Indian Ocean and contributed to the THC via Agulhas leakage, similar to the indirect route proposed by Gordon et al. (1992). The intermediate water gained buoyancy in the Brazil-Malvinas Confluence area and in the southwest Indian Ocean. The South Atlantic contributed mainly intermediate water to the North Atlantic.

Various general circulation models have been used to analyze the South Atlantic upper branch of the THC. In general, models with a higher resolution show a larger Agulhas leakage. The estimates of Agulhas leakage in global ocean circulation models range therefore from no Agulhas leakage (Drijfhout et al., 1996) to a significant leakage of 9 Sv thermocline water (Thompson et al., 1997).

The object is to make a detailed comparison between a Lagrangian description of the South Atlantic upper branch of the THC in OCCAM and the circulation inferred from various observational studies. In particular, we address whether similar box model calculations, as performed in the observational studies, would lead to different conclusions than offered by the Lagrangian description, and to what extent the box model transports in OCCAM differ from observational estimates.

OCCAM shows a dominant role for inflow from the Indian Ocean and mainly contributes thermocline water to the North Atlantic (Drijfhout et al., 2003a). Most observational studies show an important role for intermediate water and direct flow from Drake Passage. In particular we want to assess whether the discrepancies can be explained by: 1) invalid assumptions to infer the circulation from section-integrated transports in box-models, the sparse observational

datasets and the use of inconsistent combinations of datasets or large variability, or, 2) deficiencies in the general circulation model that cause the model to drift away from the observed circulation.

Also, it is clear from the conflicting conclusions that were drawn from the various inverse model studies that simply equating the warm water route with inflow of thermocline water and the cold water route with inflow of intermediate water is not justified. The water from Drake Passage that spills northward to feed the upper branch of the THC is dominated by intermediate waters with a southern hemispheric subpolar origin. Such waters have been found to flow northward in the South Atlantic, mainly inbetween the thermocline waters and the southward flowing NADW (Stramma and England, 1999), but it is unclear whether this circulation is part of the upper branch of the THC. Also, it is unclear to what extent the intermediate waters from Drake Passage that do take part in the upper branch of the THC keep their characteristics or are transformed into lighter density classes along their way. On the other hand, Agulhas leakage is dominated by warm water with a subtropical origin from the South Indian Ocean (Garzoli and Gordon, 1996), and when it flows into the South Atlantic this water would mainly be found in the thermocline layers. However, many Agulhas Rings in the South Atlantic are subject to winter cooling and part of the thermocline water may be transformed into denser, intermediate water. Also, a significant part of the Agulhas Rings consists of intermediate water that may even have its origin in the Pacific Ocean, entering the Indian-Atlantic basin by Drake Passage. Intermediate water from the Indian Ocean has been found to spread in the South Atlantic (Boebel et al., 2003), but as the circulation on larger depth is weaker, intermediate water may easily become detached from the propagating cyclones and anticyclones that are spawned from the Agulhas Current system and may take another route in the South Atlantic than the thermocline water contained within these vortices. In short, a Lagrangian description of the interocean exchange in the South Atlantic is incomplete without an examination of the watermasses involved and the inherent watermass transformations in the South Atlantic basin.

The Lagrangian analysis of the model data is performed with the method described in section 2.2. The pathways of different water masses are quantified and their conversions are diagnosed along the pathway with the off-line calculation of large amounts of Lagrangian trajectories. With this method it is possible to discriminate between direct routes and recirculations. Also, the role of eddies can be included by means of the bolus velocity (see section 2.5). In this study two datasets have been used. For the Lagrangian trajectory analysis the annual mean dataset with bolus transports included was used. For the comparison to other inverse model studies the annual mean dataset without bolus transports was used. Both datasets include data of 3 model years. The importance of the bolus velocity is discussed in section 3.4.3.

In the comparison of the OCCAM model to individual inverse models we use the same definitions for the isopycnal layers and the same locations of the hydrographic sections. We used the annual mean dataset without the bolus velocity, because the bolus transport is not considered in the inverse models. The

diapycnal transports in the area enclosed by hydrographic sections are calculated from the divergence of the isopycnal mass fluxes across the hydrographic sections.

We also calculated the standard deviation of the mass fluxes across the different hydrographic sections. The inverse models exclude the highly variable Ekman transport. In the calculation of the variability of the OCCAM model we therefore excluded the Ekman layer, which we defined as the top 25 m. The Ekman transport is mainly compensated by barotropic waves (Ganachaud, 2000). Barotropic waves take approximately 17 days to cross the South Atlantic. To remove the effects due to these barotropic waves, we averaged over a period of 20 days.

To decide whether there is a significant deviation between OCCAM and the inverse models, we used the criterion that the difference should be larger than two standard deviations. This enables us to discriminate if the differences between OCCAM and inverse models are caused by baroclinic variability or by something else.

It has been shown that the OCCAM model shows a large drift (Lee et al., 2001, see also section 2.3). In section 3.4.4 we estimate the impact of drift on the horizontal mass fluxes. We analyzed time-series of 219 5-day average mass transports and show that a linear trend in these time-series is not statistically significant.

This chapter is structured as follows. In section 3.2 we analyze the South Atlantic upper branch in OCCAM with the Lagrangian method. In the third section we compare the relevant box model transports in OCCAM to the results from various observational studies. In section 3.4 we discuss the discrepancies between model and observations and the difference between the circulation inferred from Lagrangian trajectories and section-integrated box-model transports in OCCAM. Finally, in section 3.5 we present the conclusions.

3.2 Lagrangian analysis of interocean exchange in OCCAM

3.2.1 Upper branch of the cross-equatorial return flow of the THC

We calculated the sources of the South Atlantic upper branch of the THC in OCCAM with the trajectory method discussed before. All particles that cross the Atlantic equator in a northward direction and that are lighter than the potential density $\sigma_1 = 32.16\,\mathrm{kg\,m^{-3}}$ were traced backward in time. This comprises particles with a density that is lighter than that of the NADW. The trajectory ends when it arrives at 20°E, Drake Passage (70°W) or when it curves back to the Atlantic equator. The streamfunction of particles that leave the South Atlantic towards the North Atlantic can be seen in Fig. 3.1. The strength of the upper branch is 16.2 Sv, of which 15.2 Sv originates from the Indian Ocean and

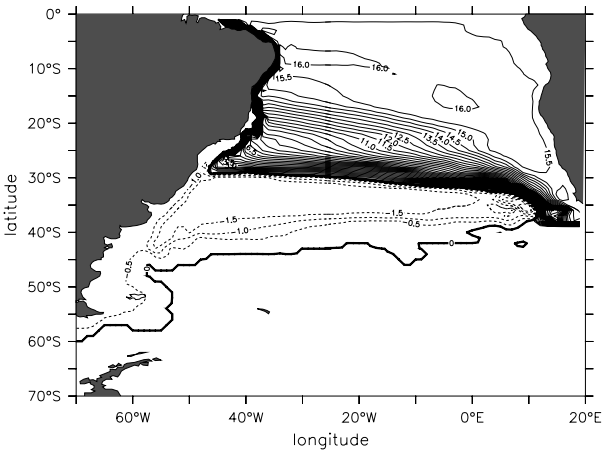

Figure 3.1: *Streamfunction in Sv (1 Sv≡ $10^6\ m^3\ s^{-1}$) of particles traced backward from the Atlantic equator to 20° E or Drake Passage. Only particles lighter than $\sigma_1 = 32.16\,\mathrm{kg\,m^{-3}}$ are included.*

1.0 Sv from Drake Passage. Less than 2 Sv recirculates in the South Atlantic subtropical gyre before flowing equatorward.

More than 90% of the flow toward the North Atlantic originates from the Indian Ocean. To obtain a more complete picture of the inflow of the South Atlantic Ocean we therefore looked at the vertical structure of the Agulhas leakage at 20°E. To this end, trajectories have been traced forward in time starting at 20°E. Agulhas leakage from the Indian to the Atlantic Ocean as a function of depth and density can be seen in Fig. 3.2. The figure divides the transport into water that is part of the upper branch of the THC (solid line) and water that recirculates in the South Atlantic subtropical gyre and returns to the Indian Ocean (dashed line). To ensure that we only included particles which either recirculated in the South Atlantic subtropical gyre, or took part in the cross-equatorial transport, we only included particles that crossed 20°W. This procedure removes the Agulhas Current transport that directly enters the Agulhas Return Current. From the Indian Ocean 22.2 Sv leaks into the South Atlantic subtropical gyre, of which 15.5 Sv is transported to the equator. 6.7 Sv recirculates in the South Atlantic subtropical gyre, and flows back to the Indian Ocean. The vertical distribution of Agulhas leakage shows that the upper branch of the THC is concentrated in the upper 1200 m. Recirculation of Indian Ocean water in the South Atlantic subtropical gyre takes place in the upper 100 m and between 1000 m and 2000 m. In Fig. 3.2b transport as a function of potential density σ, with vertical axes for reference levels at the surface (σ_0), at 1000 m depth (σ_1), and neutral density γ_n is plotted. Very light water masses ($\sigma_0 < 25.5\,\mathrm{kg\,m^{-3}}$, or warmer than 18 °C) are equally divided between a recirculation that flows back into the Indian Ocean and transport toward the Atlantic

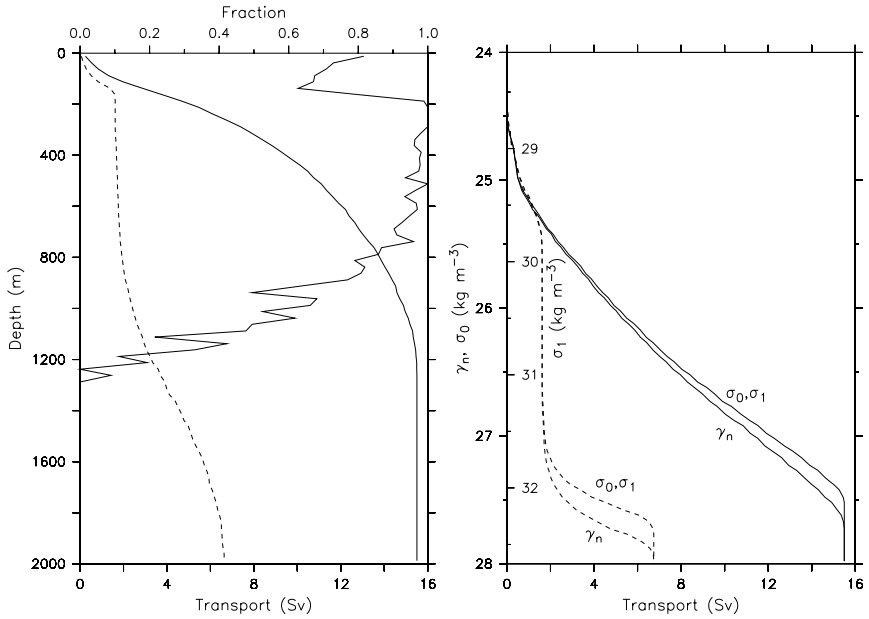

Figure 3.2: *The Agulhas leakage (in Sv) accumulated with (a) depth and (b) density at 20°E that reaches the Atlantic equator (solid) or recirculates within the South Atlantic subtropical gyre (dashed). The thin line in Fig. (a) indicates the fraction of the Agulhas leakage that is transported to the Atlantic equator. Figure (b) shows two curves for both potential density (σ_0 and σ_1) and neutral density (γ_n). The double vertical axis shows the nearly equivalent values of σ_0 and σ_1 (To discriminate between an overshoot of the Agulhas Current and the subtropical gyre circulation we excluded all transport not crossing 20°W, which is roughly halfway between the western limit of the Agulhas retroflection and the western boundary of the subtropical gyre).*

equator. Cold water masses ($\sigma_0 > 27.4\,\mathrm{kg\,m^{-3}}$, or colder than 5 °C) are mostly recirculated back into the Indian Ocean. The water masses between σ_0 25.5 and 27 are virtually all transported toward the equator.

To simplify the analysis of the upper branch in the South Atlantic, we define some isopycnal layers. On the basis of Fig. 3.2b and the layers defined by Rintoul (1991) we use 2 layers: thermocline ($\sigma_0 < 26.8\,\mathrm{kg\,m^{-3}}$) and intermediate ($\sigma_0 > 26.8\,\mathrm{kg\,m^{-3}}$ and $\sigma_1 < 32.16\,\mathrm{kg\,m^{-3}}$). Although 1.7 Sv very light water recirculates, most Agulhas leakage in the thermocline layer is transported toward the Atlantic equator. Half of the leakage of intermediate water recirculates in the South Atlantic subtropical gyre and flows back into the Indian Ocean.

The Lagrangian transports for the thermocline and intermediate layers in the South Atlantic upper branch of the THC at the start and end sections are shown in Fig. 3.3a. As in Fig. 3.1, we backtraced particles from the Atlantic equator. Note that the transports are only a subset of the total transport across a section.

A minor amount of 0.8 Sv thermocline water transforms into intermediate water in the South Atlantic Ocean. This mainly takes place north of 30°S, in the South Equatorial Current and along the western boundary. The area-averaged advection-diffusion balance can be approximated by:

$$\rho_t + w^* \rho_z = (\kappa \rho_z)_z = \kappa_z \rho_z + \kappa \rho_{zz} \tag{3.1}$$

where for simplicity the effects of horizontal advection and cabbeling are neglected. OCCAM uses the Pacanowski and Philander (1981) scheme for the vertical diffusivity, which implies that $\kappa > 0$ and for the region of interest with nowhere significant increase of shear with depth $\kappa_z \approx 0$. This implies that no balance between vertical advection and diffusion can arise as $w^* > 0$ and $\rho_{zz} < 0$. To balance the downwelling $\rho_t \approx -w^* \rho_z$, which implies drift.

It is remarkable that the water flowing from Drake Passage to the equator is mostly very light water in the thermocline layer. Apparently, in the Atlantic sector only the lightest water masses are sufficiently affected by the Ekman transport to escape the ACC to the north.

3.2.2 Interocean exchange in the South Atlantic

There is a large exchange of water between the South Atlantic and Indian Oceans. To obtain a complete picture of the South Atlantic interocean exchange of thermocline and intermediate waters we also analyzed the flow leaving the South Atlantic ocean at 20°E. The transports are shown in Fig. 3.3b. Of the 48.6 Sv of water in the thermocline layer that leaves the Atlantic sector at 20°E, 5.2 Sv upwells from the intermediate layer in the South Atlantic. This upwelling occurs in a zone around 45°S along the path of the ACC (not shown). All of this upwelled water originates from Drake Passage.

Figure 3.3c is the sum of the Figs. 3.3a and 3.3b, and represents all the interocean exchange above the NADW in the South Atlantic. The Lagrangian picture of the interocean exchange and the different pathways is not evident

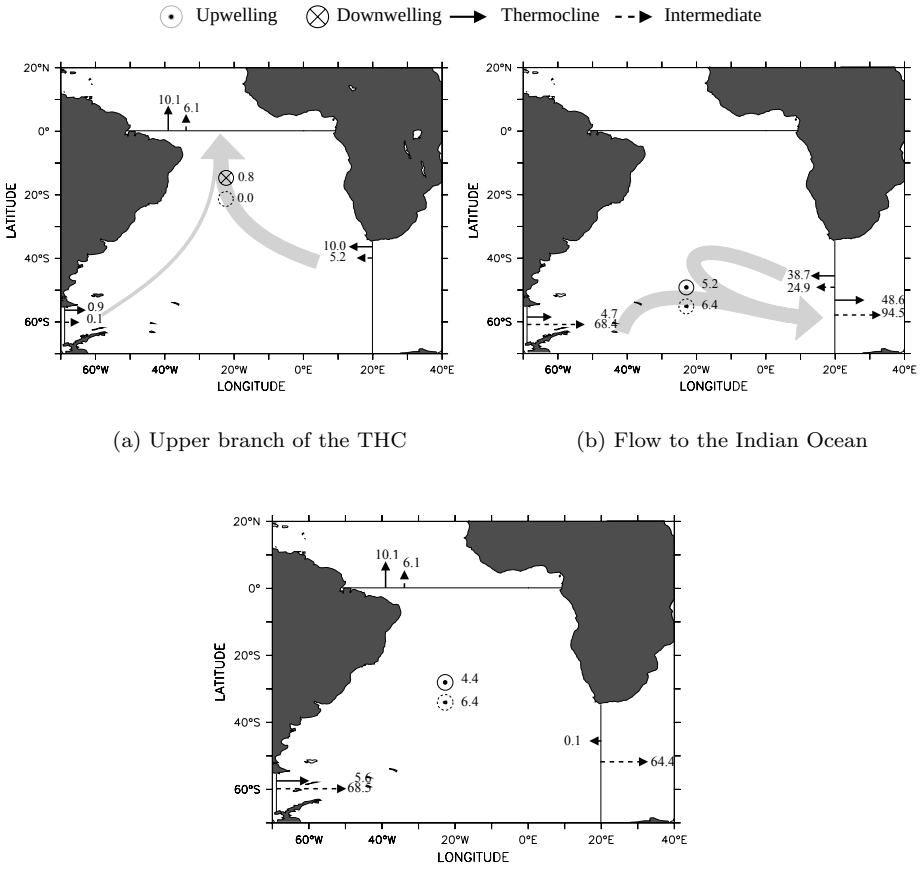

(a) Upper branch of the THC

(b) Flow to the Indian Ocean

(c) Sum of (a) and (b)

Figure 3.3: *Mass fluxes (in Sv) that (a) contribute to the upper branch of the South Atlantic and (b) the flow into the Indian Ocean sector in OCCAM. The sum of (a) and (b) is plotted in (c). Solid arrows represent the thermocline layer, and dashed arrows the intermediate layer. Also the diapycnal mass fluxes for the thermocline-intermediate layer interface (solid) and the intermediate-deep layer interface (dashed) are included. (a) Upper branch of the THC (b) Flow to the Indian Ocean (c) Sum of (a) and (b)*

from this figure. The sum of the mass fluxes at 20°E in the thermocline layer gives a total net mass flux of 0.1 Sv from the Indian Ocean into the Atlantic Ocean. So, while OCCAM shows a large contribution from the warm water route, no significant net influx of thermocline water across 20°E is necessary for this to occur. Similarly as was hypothesized in Rintoul (1991), Fig. 3.3c suggests that most of the cross-equatorial flow originates from Drake Passage: At Drake Passage 68.5 Sv intermediate waters enters the Atlantic sector, but only 64.4 Sv leaves the Atlantic at 20°E. There is also an influx from Drake Passage of 5.6 Sv of water in the thermocline layer with no net outflow of this water type occurring at 20°E. Apparently, the box model in Fig. 3.3c suggests a flow path that in reality does not occur. While in OCCAM the flow of intermediate water in the ACC decreases with 4.1 Sv in the Atlantic sector, only 0.1 Sv intermediate water from the Pacific contributes directly to the upper branch of the THC in the South Atlantic. The same holds for water in the thermocline layer. There is a decrease of 5.7 Sv in the Atlantic sector, but only 0.9 Sv of the inflowing water at Drake Passage contributes to the upper branch of the THC. The reason for this discrepancy is that across 20°E the eastward outflow is largely compensated by a westward inflow.

3.3 Comparisons to other studies

The previous section described the interocean exchange in the South Atlantic from a Lagrangian perspective. Here we review various observational studies and compare the results with OCCAM. To facilitate the comparison, section-integrated transports in the same density classes and boxes as used in the observational studies have been calculated for OCCAM. As the observational studies use Eulerian measurements we use the annual mean dataset without the bolus transport for this comparison. The influence of the bolus transport is further discussed in section 3.4.3. We note that comparing synoptic sections with yearly averaged model velocities is not strictly valid, even though it is an underlying assumption of box-inverse models that sections are representative of the mean. It seems, however, the best way of comparing the model to the observations.

The transport estimates of local current fields in inverse models are very uncertain due to high baroclinic variability (Ganachaud, 2000; Macdonald, 1998). However, because the net mass transports across hydrographic sections are more constrained, their estimates are less uncertain. Therefore, we only used the net transports of water masses across hydrographic sections for this comparison.

The diapycnal transports in most inverse models are not determined from observational data, but calculated by the model. In layers below the surface, the diapycnal transport is limited by the maximum diapycnal diffusivity defined for the inverse model. In layers that reach the surface, diapycnal transports can be larger due to air-sea interaction. The inverse model by Sloyan and Rintoul (2001b) uses a novel approach by explicitly calculating these surface water mass transformations from air-sea fluxes of heat, freshwater and momentum.

To assess the impact of variability in OCCAM we calculated the standard

deviation of the mass fluxes. To prevent cluttered figures, we only added the standard deviation to Fig. 3.6b. The variability is representative for the other comparisons. Whenever the difference between the inverse models and OCCAM is larger than two standard deviations, we discuss the deviations in more detail.

We first discuss the comparison with different inverse model studies in sections 3.3.1 to 3.3.4. The last section compares OCCAM to the observational study of Gordon et al. (1992). The effects of the bolus term and drift on the section-integrated transports are further discussed in sections 3.4.3 and 3.4.4.

3.3.1 Rintoul's (1991) inverse model

Rintoul (1991) used an inverse model in the South Atlantic Ocean and concluded that most of the upper branch of the THC consisted of intermediate water coming from Drake Passage. This water gained buoyancy through air-sea interactions. The South Atlantic Ocean between 30°S and 60°S is a region of net heat gain (NCEP/Reanalysis, see Kalnay et al. (1996)). This region of heat gain coincides with the maximum of westerly wind stress, which drives an equatorward Ekman flow. This divergent Ekman flow causes upwelling of cooler water. These processes simultaneously modify intermediate water to lighter water masses and transports the lighter water northward.

Both the original schematic circulation from Rintoul and the transports calculated in OCCAM at the same sections are shown in Fig. 3.4. At the 32.5°S section in the South Atlantic, the same two upper layers as in the previous chapter have been used. At the other sections the lower interface of the intermediate layer is $\sigma_1 = 32.36\,\mathrm{kg\,m^{-3}}$.

The inverse model and OCCAM show a large qualitative resemblance. Both models agree within two standard deviations at 32.5°S (not shown). In OCCAM the South Atlantic upper branch of the THC at 32.5°S is 35% stronger compared to Rintoul (1991), but the thermocline layer transport is in both cases the dominant upper branch contribution. The thermocline to intermediate layer transport ratio is in both cases almost equal, 1.6 for Rintoul (1991) and 1.7 for OCCAM. Both models show a small net transport of the thermocline layer south of Africa. While Rintoul (1991) shows a small eastward flow, OCCAM shows a small westward flow. The strength of the ACC in OCCAM is consistently overestimated, although a decrease of 10 Sv eastward transport of intermediate water in the ACC can be seen in both models. Rintoul assumed this water to leave the box at 32.5°S. Both Figs. 3.4b and 3.3c suggest that a similar circulation occurs in OCCAM. However, the Lagrangian analysis in section 3.2 showed that, at least in OCCAM, the sources of the cross-equatorial flow inferred from these section-integrated mass fluxes are ambiguous. The net decrease of 10 Sv eastward flowing intermediate water in OCCAM can be explained by 5 Sv intermediate water that is converted to thermocline water and leaves the ocean south of Africa to the Indian Ocean, and 5 Sv westward flowing intermediate water that comes from the Indian Ocean as part of the upper branch of the THC.

Both Figs. 3.3c and 3.4b suggest the cold water route, while the Lagrangian

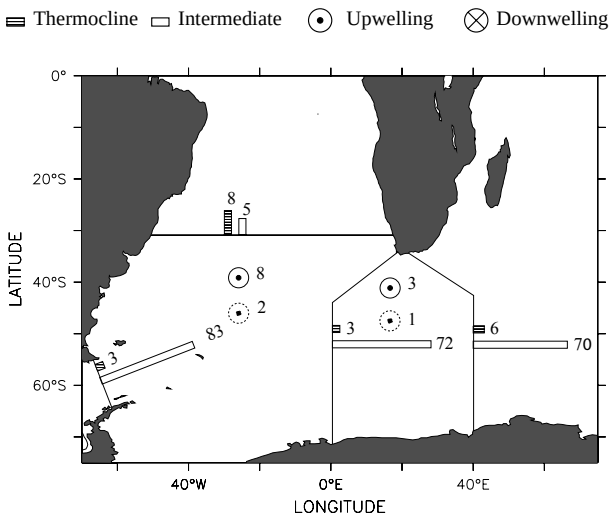

(a) Rintoul (1991)

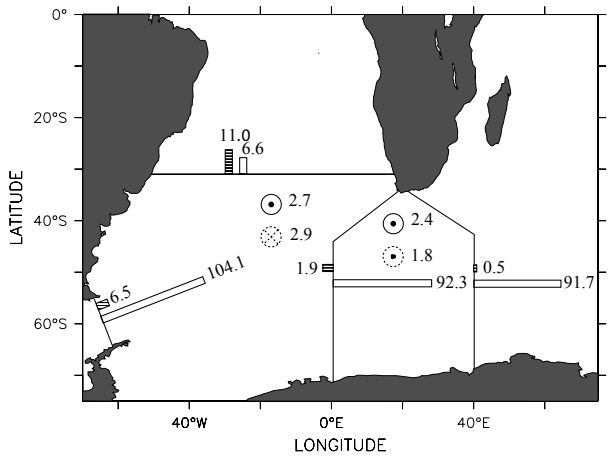

(b) OCCAM

Figure 3.4: *Comparison of the schematic circulation from Rintoul (1991) to mass fluxes calculated at the same sections in OCCAM. Diapycnal mass fluxes as in Fig. 3.3 (all mass fluxes in Sv). (a) Rintoul (1991) (b) OCCAM*

calculation shows that the warm water route is dominant in OCCAM. We see from Figs. 3.3a and 3.3b that there is both $O(50\,\mathrm{Sv})$ east- and westward flow of thermocline water across 20°E. So, a warm water route is possible without any net warm water transport across this section.

3.3.2 Macdonald's (1998) inverse model

Macdonald and Wunsch (1996) for the first time performed a consistent, quantitative study of the global ocean circulation with an inverse model and a global dataset of hydrographic sections. A comprehensive study of the model (Macdonald, 1998) suggested that the cold water route should be the most consistent source of the South Atlantic upper branch of the THC. The importance of the warm water route in that inverse model was much more uncertain, because of its intermittent character, but it might be an important, or even at times dominant, source for the South Atlantic upper branch.

The lower bound of the intermediate layer is at $\sigma_1 = 32.0\,\mathrm{kg\,m^{-3}}$. Compared to the isopycnal used in the previous section, the changed lower bound has a negligible impact on the total transport of intermediate water in the upper branch of the THC in OCCAM.

Macdonald (1998) shows a strong upper branch of 23 Sv at 11°S, while the upper branch is 13 Sv at 23°S (Fig. 3.5a). Macdonald finds at all latitudes in the South Atlantic a dominant thermocline layer flow. OCCAM shows comparable transports at 23°S, but the increase of the strength of the upper branch at 11°S is absent (Fig. 3.5b). Although the differences are large, the transports at 11 and 23°S agree within two standard deviations.

The upwelling of 10 Sv of deep to intermediate water between 11°S and 23°S differs substantially from OCCAM. Since the deep layer does not surface in this area, this must be provided by internal mixing. We calculated the diapycnal diffusivity κ needed to provide this diapycnal flux. The interface between deep and intermediate water is inbetween 800 and 1100m here. The upwelling has either to be balanced by $\kappa_z \rho_z$ or $\kappa \rho_{zz}$ (see Eq. 3.1). Below the pycnocline but well above the topography κ_z is not significantly different from zero (Polzin et al., 1997; Toole et al., 1994). If $\kappa \rho_{zz}$ provides for the diapycnal flux of 10 Sv, the average κ would be $4\,\mathrm{cm^2\,s^{-1}}$. Although some measurements do show values up to $30\,\mathrm{cm^2\,s^{-1}}$ locally (Kunze and Toole, 1997), such high values are only found within a few hundred meters above rough bottom topography. In the interior ocean κ is much less than $1\,\mathrm{cm^2\,s^{-1}}$ (Ledwell et al., 1998). A diapycnal diffusivity of 4 $\mathrm{cm^2\,s^{-1}}$ is neither supported by observations, nor by theories of enhanced vertical mixing (Laurent et al., 2002) and therefore probably unrealistically large.

In the inverse model, all northward flow at 30°S is concentrated at the northern section of the box that encloses the Benguela region. The strong eastward flow at the other sections enclosing the Benguela region box suggests that the flow from the western South Atlantic is the most important source for the northward flow. Although OCCAM does show some inflow of thermocline water from the Indian Ocean, most of the northward flow seems to be provided

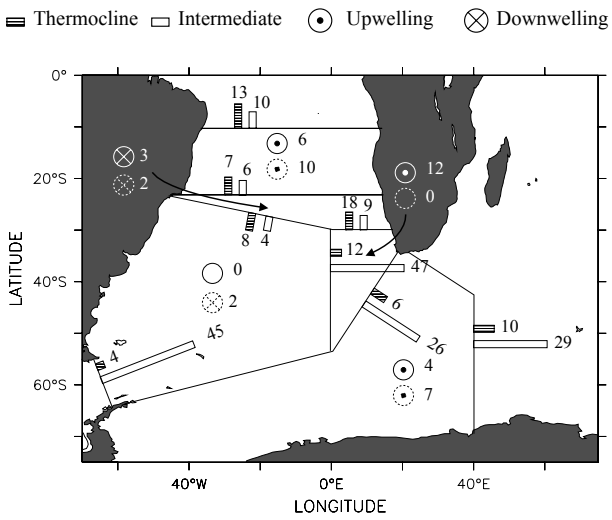

(a) Macdonald (1998)

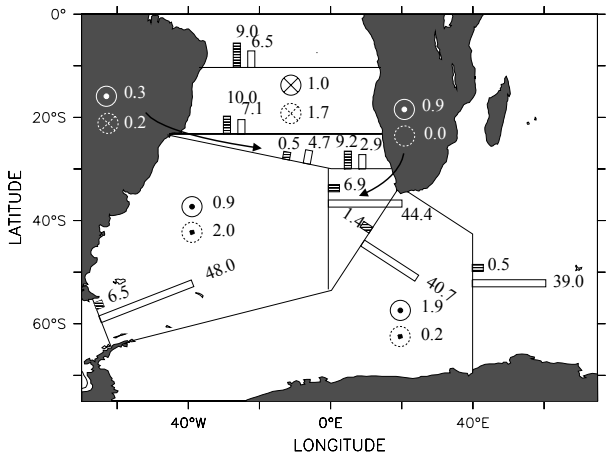

(b) OCCAM

Figure 3.5: *Comparison of the schematic circulation from Macdonald (1998) to transports calculated at the same sections in OCCAM. Diapycnal mass fluxes as in Fig. 3.3 (all mass fluxes in Sv). (a) Macdonald (1998) (b) OCCAM*

from the western South Atlantic as well. Here, also the section-integrated mass fluxes suggest a different circulation than is known to occur from the Lagrangian analysis.

The differences with the OCCAM model at the section at 30°S east of 0°E (8.8 Sv and 6.1 Sv) are larger than two standard deviations (7.8 Sv and 5.8 Sv, not shown). Because these sections stop in mid-ocean, the variability is much larger than for a hydrographic section which crosses an ocean basin. Therefore we attribute the discrepancies partly to the small extent of the section. If the section is prolonged westward of 0°E to the coast of South America, the integrated fluxes of the inverse model and OCCAM differ within two standard deviations.

Macdonald shows a strong upwelling of 12 Sv intermediate to thermocline water in the Benguela region box. Because the intermediate layer surfaces in this region, the transformation could be caused by air-sea interaction. This large conversion, however, implies a mean surface heat flux of 141 $\mathrm{W\,m^{-2}}$ in that box. The net surface heat flux in the South Atlantic shows areas with a heat gain above 100 $\mathrm{W\,m^{-2}}$ (NCEP/Reanalysis, Kalnay et al. (1996)), but the annual mean surface heat flux averaged over that area is 16 $\mathrm{W\,m^{-2}}$ with a strong seasonal cycle. The upwelling of 12 Sv of intermediate water in the Benguela region therefore seems unrealistic and in general the watermass transformations in the inverse model of Macdonald are very large. This makes the quantification of the cold and warm route in that model very uncertain.

3.3.3 Ganachaud's (2000) inverse model

Ganachaud (2000) used the global high-quality hydrographic data from the World Ocean Circulation Experiment to improve the estimates of the global circulation and heat fluxes. Ganachaud (2000) concluded that the vertical structure of the South Atlantic upper branch (in total 14 to 20 Sv) showed an equipartition between intermediate and thermocline flow. Because of the enhanced eddy field in the Benguela region he did not attempt to distinguish the sources of the South Atlantic upper branch of the THC.

Ganachaud used neutral surfaces (Jackett and McDougall, 1997; McDougall, 1987) to define isopycnal layer boundaries. We therefore also used neutral density to calculate layer transports in OCCAM. The lower interfaces of the thermocline and intermediate layer are respectively $\gamma_n = 26.8\,\mathrm{kg\,m^{-3}}$ and $27.72\,\mathrm{kg\,m^{-3}}$.

Ganachaud (2000) shows a dominant flow of thermocline water at 11°S and 45°S, while at 30°S the intermediate water dominates (Fig. 3.6). A strong formation of 11.5 Sv intermediate water is needed between 30° and the WOCE A11 section at 45°S. OCCAM shows an almost equal partition in the South Atlantic north of 30°S, and a dominant transport of intermediate water at 45°S. While Fig. 3.6b shows an equipartition between thermocline and intermediate water, in Fig. 3.5b thermocline water dominates; the relative importance of thermocline to intermediate water masses in composing the cross-equatorial NADW-return flow is therefore more a matter of layer definition rather than fundamental.

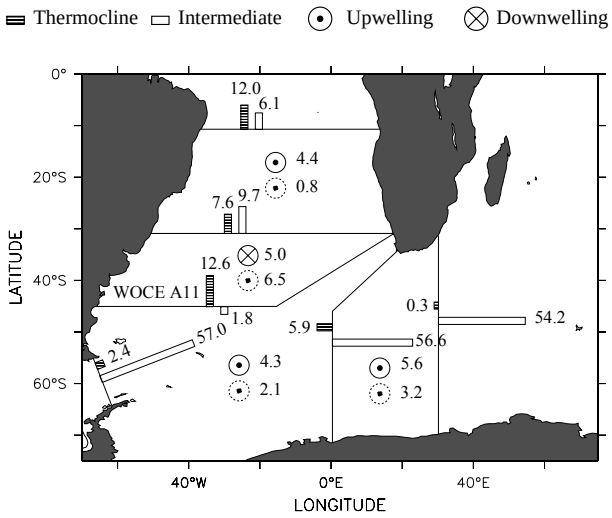

(a) Ganachaud (2000)

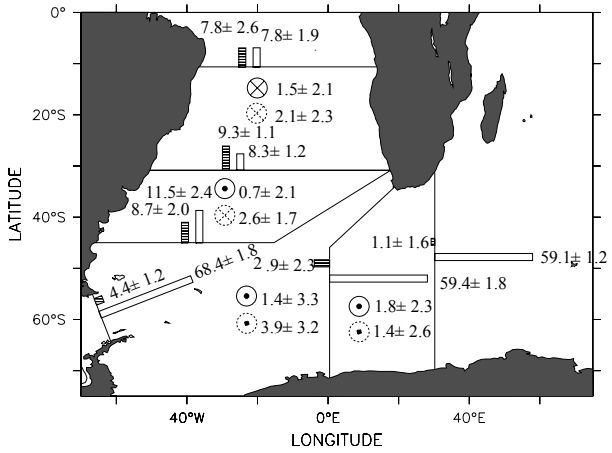

(b) OCCAM

Figure 3.6: *Comparison of the circulation scheme from Ganachaud (2000) to transports calculated at the same sections in OCCAM. Figure (b) also shows the standard deviation of the mass fluxes due to variability (all mass fluxes in Sv). (a) Ganachaud (2000) (b) OCCAM*

In contrast to the inverse models of Rintoul (1991) and Macdonald (1998), Ganachaud shows a large net westward flow of thermocline water at 0°E (5.9 Sv), even more than occurs in OCCAM (2.9 Sv). The model of Ganachaud is the first inverse model that suggests that the upper branch of the THC may have a significant contribution from the Indian Ocean. Nevertheless Ganachaud could not estimate the inflow from the Indian Ocean due to the large error bars.

To assess the effect of baroclinic variability we calculated the standard deviation of the mass fluxes in OCCAM from 5 day averages. The numbers have been added to Fig. 3.6b. Most of the fluxes agree within one standard deviation with the inverse model estimates. Only the intermediate flow at Drake Passage and across WOCE A11 differs strongly between the two models. The discrepancy at Drake Passage is probably due to the too strong ACC in OCCAM. The large difference at WOCE A11 between OCCAM and Ganachaud's inverse model also occurs for other inverse models using the nearby SAVE leg 4, and will be discussed separately in section 3.4.

Also, for all isopycnals which do not reach the surface the variability of the diapycnal fluxes is very large: in the OCCAM model the standard deviation is larger than the mean value. This suggests that it may not be possible to derive area-averaged diapycnal mass fluxes from inverse models based on one-time hydrographic sections.

Both the inverse model and the OCCAM model show some unrealistic features. There is 6.5 Sv upwelling of deep water between 30 and 45° S in the inverse model. At the depth of this isopycnal (900-1600m) κ_z is about zero (Polzin et al., 1997), and the κ needed for this transformation would be $6\,\mathrm{cm^2\,s^{-1}}$, which seems unrealistically high for an isopycnal layer well above the rough topography. The downwelling of 2.6 Sv intermediate water in OCCAM is also unrealistic, because it cannot be balanced by the diffusive flux and is thus associated with drift (see section 3.4.4).

In general, the transports in OCCAM across sections are similar to those in the inverse model solution from Ganachaud, except at the WOCE A11 section. The section-integrated fluxes even seem to suggest that the cold water route plays a more important role in OCCAM than in Ganachaud's inverse model, although the Lagrangian analysis shows a marginal contribution of the cold water route to the South Atlantic upper branch of the THC in OCCAM. As Ganachaud (2000) also noted, in the inverse model the error bars are too large to determine the relative importance of both routes.

3.3.4 Sloyan and Rintoul's (2001) inverse model

Sloyan and Rintoul (2001a) used an inverse model to determine the ocean circulation of the Southern Hemisphere. They improved the inverse model of Wunsch (1978) with the inclusion of observational datasets for air-sea fluxes of heat, freshwater and momentum and their implied water mass transformations (Sloyan and Rintoul, 2000). They concluded that the South Atlantic upper branch of the THC consisted mainly of intermediate water from Drake Passage. Like Ganachaud (2000), they also used neutral surfaces to define layer

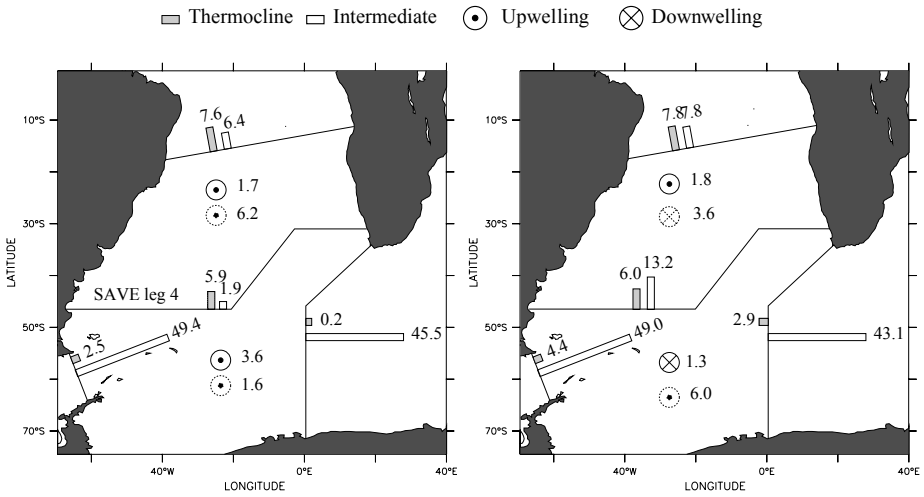

(a) Sloyan and Rintoul (2001a)

(b) OCCAM

Figure 3.7: *Comparison of the circulation scheme from Sloyan and Rintoul (2001a) to transports calculated at the same sections and with the same layers in OCCAM (all mass fluxes in Sv). (a) Sloyan and Rintoul (2001a) (b) OCCAM*

boundaries. The lower interfaces of the thermocline and intermediate layer are $\gamma_n = 26.8\,\mathrm{kg\,m^{-3}}$ and $\gamma_n = 27.6\,\mathrm{kg\,m^{-3}}$.

Sloyan and Rintoul show a dominant thermocline layer transport in the South Atlantic both at 14°S and at 30°-45°S (Fig. 3.7). The net northward transport increases northward in the South Atlantic, which indicates that a large source (6.2 Sv) for the upper branch of the THC is the upwelling of deep to intermediate water in the South Atlantic between 14°S and 45°S. To sustain this flux, assuming again that $\kappa_z \approx 0$ at this depth (900-1300m), a diapycnal diffusivity of $2.3\,\mathrm{cm^2\,s^{-1}}$ would be needed for this area. Compared to observations (Ledwell et al., 1998), this seems an unrealistic value for an isopycnal level in the interior ocean. Downwelling of intermediate water in the same area of the OCCAM model is not balanced by the diffusive flux and can be ascribed to drift (see section 3.4.4).

Sloyan and Rintoul (2001a) included enough light density layers to fully resolve the upper layers of the Agulhas Current. From the surface down to the $\gamma_n = 26.5$ isopycnal the inverse model shows a net inflow into the South Atlantic Ocean of 1.7 Sv. The OCCAM model shows a net inflow of 4.1 Sv. Both OCCAM and the inverse model show a net westward transport below the $\gamma_n = 26.5$ isopycnal. Although the net mass flux into the South Atlantic ocean increases if lighter density levels are considered, the net transport of thermocline water still underestimates the Agulhas leakage into the South Atlantic by 150%.

Almost all inverse model mass transports agree well to those of the OCCAM model within two standard deviations. However, the northward transport of intermediate water across the "South Atlantic Ventilation Experiment" (SAVE) leg 4, located between 30 and 45°S, is much larger in OCCAM than in the inverse model. This was also noted for Ganachaud's inverse model, and this discrepancy is therefore further discussed in section 3.4.2. The section-integrated transports between Africa and Antarctica largely conceal the contribution of the Indian Ocean to the South Atlantic upper branch of the THC in OCCAM.

3.3.5 The analysis of Gordon et al (1992)

Gordon et al. estimated transports across the SAVE leg 4 section, and determined the origins of these transports from CFM and salinity data. They concluded that most water in the South Atlantic upper branch of the THC consisted of water from the Indian Ocean. The South Atlantic partially converted thermocline water to intermediate water and transported mainly intermediate water to the North Atlantic. Gordon et al. (1992) defined the layers as a function of temperature: Thermocline water was defined as water warmer than 9°C and intermediate water colder than 9°C but shallower than 1500 db.

Gordon et al. (1992) explicitly calculated mass fluxes at only one hydrographic section, while tracers were used to estimate the sources of the various watermasses. Although Gordon et al. (1992) did not have explicit Lagrangian observations at their disposal, they combined their data to arrive at an almost Lagrangian circulation scheme. We therefore used a Lagrangian trajectory analysis to compare Gordon et al. (1992) to OCCAM. We backtraced both the northward flow at the Atlantic equator and the eastward flow at 20°E. As in Fig. 3.3c, we added the flow paths and mass fluxes of both runs, only now with the layers and sections from the study of Gordon et al.

Gordon et al. concluded that 60%-65% of the thermocline water in the Benguela Current originated from the Indian Ocean (Fig. 3.8), slightly less than in OCCAM (12.3 Sv/16.9 Sv=73%), the other 35%-40% recirculates in the South Atlantic subtropical gyre. They showed that the input of Indian Ocean water decreased with depth. They estimated that 50% of the intermediate water comes from the Indian Ocean. OCCAM shows only a slight decrease of Indian Ocean water input with depth: 5.9 Sv (5.9/8.6=69%) of the intermediate water comes from the Indian Ocean.

There is a large discrepancy in transport of intermediate water across SAVE leg 4 between the study of Gordon et al. and OCCAM. Gordon et al. estimated that the Malvinas Current transports 8 Sv northward across 47°S, while this is more than 40 Sv for OCCAM. The discrepancy is due to the fact that Gordon et al. excluded the flow of intermediate water south of the Subantarctic Front, located at 43°S. As 5.9 Sv thermocline water is supplied by modified intermediate water from the Malvinas Current in OCCAM, Gordon et al. probably exclude an important part of the circulation.

As a result, the large difference between Gordon et al. and OCCAM in the estimated flow toward the North Atlantic can be linked to the conversion of

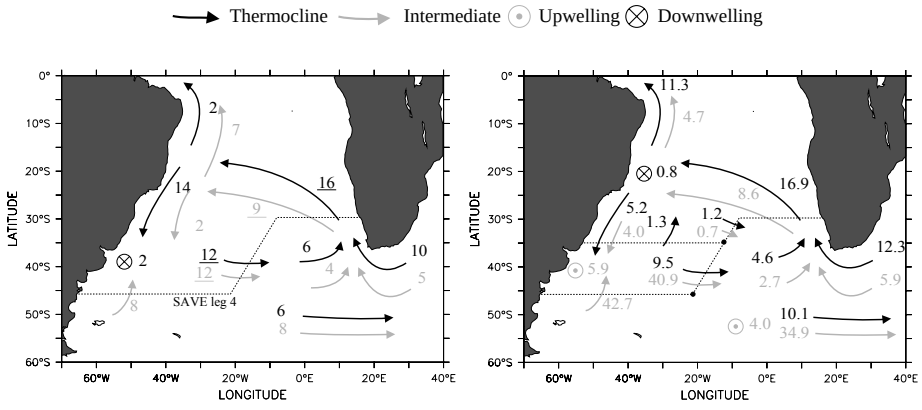

(a) Gordon et al. (1992)

(b) OCCAM

Figure 3.8: *Schematic circulation from Gordon et al. (1992) in comparison to the analogue scheme for OCCAM. Black arrows indicate the thermocline layer ($T > 9°C$), grey indicates the intermediate layer ($T < 9°C$, shallower than 1500 db). The dashed line in (a) is the hydrographic section SAVE leg 4 used for the study of Gordon et al. The fluxes across sections between • in (b) are calculated from two trajectory analyses (all mass fluxes in Sv). Underlined transports are calculated explicitly from hydrographic data, all other transports in Fig. (a) are estimated from chemical tracers and salinity. (a) Gordon et al. (1992) (b) OCCAM.*

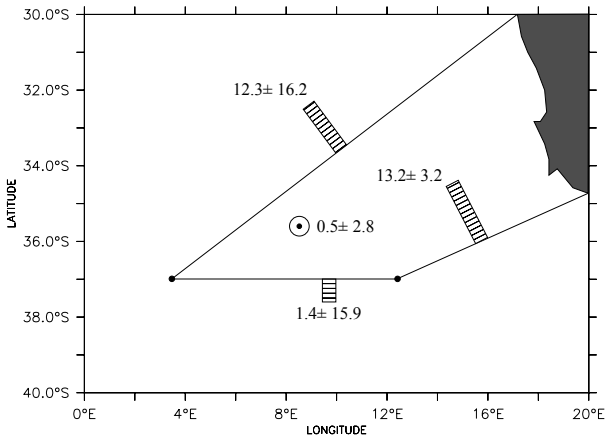

Figure 3.9: *Mass transports and their standard deviations for the thermocline layer in a subbox close to the South African coast.*

water masses in the Confluence zone. Gordon et al. assume a conversion of 2 Sv thermocline to intermediate water north of SAVE leg 4. A large southward flow of thermocline water in the Brazil Current closes the circulation loop of Gordon et al. This leaves only 2 Sv of thermocline water available to the North Atlantic. In OCCAM, the conversion of intermediate to thermocline water at the Brazil-Malvinas Confluence (5.9 Sv) together with a much smaller southward flow of thermocline water in the Brazil Current results in a much larger transport of thermocline water to the North Atlantic (11.3 Sv). This difference in watermass conversion (7.9 Sv) explains most of the difference in cross-equatorial thermocline water transport (9.3 Sv).

3.4 Discussion

3.4.1 Discrepancy between the section-integrated and the Lagrangian estimates of Agulhas leakage

In the previous section it is shown that the estimated leakage of thermocline water from the Indian Ocean to the South Atlantic Ocean from section-integrated transports at 0°E underestimates the actual leakage of thermocline water from the Indian Ocean. The reason for this discrepancy is that part of the westward flow connects with the cross-equatorial flow in the Atlantic, while the eastward flow is partly derived from upwelled intermediate and thermocline water that originates from Drake Passage.

On basis of the model results we have tried to devise a subbox in which the Agulhas leakage of thermocline waters could be better estimated. This estimate is possible if another hydrographic section would be carried out. We imagine a subbox defined by the WOCE A11 section and the section at 0°E of Fig. 3.6

starting from Africa and add a zonal section along 37°S (see Fig. 3.9). The net westward flow at the eastern section of this subbox in the annually averaged dataset above $\sigma_0 = 32.16$ is 13.2 Sv, further south the flow is eastward. The standard deviation of the leakage is 3.2 Sv. This is very close to the total Agulhas leakage of thermocline water estimated at 11.9 Sv in the Lagrangian calculation. This 11.9 Sv consists of both water that recirculates in the South Atlantic subtropical gyre and then flows back into the Indian Ocean and water that is transported toward the North Atlantic (see Fig. 3.2). The net westward transport of thermocline water, however, is very sensitive to the southern latitude of the subbox, as can be seen in Fig. 3.1. At the western section of this subbox the flux of thermocline water shows a much larger standard deviation of 16.2 Sv on a total amount of 12.3 Sv. This suggests that an inverse model with a one-time hydrographic section would be unable to quantify the flow across this section. To obtain a robust estimate the hydrographic survey should be carried out several times.

3.4.2 Discrepancies at the WOCE A11 and SAVE leg 4 sections

There is a large discrepancy (approximately 12 Sv, or 5 times the standard deviation) between the box model calculations in OCCAM and the inverse model calculations of the northward transport of intermediate water across SAVE leg 4 and WOCE A11 (Ganachaud, 2000; Gordon et al., 1992; Macdonald, 1998). The strong northward transport of intermediate water across these sections in OCCAM is due to intermediate water coming from Drake Passage. This water transforms to thermocline water within the South Atlantic north of the SAVE leg 4 and WOCE A11 sections, and crosses the same section in the opposite direction as thermocline water. The sections cross two regions of high eddy activity: the Benguela and Confluence regions. These regions cause enhanced variability in intermediate water transport. Both effects could influence the estimates of northward flow of intermediate water across these sections.

The net surface heat flux (NCEP/Reanalysis, Kalnay et al. (1996)) shows a strong heating of the waters in the Malvinas Current. If the intermediate water surfaces, it is transformed to lighter water masses there. The average position of the intermediate water outcrop in OCCAM is biased to the north (not shown). Due to this bias, the transformation of intermediate to thermocline water is located further northward in the OCCAM model than in the observations. This transformation itself has a strong seasonality. The pathway between its formation site and the point where the newly formed thermocline water crosses the WOCE A11 and SAVE leg 4 sections, however, is so long that a clear seasonality in the net fluxes across these sections has disappeared. In the observations the outcrop occurs only 4 months per year to the north of these sections and the path for the southward flowing thermocline flow to cross these sections is much shorter. It is expected that the observations would show a stronger seasonality in the net fluxes across the two sections. Both hydrographic surveys were taken in austral summer, just after the period when the transformation of intermediate

to thermocline water occurs to the north of these sections. As a result the net northward flow of intermediate water at these sections may be underestimated in the inverse models, while it is probably overestimated in OCCAM. The total amount of upwelled intermediate water involved can explain roughly 6 Sv or half of the difference between OCCAM and the inverse models (see Fig. 3.8b).

The Benguela and Brazil-Malvinas Confluence are both regions of high eddy activity. Both the SAVE leg 4 and WOCE A11 cross these two regions. The mass flux of intermediate water has a baroclinic variability of 2.5 Sv in OCCAM. If we assume that the mass fluxes estimated from a one-time hydrographic section will deviate on average one standard deviation, the variability could account for 20%-25% of the discrepancy.

Although we are not able to fully explain the discrepancies between the inverse models and OCCAM, a different representation of the water mass transformations in the Confluence area in OCCAM and the inverse models and the large baroclinic variability of the transports across these sections are probably the most important factors. The large discrepancy suggests that inverse models could do better avoiding these regions of high eddy activity and large water mass transformations. To obtain a better estimate of the net fluxes across sections in this region, more time-sampling is needed, with at least one survey during austral spring.

3.4.3 Bolus transport

In the calculation of Lagrangian trajectories we used the datasets with the bolus transport, while for the comparison to other studies we used the datasets without the bolus term. The bolus term is most important in the upper layers. As already noted, the bolus transport is merely a vertical redistribution of the horizontal fluxes. The vertical fluxes are calculated from the continuity equation, and are therefore directly linked to the divergence of the horizontal fluxes. As a result, the vertical transport is strongly influenced by the bolus term. Since the bolus effect is integrated along the path of the trajectory, its water mass transformation is very sensitive to the bolus term, even at locations without a large bolus effect (Drijfhout et al., 2003a). The influence of the bolus effect on section-integrated transports is only important at sections with strong eddy activity.

The effect of bolus velocity on the trajectory analysis can be seen in Fig. 3.10, showing the Lagrangian transport for the thermocline and intermediate water toward the North Atlantic across the sections denoted in the figure. The bolus term has a large impact on the water mass transformation of the Lagrangian trajectories, especially in the Southern Ocean. Water mass transformations are overestimated by roughly a factor of 2 if the bolus term is omitted.

The impact of the bolus effect on the section-integrated transports is also calculated, but not shown. The bolus term induces corrections typically in the order of 10% at most sections. Larger effects are found in regions of strong eddy activity. In the Agulhas region the westward flow of thermocline water into the South Atlantic increases from 2.9 to 4.5 Sv (+55%). The upwelling of

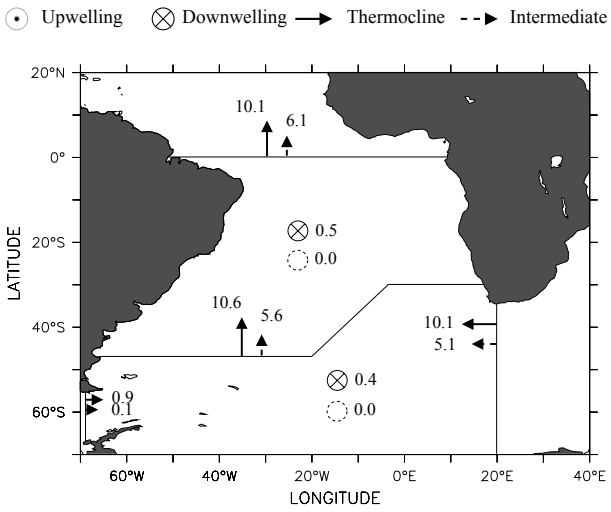

(a) Lagrangian with bolus

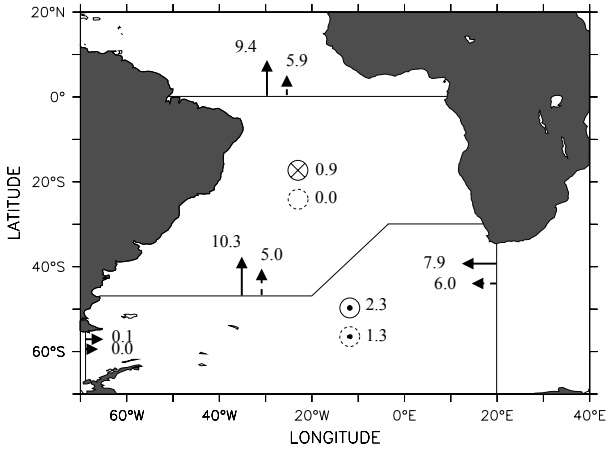

(b) Lagrangian without bolus

Figure 3.10: *Transports (in Sv) with Lagrangian trajectories in the thermocline and intermediate layer in the South Atlantic (thermocline to* $\sigma_0 = 26.8\,\mathrm{kg\,m^{-3}}$*, intermediate to* $\sigma_1 = 32.16\,\mathrm{kg\,m^{-3}}$*). (a) Lagrangian with bolus (b) Lagrangian without bolus.*

deep water in the Southern Ocean decreases from 6.0 to 3.5 Sv (-40%) if the bolus term is included.

3.4.4 Drift

As mentioned in the introduction, OCCAM is not in an equilibrium state. The model drifts away from the initial climatology, especially in the deeper layers (Lee et al., 2001). More NADW leaves the South Atlantic at 35°S than enters at the Atlantic equator, because NADW formation decreases with time. The consequence of drift for this study is that there is an apparent formation of NADW in the South Atlantic ocean. The drift has primarily an impact on the section-integrated fluxes used for the comparison to the various inverse model studies. In the Lagrangian analysis in OCCAM the drift hardly plays a role, since only the particles are included that leave the South Atlantic as thermocline or intermediate water. Those particles that have transformed to deep water are not considered.

While at 35°S 18.4 Sv thermocline and intermediate water enters the South Atlantic, only 13.8 Sv leaves the South Atlantic at the equator. The evaporation loss is negligible. The apparent formation of deep water is 4.6 Sv. The deep layer does not surface between the equator and 35°S. This downwelling is not balanced by a diffusive flux in OCCAM and is associated with drift.

The impact of drift on the various mass transports presented in the former section is twofold. Firstly, all time series of the mass transports may show long term trends and could be biased. We estimated the significance of long-term trends in the time-series of horizontal mass fluxes at different locations in the South Atlantic Ocean. With linear regression analysis we calculated the linear trend of the time-series. To estimate the significance of the trends, we first determined the decorrelation time-scales of the different time-series. These are generally around 100 days. The decorrelation time scale determines the degrees of freedom, needed to calculate the significance of the trend. We found that none of the time-series showed a statistically significant trend above the 90% confidence level. The drift in the mass fluxes as determined from linear regression analysis and its significance has been tabulated in table 3.1. We concluded that the time series of the horizontal mass fluxes show no significant effect of drift in the model.

Secondly, an imbalance may arise between the transports of a certain water mass across a section and the amount of upstream formation of that water mass. To close the balance spurious water mass formation is needed. There is no evidence that the transformation from intermediate to thermocline and vice-versa and the transformation from deep to intermediate water is biased in the model. When driven by internal diffusion the transformation rates are lower than what is estimated in the inverse models and there are no places where the transformation rates seem unrealistic. Only the transformation from intermediate to deep water in the South Atlantic, north of 35°S is unequivocally spurious.

	thermocline	significance (%)	intermediate	significance (%)
5°S	-3.8	71	-0.8	36
15°S	-4.0	87	-1.9	65
25°S	-2.0	75	-2.2	70
35°S	+1.7	70	-3.6	86

Table 3.1: *Table with the decline of the transports at different latitudes the South Atlantic during the total 3 year run of OCCAM (in Sv) calculated with linear regression analysis. The third and fifth and columns show the significance of the trend taking into account the decorrelation time-scales of the time-series.*

To estimate the impact on the section-integrated transport estimates in OCCAM of this water mass transformation, we calculated the Lagrangian trajectories that are converted to deep water. The associated horizontal fluxes at the different hydrographic sections are then subtracted from the section-integrated Eulerian fluxes. It appears that the general characteristics are unchanged. There is still a decrease of intermediate flow between Drake Passage and 0°E, and at SAVE leg 4 the northward flow of intermediate water is still dominant.

3.5 Conclusions

The exchange of water masses between the Pacific, Indian and North Atlantic Oceans that occur in the South Atlantic have been investigated with a path following technique in OCCAM. OCCAM clearly shows that 90% of the upper branch of the THC is derived from the inflow of Indian Ocean water into the South Atlantic. The Agulhas leakage takes place in the upper 2000 m, but 95% of all the transport that contributes to the upper branch of the Atlantic THC is found in the upper kilometer below the surface mixed layer. The partition between thermocline and intermediate water depends slightly on the density variable used, although in none of the cases intermediate water played a dominant role. Apart from 1 Sv that flows to the equator, all of the water from Drake Passage leaves the Atlantic sector of the Southern Ocean, south of Africa. More than 5 Sv of intermediate water from Drake Passage upwells to thermocline water while it traverses the Atlantic sector of the Southern Ocean. This upwelling of intermediate water takes place at the Brazil-Malvinas Confluence and eastward along 45°S and is probably driven by air-sea interaction. These results are at odds with conclusions drawn from section-integrated mass fluxes from various inverse model studies which show a dominance or significant influence of the cold water route.

However, the comparison of section-integrated mass fluxes across boxes from various inverse models and observational studies and OCCAM shows a reasonable agreement. In OCCAM the section-integrated mass fluxes suggest the dom-

inance of the cold water route as well, while the Lagrangian calculation clearly shows that the upper branch of the THC follows the warm water route. The reason for this discrepancy is that to the south of Africa the net mass flux consists of opposing, and in the thermocline layer nearly compensating, east- and westward flows. The westward thermocline flow connects with the cross-equatorial flow in the Atlantic. The eastward flow is mostly derived from upwelled intermediate and thermocline water that originates from Drake Passage. There is no indication that drift significantly corrupts the section-integrated transports in OCCAM. In general, the implied water mass conversions that are needed to close the budgets are smaller in OCCAM than in the various inverse models. Due to the high baroclinic variability, area-averaged diapycnal diffusivities cannot be estimated from inverse models using one-time hydrographic sections only.

There is a contradiction between OCCAM and the inverse models concerning the northward flow of intermediate water across the hydrographic surveys WOCE A11 and SAVE leg 4. OCCAM shows here a strong, northward flow of intermediate water, while the inverse models show almost no flow of intermediate water. In OCCAM the net northward flow of intermediate water has two sources. One source is the northward flow of intermediate water in the Malvinas Current, which is converted to thermocline water north of these sections, before it flows back across these sections. The second source is the intermittent leakage of intermediate water from the Indian Ocean. The intermittent leakage is hard to represent in a hydrographic survey, while the water mass transformations in OCCAM are located northward of what is observed. As a result, the flow of intermediate water across these sections strongly differs.

The bolus term is important for the water mass transformation of the trajectories. In the Eulerian fluxes the bolus term induces corrections, which are typically in the order of 10%. Especially in the ACC, upwelling of deep water into the intermediate layer decreases by 40% if the bolus term is not taken into account. Also, recirculations are well accounted for in the Lagrangian analysis and hard to distinguish in the Eulerian analysis.

The contribution to the South Atlantic upper branch of the THC from the Indian Ocean is not well resolved by the section-integrated mass fluxes. OCCAM and one inverse model show a larger net inflow of thermocline water from the Indian Ocean if layers with lower densities are considered, although in OCCAM the flow to the Atlantic equator is still underestimated by 150% compared to the Lagrangian analysis as long as the boxes are bounded by a whole section from South Africa to Antarctica.

Opposite currents across hydrographic sections are in principle separately resolved by inverse models. The transports of these separate currents, however, are mostly not or only marginally significant due to baroclinic variability and therefore hampers the determination of sources and destinations of water within these currents. This could prevent the determination of pathways within the world ocean from inverse model results.

Chapter 4

Water mass transformation and subduction

The transformation of water masses induced by air-sea fluxes in the South Atlantic is calculated with OCCAM and has been compared with several observational datasets. Air-sea interaction supplies buoyancy to the ocean at almost all density levels. The uncertainty of the estimates of water mass transformations is at least 10 Sv, largely caused by the uncertainties in heat fluxes. Further analysis of the buoyancy budget of the mixed layer in the OCCAM model shows that diffusion extracts buoyancy from the water column at all densities. In agreement with observations, water mass formation of surface water due to air-sea interaction is completely balanced by consumption due to diffusion. There is a large interocean exchange with the Indian and Pacific Oceans. Intermediate water is imported from the Pacific and light surface water is imported from the Indian Ocean. South Atlantic Central Water and denser water masses are exported to the Indian Ocean. The air-sea formation rate is only a qualitative estimate of the sum of subduction and interocean exchange. Subduction generates teleconnections between the South Atlantic and remote areas where these water masses re-emerge in the mixed layer. Therefore, the subduction is analyzed with a Lagrangian trajectory analysis. Surface water obducts in the South Atlantic, while all other water masses experience net subduction. The subducted Antarctic Intermediate Water and Subantarctic Mode Water re-emerge mainly in the Antarctic Circumpolar Current further downstream. Lighter waters re-emerge in the eastern Tropical Atlantic. As a result, the extratropical South Atlantic has a strong link with the Tropical Atlantic basin, and only a weak direct link with the extratropical North Atlantic. The impact of the South Atlantic on the upper branch of the thermohaline circulation is rather indirect: water is significantly transformed by air-sea fluxes and mixing in the South Atlantic, but most of it re-emerges and subducts again further downstream.

Accepted as Donners et al. (2004b)

4.1 Introduction

The South Atlantic basin has both strong, local air-sea interaction of heat and freshwater and large interocean exchange with adjacent basins. These air-sea interaction processes cause water mass transformations in the South Atlantic, with a possibly large remote impact on the ocean circulation in other basins (Karstensen and Quadfasel, 2002b; Sloyan and Rintoul, 2001a). Due to the thermohaline circulation (THC), the South Atlantic exports about 15 Sverdrup ($\mathrm{Sv} \equiv 10^6\,\mathrm{m}^3\,\mathrm{s}^{-1}$) of North Atlantic Deep Water (NADW). This requires a compensating flow toward the North Atlantic at other levels. The water masses that make up the return flow are modified within the South Atlantic basin, with potential impacts on the THC (Weijer et al., 2002). In this chapter we discuss the effects of mixing and surface buoyancy fluxes of heat and freshwater on the volume and buoyancy balance of the South Atlantic mixed layer. Furthermore, with Lagrangian analysis, the impact of water mass modification in the South Atlantic on the THC is estimated.

Two distinct methods are available to analyze the impact of mixed layer processes on the ocean circulation. First, the oceanic circulation induced by the thermal surface fluxes has been quantified by Walin (1982). He combined the ocean state with air-sea fluxes of heat to estimate the oceanic 'Hadley cell'. With an extension of this theory (Tziperman, 1986) net sources and sinks of specific water masses can be calculated from the combination of heat and freshwater fluxes and sea surface salinity and temperature. The change of density of seawater due to surface fluxes is called water mass transformation (WMT). The convergence of water within a specific density interval due to WMT is called water mass formation. Water mass transformation rates have been calculated for the North Atlantic (Speer and Tziperman, 1992) and the global ocean (Speer et al., 1995).

Second, a kinematic approach can be used to estimate the exchange between the mixed layer and the underlying stratum, and to assess the impact of surface processes on the internal ocean. In winter, the mixed layer deepens, and, consequently, mass is transferred from the ocean interior into the mixed layer. This process, caused mostly by turbulent mixing at the mixed layer base, is called entrainment. Water masses are transformed due to air-sea fluxes and mixing in the surface mixed layer. When the upper ocean restratifies in spring, the mixed layer shallows. Detrainment is the process where water masses leave the turbulent mixed layer and enter the interior ocean. After detrainment, the water masses move largely adiabatically within the interior ocean. Subduction is a fraction of the detrained mass flux: it refers to that part of the detrained water mass that is not entrained in the next winter (Cushman-Roisin, 1987). The opposite process is sometimes referred to as obduction. The physics involved in subduction and obduction, however, are completely different.

In a closed basin and in steady state, the mixed layer is in a balance between transport across the winter mixed layer base, the water mass formation by air-sea fluxes, and mixing. This mixing within and across the winter mixed layer has been studied extensively by Nurser et al. (1999). In general, mixing counteracts

water mass transformation by air-sea fluxes.

Marshall et al. (1999) combined WMT and subduction into one theoretical framework and analyzed the total mass balance of the water volume delimited by the winter mixed layer depth. It was shown that mixing is important everywhere, and that subduction and WMT can not easily be equated. Karstensen and Quadfasel (2002a) compared WMT rates to subduction rates for the three ocean basins of the southern hemisphere using observational and reanalysis data. They concluded that 13 Sv of newly formed water within the South Atlantic mixed layer is exported toward the Indian Ocean before it subducts into the interior.

Most studies on subduction and WMT concentrate on the North Atlantic or show a globally averaged picture. The aim of this study is to show WMT and subduction within the South Atlantic. The South Atlantic is a data sparse region and we therefore compare WMT rates deduced from different datasets. This gives an indication of the errors involved in the air-sea flux estimates across the South Atlantic (Sterl, 2001). From observational datasets of Ekman pumping and wind stress, Lagrangian trajectories can be calculated via the Sverdrup balance. These can be used to calculate subduction and obduction rates (Qiu and Huang, 1995). This approach, however, is not easily implemented for the Southern Hemisphere since it is not straightforward to apply the Sverdrup balance to the Antarctic Circumpolar Current (Gnanadesikan and Hallberg, 2000). Therefore, we study subduction in more detail with a Lagrangian trajectory analysis of the OCCAM model. This enables us to estimate the influence of subduction in the South Atlantic on the global ocean. A detailed buoyancy analysis of the mixed layer shows the relative importance of WMT, mixing, interocean exchange, and subduction.

The chapter is set up as follows: the next section introduces the theoretical framework of WMT and subduction. In sections 4.3 and 4.4 the water mass transformations calculated from different datasets are discussed. Section 4.5 shows the buoyancy budget of the South Atlantic for the OCCAM model. Section 4.6 treats the Lagrangian view of the water subducted within the South Atlantic. Sections 4.7 and 4.8 contain the discussion and conclusions.

4.2 Theoretical framework

Air-sea fluxes of heat and freshwater cause a change of buoyancy (or, equivalently, density) of ocean water directly at the surface. Due to advection and mixing processes in the surface mixed layer, this buoyancy change is carried further down into the interior ocean. The dynamical balance of the ocean determines how the ocean water is carried further below the mixed layer.

The volume and buoyancy balances of the mixed layer connect the kinematic and thermodynamic processes within the mixed layer. In this section we show the links between the different processes of surface forcing of heat and freshwater fluxes, the subduction process, the exchange of water with adjacent ocean basins, and diffusion.

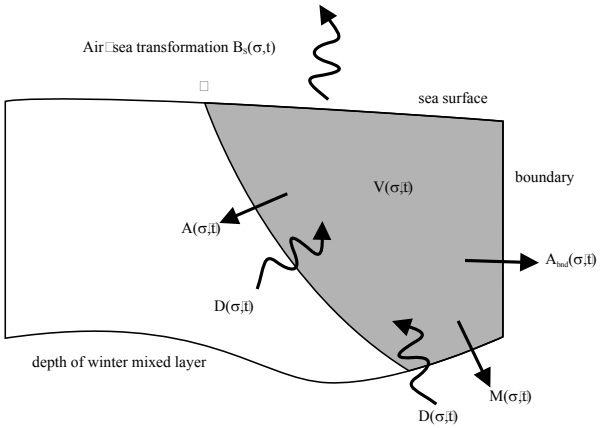

Figure 4.1: *Schematic diagram which shows the relation between air-sea transformation, diffusion and subduction within an open ocean region. The grey area is bounded by the horizontal region R, the sea surface, the isopycnal σ and the depth of the winter mixed layer. The arrows point in the direction for which the quantity is defined positive.*

In Fig. 4.1 the framework is drawn which shows the relation between air-sea transformation, subduction and mixing. The framework is based on both Marshall et al. (1999) and Walin (1982). The following symbols are used throughout the chapter:

σ	potential density anomaly $[\,\mathrm{kg\,m^{-3}}]$
t	time [s]
R	region of interest
$H(x,y)$	deepest mixed layer within R [m]
$V(\sigma,t)$	volume of water with a density lower than σ, bounded by the region of interest, the deepest mixed layer, and the sea surface $[\mathrm{m^3}]$
$M(\sigma,t)$	volume flux from $V(\sigma,t)$ into the interior ocean $[\,\mathrm{m^3\,s^{-1}}]$
$A_{\mathrm{bnd}}(\sigma,t)$	volume flux from $V(\sigma,t)$ to adjacent basins $[\,\mathrm{m^3\,s^{-1}}]$
$A(\sigma,t)$	diapycnal volume flux across isopycnal σ within $H(x,y)$, positive for flow towards increasing σ $[\,\mathrm{m^3\,s^{-1}}]$
$B(\sigma,t)$	total buoyancy loss of $V(\sigma,t)$ $[\,\mathrm{kg\,s^{-1}}]$
$B_s(\sigma,t)$	buoyancy loss through the sea surface of $V(\sigma,t)$ $[\,\mathrm{kg\,s^{-1}}]$
$D(\sigma,t)$	diffusion across bounding surface of $V(\sigma,t)$ $[\,\mathrm{kg\,s^{-1}}]$

The potential density anomaly σ is referenced to the surface pressure. Note that V, A_{bnd}, M, B, B_S, and D are quantities integrated over all densities lower than σ, while A is a volume flux across the isopycnal σ. The volume balance of V can be stated as follows:

$$\frac{\partial V(\sigma,t)}{\partial t} = -A(\sigma,t) - A_{\mathrm{bnd}}(\sigma,t) - M(\sigma,t) \tag{4.1}$$

The freshwater loss due to evaporation and precipitation in the South Atlantic of the OCCAM model is 0.5 Sv and can be neglected for the volume balance. However, evaporation and precipitation is included in the buoyancy forcing $F(\sigma, t)$. If we assume that the ocean is in a steady state and that the transport through the boundaries A_{bnd} is small or known, the net advective diapycnal flux $A(\sigma, t)$ can be equated to $M(\sigma, t)$. The volume flux $M(\sigma, t)$ represents the annual mean mass flux across the deepest mixed layer:

$$M(\sigma, t) = M_{\mathrm{Eul}}(\sigma, t) = \iint [-\mathbf{u}_H \cdot \nabla H(x, y) - w_H] \, \mathrm{d}x \, \mathrm{d}y \tag{4.2}$$

with $\mathbf{u}_H$ the two-dimensional annual mean velocity field at the depth H. The vertical velocity at depth H is represented by w_H. The two-dimensional integral includes all locations with a density lower than σ. Because M is the volume flux through a fixed surface, it is a Eulerian quantity. The transformation caused by mixing below the mixed layer in summer is assumed to be small in comparison to the vigorous mixing within the mixed layer and the entrainment. Therefore we took the deepest mixed layer depth as a control volume. Note that M_{Eul} could be both positive and negative. The sum of the fluxes through the winter mixed layer base from V is defined as the Eulerian subduction S_{eul}. The sum of the fluxes into V is defined as Eulerian obduction O_{Eul}. Equation 4.2 has been used by Marshall et al. (1993) in their data analysis of net subduction in the North Atlantic.

The subduction process, however, is a quantity with a Lagrangian definition (Cushman-Roisin, 1987). Water is subducted if it does not reenter the mixed layer during deepening of the mixed layer in the following year. We denote this Lagrangian quantity with S_{Lag}. Water that enters the mixed layer, after remaining below the mixed layer for more than one year, has been obducted (O_{Lag}). To determine if water particles resided longer than one year within the interior ocean, a Lagrangian trajectory calculation is needed. The Lagrangian net subduction M_{Lag} is the sum of Lagrangian subduction and obduction.

The Eulerian and Lagrangian subduction are in general not equal. Not all the water that enters V through the mixed layer base has resided below the mixed layer for more than one year, and some of the water that leaves V could reenter the mixed layer within a year. Another discrepancy is the change in time of the ocean circulation. While the Eulerian subduction is an annually averaged quantity across a fixed surface, the Lagrangian subduction depends on the time-varying ocean circulation along the path after the water has left the mixed layer.

The volume balance of the control volume V relates the diapycnal fluxes $A(\sigma, t)$ to the fluxes through the side and bottom boundaries of V. So far, only kinematics have been used to derive this relation. However, the diapycnal volume flux $A(\sigma, t)$ is closely connected to the buoyancy budget of V. To show this relation, we first write down the buoyancy budget (or equivalently, mass budget) for V:

$$\int_{-\infty}^{\sigma} \sigma' \frac{\partial^2 V(\sigma', t)}{\partial \sigma' \partial t} \, \mathrm{d}\sigma' = -\sigma A(\sigma, t) - \int_{-\infty}^{\sigma} \sigma' \frac{\partial \{A_{\mathrm{bnd}}(\sigma', t) + M(\sigma', t)\}}{\partial \sigma'} \, \mathrm{d}\sigma' + B(\sigma, t) \tag{4.3}$$

The buoyancy balance (eq. 4.3) has a similar form as the volume balance (eq. 4.1), because mass fluxes are equal to volume fluxes times the density. The quantity σA is the advective diapycnal mass flux across the isopycnal σ. The other terms, V, A_{bnd} and M need to be integrated for all densities lower than σ. The buoyancy term B appears in the buoyancy budget and not in the volume budget, because the density of water is changed without a volume flux. If we calculate the derivative to σ of both the volume (eq. 4.1) and the mass balance (eq. 4.3), we get:

$$\frac{\partial^2 V}{\partial \sigma \partial t} = -\frac{\partial A}{\partial \sigma} - \frac{\partial A_{\mathrm{bnd}}}{\partial \sigma} - \frac{\partial M}{\partial \sigma} \tag{4.4}$$

$$\sigma \frac{\partial^2 V}{\partial \sigma \partial t} = -A - \sigma \frac{\partial A}{\partial \sigma} - \sigma \frac{\partial A_{\mathrm{bnd}}}{\partial \sigma} - \sigma \frac{\partial M}{\partial \sigma} + \frac{\partial B}{\partial \sigma} \tag{4.5}$$

Multiplying equation 4.4 by σ and subtracting from equation 4.5 gives:

$$A(\sigma, t) = \frac{\partial B(\sigma, t)}{\partial \sigma} \tag{4.6}$$

The total non-advective supply of buoyancy to V can be written as follows:

$$B(\sigma, t) = -\int_{V(\sigma,t)} \nabla \cdot \mathbf{N}_\sigma \, \mathrm{d}V \tag{4.7}$$

with $\mathbf{N}_\sigma$ the non-advective flux of potential density. If we ignore internal sources of buoyancy like cabbeling, $B(\sigma, t)$ can be calculated from the integral of the buoyancy flux across the boundary of $V(\sigma, t)$. This buoyancy supply can be divided into two distinct components: internal diffusion processes $D(\sigma, t)$ and buoyancy fluxes through the surface $B_S(\sigma, t)$:

$$B = B_s - D \tag{4.8}$$

$$D = \iint \mathbf{N}_\sigma \cdot \mathbf{n} \, \mathrm{d}A_1 \tag{4.9}$$

$$B_S = \iint \left[\frac{\alpha}{c_w} Q + \rho_0 \beta S (E - P) \right] \mathrm{d}A_2 \tag{4.10}$$

with A_1 and A_2 the surfaces that enclose the control volume $V(\sigma, t)$ respectively below and at the sea surface. The coefficients α and β represent the thermal expansion and haline contraction of sea water. The quantities Q and

$(E - P)$ are the heat and freshwater fluxes from the atmosphere to the ocean. The quantity c_w is the specific heat of seawater and S is the sea surface salinity. The transformation of seawater due to air-sea fluxes is separately defined as F:

$$F(\sigma, t) = \frac{\partial B_S(\sigma, t)}{\partial \sigma} \tag{4.11}$$

The diapycnal fluxes $A(\sigma, t)$ are difficult to measure in the ocean. However, the diapycnal fluxes within the mixed layer can be eliminated from the balance if we combine eqs. 4.1 and 4.6:

$$\frac{\partial V}{\partial t} = -F + \frac{\partial D}{\partial \sigma} - A_{\text{bnd}} - M \tag{4.12}$$

Water masses in oceanography are normally labeled by a specific density interval. To analyze the balance of a water mass defined by two isopycnals σ_1 and σ_2, we have to subtract the integrated balance for these two isopycnal levels:

$$\begin{aligned}\frac{\partial [V(\sigma_2) - V(\sigma_1)]}{\partial t} &= -F(\sigma_2) + F(\sigma_1) + \\ \frac{\partial [D(\sigma_2) - D(\sigma_1)]}{\partial \sigma} &- A_{\text{bnd}}(\sigma_2) + A_{\text{bnd}}(\sigma_1) - M(\sigma_2) + M(\sigma_1)\end{aligned} \tag{4.13}$$

In section 4.4 we compare the transformation due to air-sea fluxes $F(\sigma, t)$ calculated from different datasets. The volume budget of V (Eq. 4.12) is described in section 4.5, where we show the importance of the different quantities B_S, D, M, A_{bnd}, and the drift of the control volume V.

4.3 Other datasets used: DaSilva, NCEP, ECCO, and ERA40

To assess the uncertainty of WMT rates, we selected different datasets for comparison to OCCAM. We use a compilation of the Comprehensive Ocean-Atmosphere Dataset, a dataset based on in-situ observations from ships and parameterizations of the air-sea interaction (henceforth DaSilva) (Da Silva and Young, 1994). We used a monthly climatology for the period from 1945 to 1993. It is known that fields of observed air-sea fluxes are uncertain due to the limited number of observations available, especially for the Southern Hemisphere (Sterl, 2001). Furthermore, the European Center for Medium-Range Weather Forecasts 40 year Re-analysis (ERA40) (Simmons and Gibson, 2000) and National Centers for Environmental Prediction Reanalysis (NCEP) (Kalnay et al., 1996) data have been used. Both datasets are atmospheric reanalysis products. The ECCO dataset has been derived from the project Estimating the Circulation and Climate of the Ocean (ECCO). We used the monthly data from the 2° adjoint model (Stammer et al., 2000). For both reanalysis products and the ECCO dataset we used the period from 1992 to 1997, which overlaps the period that has been used for the forcing of the OCCAM model (1993 to 1995).

Both reanalysis products and the DaSilva dataset have no data on the SSS. To calculate the WMT as a function of density, however, SSS is a necessary variable. We used the monthly SSS climatology from the World Ocean Atlas 1998 (Boyer et al., 1998) for these datasets. For the ocean models OCCAM and ECCO we used the model output of SSS to calculate the WMT rates.

4.4 Comparison of water mass transformations

To analyze the complete volume and buoyancy balance of the South Atlantic (eq. 4.12), we use the OCCAM model, which is described in chapter 2. The use of an ocean model ensures that all terms can be calculated in a consistent manner. Although separate terms of the volume balance can be estimated from observations, the errors are undoubtedly significant as observations in the Southern Ocean outside the summer season are sparse. To assess the realism of this model, we first compare the WMT $F(\sigma)$ of different datasets (see eq. 4.11). This gives an idea of the uncertainty of the WMT, and of all processes that are linked to it through the volume and buoyancy balance.

A density interval of $0.1\,\mathrm{kg\,m^{-3}}$ is used for the calculation of the transformation rate for all datasets. We use the region located from the Atlantic equator to 60°S and from 70°W to 20°E. The WMT $F(\sigma)$ for all datasets is plotted in Fig. 4.3. A positive transformation denotes a densification of water masses due to air-sea interaction. The gradient of the transformation ($\partial F/\partial\sigma$) curve denotes the amount of water mass that is formed within that particular density interval. To simplify the analysis, we also consider 6 water masses for the South Atlantic basin, based on observational studies. The definitions are tabulated in Table 4.1. The formation rates for the different water masses are tabulated in Table 4.2. The surface water (SW) consists mainly of Salinity Maximum Water (Blanke et al., 2002a), that subducts in the western tropical Atlantic. Water masses with a density below $\sigma = 24.2$ are formed in the equatorial South Atlantic, primarily north of 5°S. According to Tomczak and Godfrey (1994), part of the light South Atlantic Central Water (lSACW) is Indian Central Water (ICW) brought into the South Atlantic Ocean by Agulhas Current intrusions because the T-S curves of lSACW and ICW are virtually the same. The South Atlantic Subtropical Mode Water (SASTMW) consists of a light variety of subtropical mode waters (Provost et al., 1999), formed mainly in the Brazil Current overshoot, and 13°C mode water, presumably formed by mixing in Agulhas Rings (Tomczak and Godfrey, 1994). The Subantarctic Mode Water (SAMW) is formed along the Subantarctic Front (SAF), located between 45°S and 50°S. South Atlantic Central Water (SACW) is a combination of the water masses lSACW, SASTMW and SAMW. The Antarctic Intermediate Water (AAIW) is characterized by a salinity minimum and is formed in the eastern South Pacific and western South Atlantic (Stramma and England, 1999). The oceanic heat gain along the SAF at 50°S converts AAIW into SAMW. The Deep water (DW) is defined as the water mass below the AAIW. The locations of the density fronts agree closely during winter, but there is a northward bias during

Water mass	Definition
Surface water	$\sigma < 25.5$
lSACW	$25.5 < \sigma < 26.2$
SASTMW	$26.2 < \sigma < 26.6$
SAMW	$26.6 < \sigma < 27.0$
AAIW	$27.0 < \sigma < 27.3$
DW	$\sigma > 27.3$

Table 4.1: *Table with the different water masses and their definition in terms of the density interval.*

summer south of 40° S in the OCCAM dataset.

Figure 4.2 shows the temperature-salinity diagram for three different locations in the South Atlantic for both the OCCAM model and the Levitus climatology. The vertical salinity-gradient is weakened in the OCCAM model; while the AAIW at 30°S is too saline, the SW is too fresh. The location of the 34.2 psu contour compares well with observations (Tomczak and Godfrey, 1994). The contours between 34.3 and 34.5 psu, however, are located too far south. This discrepancy can be explained by the northward bias of density fronts in the ACC, which causes an increased oceanic heat gain and evaporation. These effects compensate each other in the buoyancy flux. Further northward the warm and salty bias of AAIW decreases and at 10°S it has almost diasppeared in OCCAM (see Fig. 4.2). The salinity minimum is located deeper than 1100 m in the Brazil Current and the Agulhas ring corridor in the south-east Atlantic. Especially the latter may point at an overestimation of the impact of Agulhas leakage on the South Atlantic in OCCAM. This might also be a reason why the salinity minimum is too salty in the extratropical South Atlantic. The SACW is slightly too fresh, especially the lSACW. This could be caused by an underestimation of evaporation in the extra-tropical Atlantic Ocean and a strong influx of fresher central water from the Indian Ocean. Also, the Agulhas retroflection extends too far west and the Brazil-Malvinas Confluence front too far south in the model. The relaxation to the Levitus dataset corrects these model biases with a spurious cooling and freshwater forcing. This might explain the cold and fresh bias of the lighter water masses in OCCAM. In general, however, there is a good qualitative agreement of the South Atlantic mode waters between OCCAM and Tomczak and Godfrey (1994).

The different datasets show a similar qualitative behaviour, although the differences in formation rates are large. For light SW ($\sigma < 24.0$) the transformation is negative, while at the isopycnal level that separates SW and lSACW the transformation is positive (i.e. toward higher density) for all datasets. At the isopycnal that separates the SAMW and AAIW all datasets reach a second minimum transformation, i.e. water gains buoyancy. The NCEP dataset shows a large consumption rate of SW in comparison to the other datasets. Although the seasonal cycle of the WMT of the NCEP and ERA40 datasets

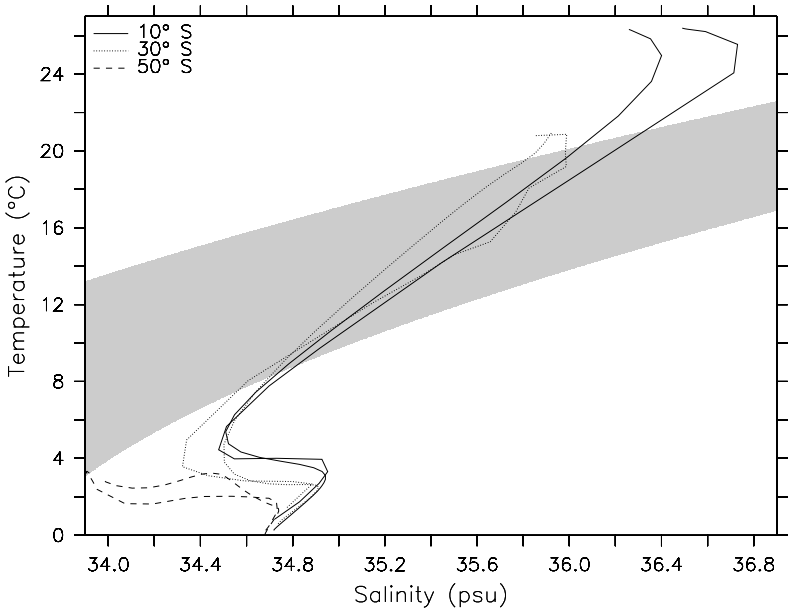

Figure 4.2: *The temperature-salinity diagram for three different latitudes (all at 25° W) in the South Atlantic. The thin lines are annual mean data from the OCCAM model, the thick lines are annual mean data from the Levitus climatology. The density range for the water mass SACW is indicated by the grey area.*

Water mass	OCCAM	ECCO	ERA40	NCEP	DaSilva
SW	-0.7± 6.8	-1.3± 7.0	-1.8 ± 5.4	-8.0 ± 3.4	-3.6
lSACW	5.6 ± 7.0	4.6 ± 7.3	-7.8 ± 4.9	6.8 ± 3.4	-0.9
SASTMW	6.0 ± 0.7	6.1 ± 4.7	10.0± 1.8	10.7 ± 3.8	6.6
SAMW	1.5 ± 0.8	2.4 ± 4.8	13.1 ± 3.0	11.9 ± 3.7	14.0
AAIW	-4.2 ± 0.5	-7.7 ± 3.2	-12.2± 1.0	-16.0 ± 1.4	-10.2
DW	-8.2 ± 1.1	-4.1 ± 0.8	-1.3 ± 0.7	-5.3 ± 1.4	-5.9

Table 4.2: *Table with formation and destruction rates for different models (in Sv, positive values denote water mass formation). For the datasets the standard deviation of the annual water mass formation is calculated.*

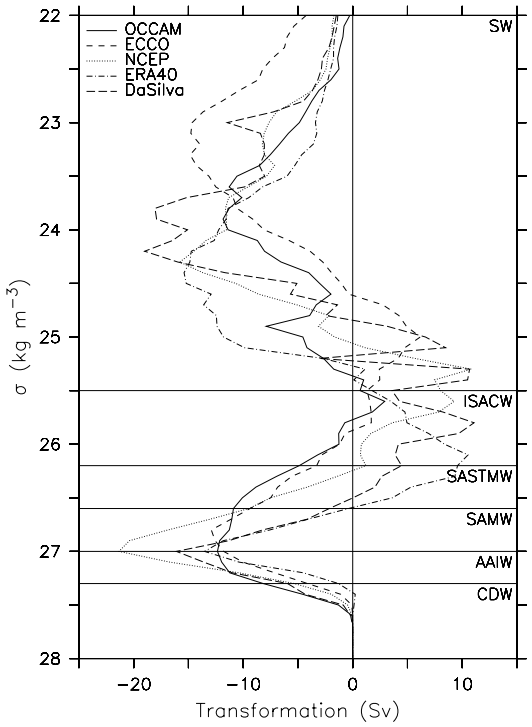

Figure 4.3: *Water mass transformation curves $F(\sigma)$ for the different air-sea flux datasets (in Sv). Positive values denote a transformation toward higher densities.*

agree reasonably well at this isopycnal level, the NCEP dataset is lower during 8 months. The WMT rates at the isopycnals that divide lSACW, SASTMW, SAMW and AAIW agree closely for the ERA40 and NCEP datasets in summer. However, the WMT rates for the ERA40 dataset are consistently higher due to the stronger surface cooling in winter. The formation of SAMW is underestimated in both ocean-only models OCCAM and ECCO. In the OCCAM model this can be attributed to the overall weak surface forcing and its small seasonal cycle. In the ECCO model the cooling of lSACW and SASTMW is too weak in winter, while in summer the warming of AAIW is too weak in comparison to the reanalysis datasets. The datasets agree on whether there is a net formation or consumption of a particular water mass in the South Atlantic, except for lSACW. The formation rate of lSACW is uncertain due to the strong transformation of SW into lSACW in the NCEP dataset and the strong transformation of lSACW into SASTMW.

The quantitative differences in WMT rates between the datasets are approximately 10 Sv. Discrepancies could be caused either by interannual variability, uncertainties in the numerical evaluation of $F(\sigma)$, or uncertainties in the observations of heat and freshwater fluxes. The interannual variability in transformation rates has a standard deviation of 3 to 4 Sv and increases with density. The accuracy of the calculation method is determined by changing the density interval of the calculation of WMT. The accuracy decreases slightly with density and is on average 2 Sv. The interannual variability together with the numerical accuracy, however, cannot explain the discrepancy in WMT rates of 10 Sv between the different datasets. This discrepancy must therefore be caused by uncertainties in the observed heat and freshwater fluxes. For SW and lSACW, the uncertainties in the WMT due to heat fluxes (10 Sv) are larger than the uncertainties in the WMT due to freshwater fluxes (5 Sv). Although the uncertainty of the freshwater fluxes themselves is larger than that of the heat fluxes, the transformation rate due to heat fluxes is stronger than the transformation due to freshwater fluxes, which explains the larger uncertainty in the transformation rate. For the other water masses the uncertainty of the WMT due to heat and freshwater fluxes is similar. There is no quantitative agreement between the different datasets, assuming that the differences should be within two standard deviations.

Even though the OCCAM model uses a relaxation condition for the SST and SSS, the transformation (F) and formation ($\partial F/\partial\sigma$) rates for water masses other than SW are in good agreement with the ECCO model with data assimilation. However, the formation rates in OCCAM are weaker than for the NCEP, ERA40 and Da Silva datasets. The OCCAM model has a broader and less strong transformation minimum (or buoyancy gain) at the isopycnal that divides SAMW and AAIW. Although the surface forcing in OCCAM could be improved, we are confident that the air-sea fluxes in OCCAM have sufficient quality to be used for this study. To be able to make a robust and quantitative estimate of transformation and formation rates, the observational dataset of air-sea fluxes needs to be improved within the South Atlantic, especially for the heat fluxes.

4.5 Buoyancy budget

In the previous section we showed that all datasets agree on the qualitative structure of the WMT rate due to air-sea interaction within the South Atlantic. In this section we study the total balance of the winter mixed layer in the South Atlantic for the OCCAM model. In the buoyancy budget of the winter mixed layer, five processes play an important role: air-sea interaction, trend, subduction, mixing, and interocean exchange (see Eq. 4.12). The total balance, however, is not easily determined from observations. Karstensen and Quadfasel (2002a) estimated the water mass transformation rates due to air-sea fluxes and subduction rates from observations for the three separate basins in the Southern Ocean. With these calculations the interocean exchange within the mixed layer (A_{bnd}) between the different basins in the Southern Ocean was estimated. However, they neglected mixing processes. With the OCCAM model we studied the volume balance in more detail. The interocean exchange A_{bnd}, Eulerian subduction M_{Eul}, and the trend in the volume of different water masses $\partial V/\partial t$ were determined explicitly, and the residual transformation must be caused by mixing processes $\partial D/\partial\sigma$.

We tried to calculate the diffusion explicitly, but we could not explain the residual of balance Eq. 4.12 for the OCCAM model. We assume that the explicit calculation of diffusion from seasonally averaged datafiles does not resolve the diapycnal mixing induced by internal waves that are generated by the high-frequency wind-forcing (Lee et al., 2001). There was, however, a qualitative agreement. For this manuscript we used the residual of the mass balance for the diffusive term.

The OCCAM model has no explicit mixed layer scheme. Hence the mixed layer depth needs to be calculated from other properties. As a criterion we used the depth at which the density is $0.1\,\mathrm{kg\,m^{-3}}$ higher than the sea surface density. For this calculation the seasonal mean fields of temperature and salinity have been used. Because seasonal mean fields smooth out the extreme values within a season, the data were corrected with an interpolation scheme described by Killworth (1996). In Fig. 4.4, the deepest winter mixed layer depth is drawn together with the isopycnals separating the outcrops of the different water masses (Table 4.1). Karstensen and Quadfasel (2002a) showed the winter mixed layer depth calculated with a similar density criterion ($0.125\,\mathrm{kg\,m^{-3}}$) from the World Ocean Atlas 98 dataset, which has a quantitative agreement to the maximum mixed layer depth in OCCAM in regions with enough observations. South of 35°S and far away from the coastlines, the in-situ data in winter are sparse which makes a quantitative comparison very uncertain. Winter mixed layers are deep in the northern part of Drake Passage and in the Malvinas Current; winter mixed layers are shallow in the Cape basin and Brazil-Malvinas Confluence regions, due to warm surface waters injected from the Agulhas Current and the Brazil Current, respectively. Talley (1999) used the depth of 95% oxygen saturation as another proxy for the winter mixed layer depth. The agreement with the OCCAM model is qualitative. Deep mixed layers (> 150 m) are found at the 0° meridian between 30°S and 50°S and in the Cape basin close to the

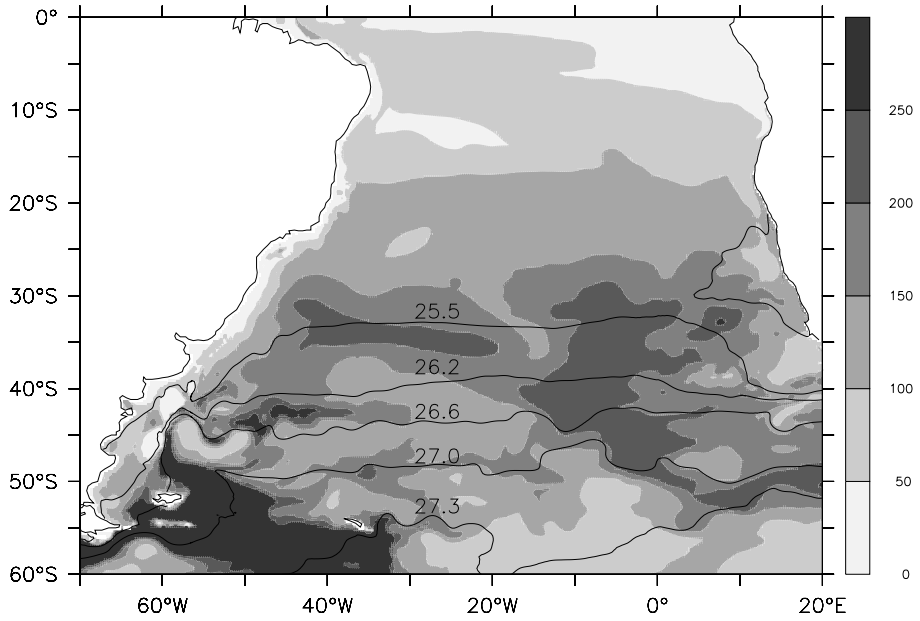

Figure 4.4: *Maximum mixed layer depth in OCCAM (in m). The surface isopycnals that divide the outcrops of the different water masses (see Table 4.1) are overlayed.*

African continent winter mixed layers are shallow. The Brazil-Malvinas Confluence is a region of shallow mixed layers flanked with deep mixed layers.

We have drawn the transformation induced by each process as a function of density for the OCCAM model in Fig. 4.5. Figure 4.5a shows the balance between buoyancy input at the ocean surface (F), diffusion ($-\partial D/\partial\sigma$), trend ($\partial V/\partial t$) and the exchange with neighbouring oceans and the interior ($M_{Eul} + A_{bnd}$). In Fig. 4.5b the processes responsible for the exchange with the interior and adjacent oceans are drawn separately. Negative values denote a volume flux into $V(\sigma, t)$. The decrease of the transformation over a density interval denotes a convergence of a water mass within that density range. The same results are summed for the different water masses in Fig. 4.6. The air-sea transformation F is negative at almost all density levels, which indicates a buoyancy gain for most water masses in the South Atlantic. The trend is a small contribution to the total buoyancy balance, but it is statistically significant. However, the average volume change of the water masses is less than 2.5% and is further neglected. Figure 4.5a shows that the diffusion is important, especially for the SW, and it acts to increase the density of ocean water at all levels. Down to $\sigma = 24.0$, primarily north of 12°S, formation by air-sea fluxes is completely balanced by consumption due to diffusion. Niiler and Stevenson (1982) showed that turbulent vertical diffusion of heat balances surface heating in tropical oceans. For the denser SW ($24.0 < \sigma < 25.5$), in the subtropical gyre and the Agulhas region, diffusion has a strong impact on the mass balance of the control volume, mainly forming water masses heavier than $\sigma = 25.0$. Diffusion is less important for water masses other than SW, south of the South Atlantic subtropical gyre.

The interocean exchange A_{bnd} is as large as the net subduction rate M_{Eul}. Light SW ($\sigma < 25.0$) is imported from the Indian ocean by the Agulhas Current. The SASTMW is formed by differential heating in the Subtropical Front (STF) (6.0 Sv). More than half of this newly formed water mass subducts (3.5 Sv). Mixing (1.7 Sv) and interocean exchange (0.8 Sv) account for the other newly formed SASTMW. The Pacific Ocean provides mainly SAMW, AAIW and DW by the Antarctic Circumpolar Current. After transformation by air-sea interaction and mixing, these water masses either subduct, or flow within the mixed layer to the Indian Ocean. All water masses except SW are exported toward the Indian Ocean (not shown). Karstensen and Quadfasel (2002a) and Sloyan and Rintoul (2001a) also concluded that water formed in the South Atlantic must flow into the Indian Ocean, where it finally subducts. For the mixed layer budget, the exchange between the North and South Atlantic basin is small. North Brazil Current rings play an important role in the net interhemispheric exchange and this process may be underestimated in the model. However, net exchange associated with the THC is realistic in OCCAM. The exchange occurs predominantly below the mixed layer. The positive density-integrated subduction rate of 15 Sv at $\sigma = 28.0$ indicates that there is a net subduction of water within the South Atlantic, provided by water imported from adjacent oceans. All water masses ranging from lSACW to DW subduct in the South Atlantic, while SW obducts. The Eulerian obduction of SW is located in the eastern

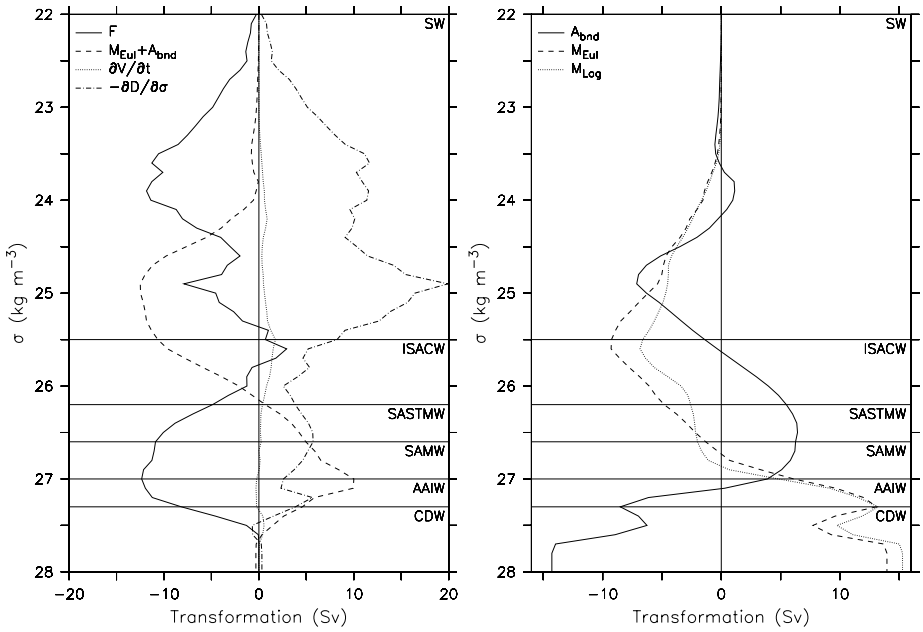

Figure 4.5: *(a) Transformation curve (in Sv) showing the balance (see eq. 4.1) within the domain between air-sea fluxes ($F(\sigma)$, solid), the density-integrated, outward flux through the control surfaces ($M(\sigma) + A_{\mathrm{bnd}}(\sigma)$, dashed), trend (dotted) and the diffusion (dash-dotted). An increase of transformation with density denotes a loss of water from the control volume. The sum of all processes is zero, because the total volume is conserved. (b) Transformation processes through the control surface: outgoing volume flux through the open boundaries: interocean exchange A_{bnd} (solid), Eulerian subduction M_{Eul} (dashed) and Lagrangian subduction M_{Lag} (dotted). The horizontal lines indicate the density bounds between different water masses (see Table 4.1).*

equatorial region, the Agulhas region and along the western boundary of the South Atlantic up to the Brazil-Malvinas Confluence area. The Lagrangian net subduction M_{Lag} has been plotted in Fig. 4.5b for comparison, which is further discussed in the next section. Although deviations are small, the Eulerian and Lagrangian net subduction are not equal.

4.6 Lagrangian connections of subduction zones

In the previous section we analyzed the volume balance of the South Atlantic mixed layer. So far, all analyses were carried out in a Eulerian framework. We have shown that the South Atlantic has a net Eulerian subduction (M_{Eul}) of more than 15 Sv in OCCAM (see Fig. 4.5c). This Eulerian subduction is the net

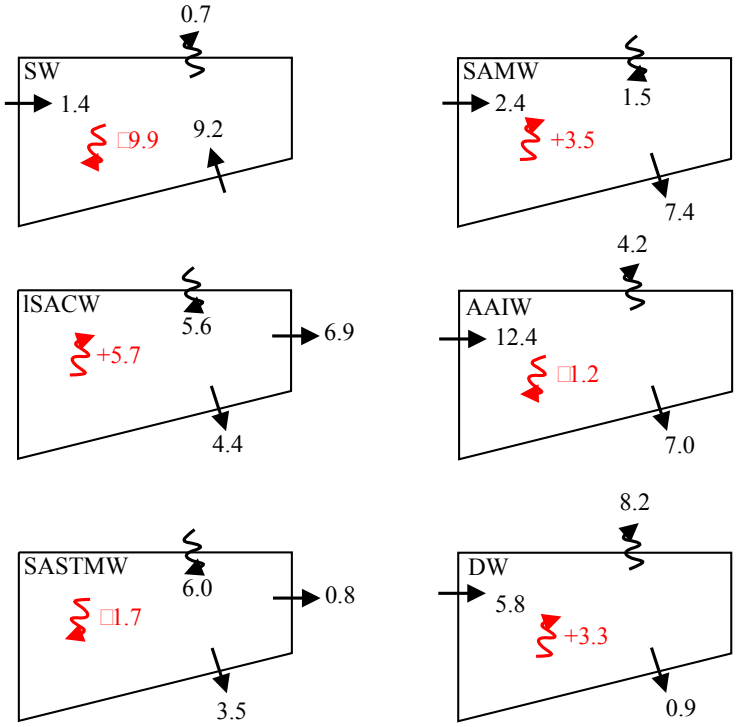

Figure 4.6: *Budget for four different water masses within the South Atlantic mixed layer. The different water masses are indicated by the name in the upper left corner of each box. Water masses are defined in Table 4.1. All numbers are in Sv. The arrows at the top of each box represent the formation from air-sea interaction. The arrows at the bottom represent the net flux across the deepest mixed layer depth. The arrows across the left or right side represent interocean exchange, while the arrow within the box indicate formation by mixing within the mixed layer.*

mass flux across the winter mixed layer base in the South Atlantic. The Eulerian subduction does not indicate whether these water masses move in the interior ocean for more than one year, nor does it give an indication of the locations that are remotely influenced by the subducted water masses. A Lagrangian analysis is needed to estimate the remote impact of subducted water masses within the South Atlantic.

The three-dimensional Lagrangian trajectory technique we use to this end has been described and applied before (Donners and Drijfhout, 2004; Döös, 1995; Hazeleger et al., 2003). With Lagrangian trajectory analysis we follow particles that enter the interior ocean through the winter mixed layer base. The properties of the water masses are set in the mixed layer prior to subduction. Particles are followed until they reach the winter mixed layer base again. The properties of the mixed layer are influenced by the water masses that re-enter the mixed layer. This gives an indication of possible teleconnections between South Atlantic subduction regions and remote obduction regions. Lagrangian subduction rates (S_{Lag}) are calculated by tracing forward in time, starting from the mixed layer base; while we obtain Lagrangian obduction rates (O_{Lag}) with backward time integration of particles that end at the mixed layer base.

Model drift influences the pathways of water masses below the mixed layer and consequently the obduction regions. However, we cannot directly quantify the effect of drift on the obduction regions, because the Lagrangian trajectory analysis requires a dataset averaged over several years. However, we can calculate the effect of drift on Eulerian water mass transports in the OCCAM model. Donners and Drijfhout (2004) showed that the drift in meridional water mass transports in the South Atlantic in the OCCAM model is not statistically significant.

Particles represent a transport of at most 10^{-3} Sv, and are evenly spread in space and time. Tens of thousands of particles have been calculated to obtain a quantitative picture of the Lagrangian subduction within the South Atlantic. The accuracy of the total transports is better than 0.1 Sv. A similar analysis for the global ocean has been done by Blanke et al. (2002b), but without distinguishing different water masses. They calculated Lagrangian trajectories between regions of subduction and obduction. We do not divide the South Atlantic into different regions, but distinguish between 6 water masses defined by density intervals (see Table 4.1).

The formation induced by air-sea interaction together with the Lagrangian subduction and re-emergence zones for all water masses except DW is plotted in Figs. 4.7 to 4.11. The results are quantified in Table 4.3. Note that the Lagrangian obduction O_{Lag} and re-emergence differ because of interocean exchange: re-emergence includes only particles that subducted in the South Atlantic, the Lagrangian obduction O_{Lag} includes all particles that obduct in the South Atlantic. The latter may have been subducted in the South Atlantic or in other basins. Also note that the formation is not equal to F. The formation is the integral over R of air-sea transformations that converge into a specific density class. This is an indication of the potential amount of newly formed water mass that could subduct. Formation and subduction of DW has not been

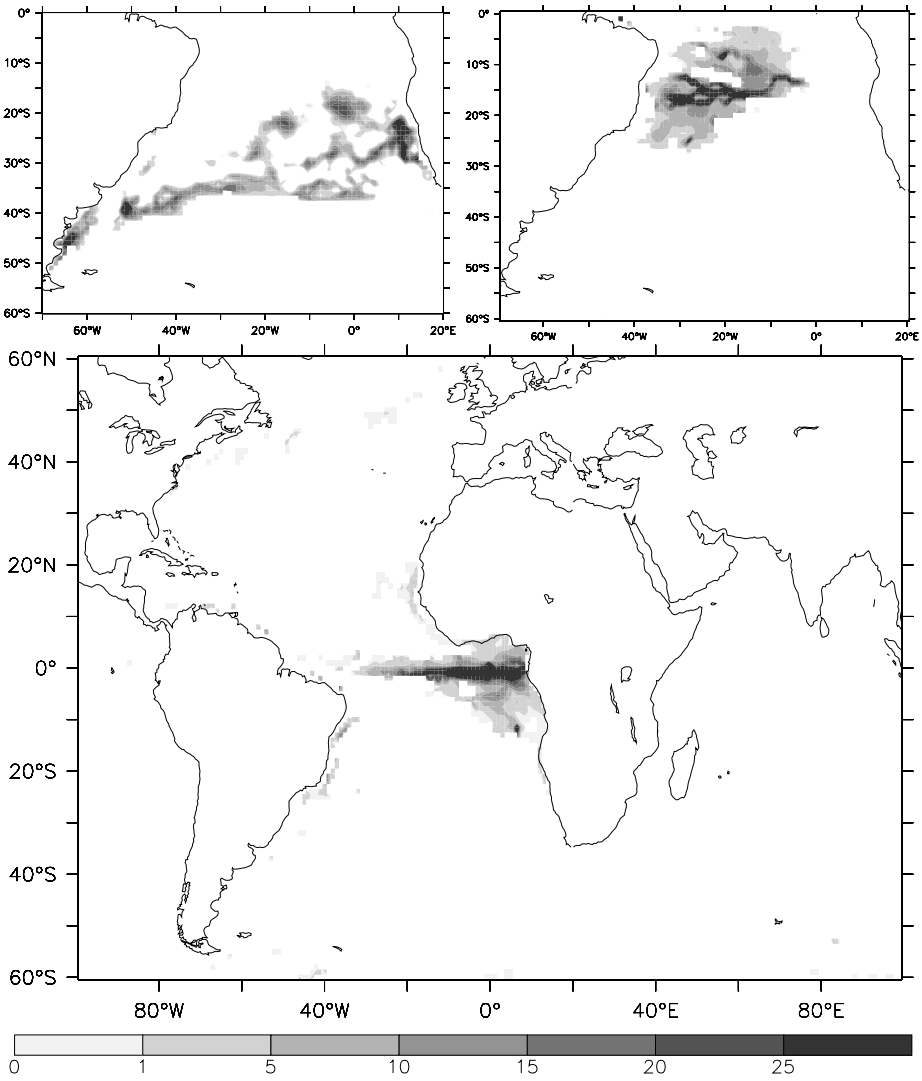

Figure 4.7: *Water mass formation due to air-sea fluxes (upper left panel) together with the subduction (upper right panel) and re-emergence regions (lower panel) for the SW (in mSv per $1^\circ \times 1^\circ$ gridbox).*

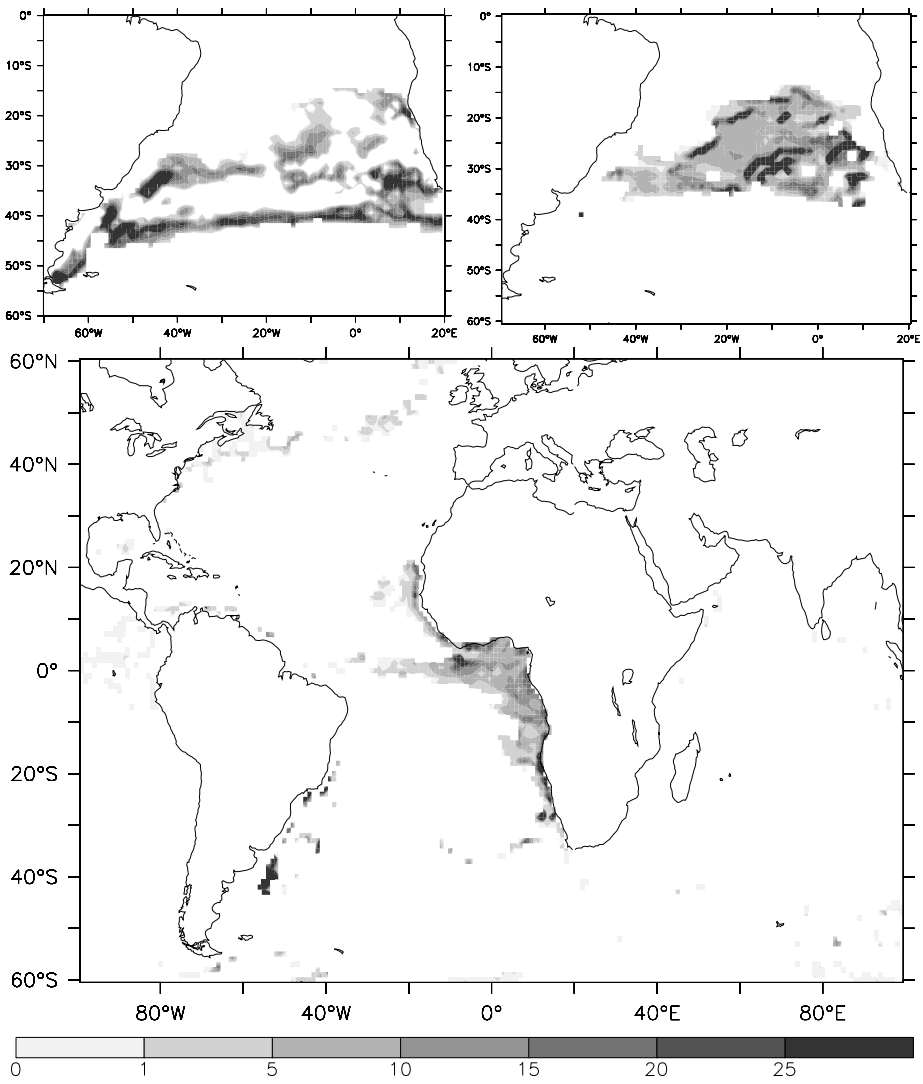

Figure 4.8: *Idem like Fig. 4.7 for the lSACW.*

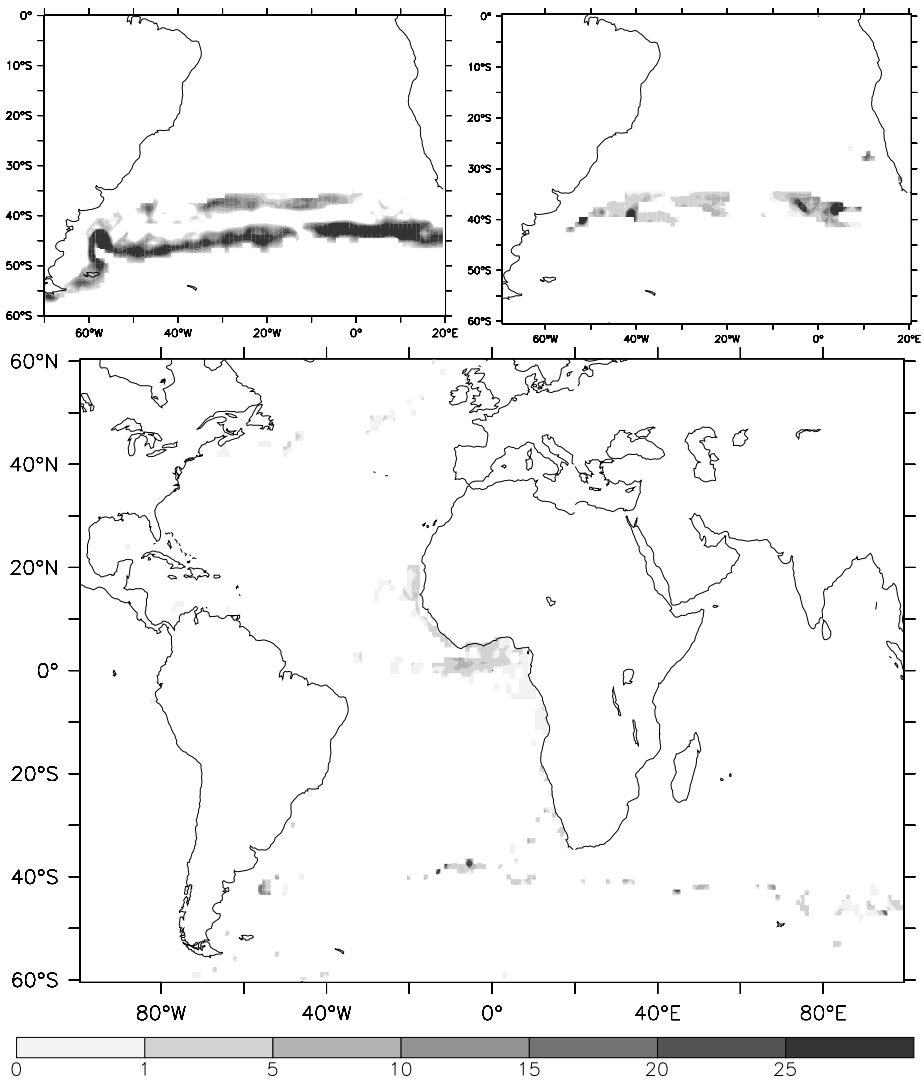

Figure 4.9: *Idem like Fig. 4.7 for the SASTMW.*

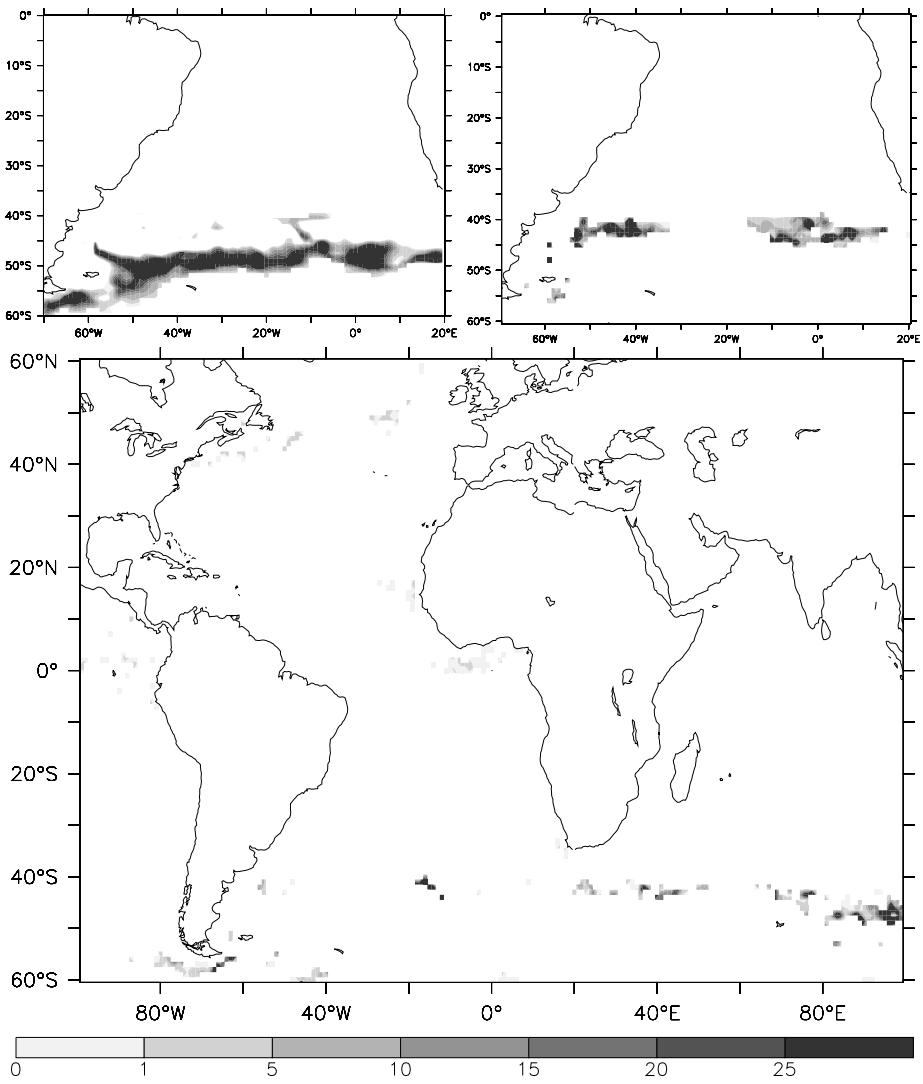

Figure 4.10: *Idem like Fig. 4.7 for the SAMW.*

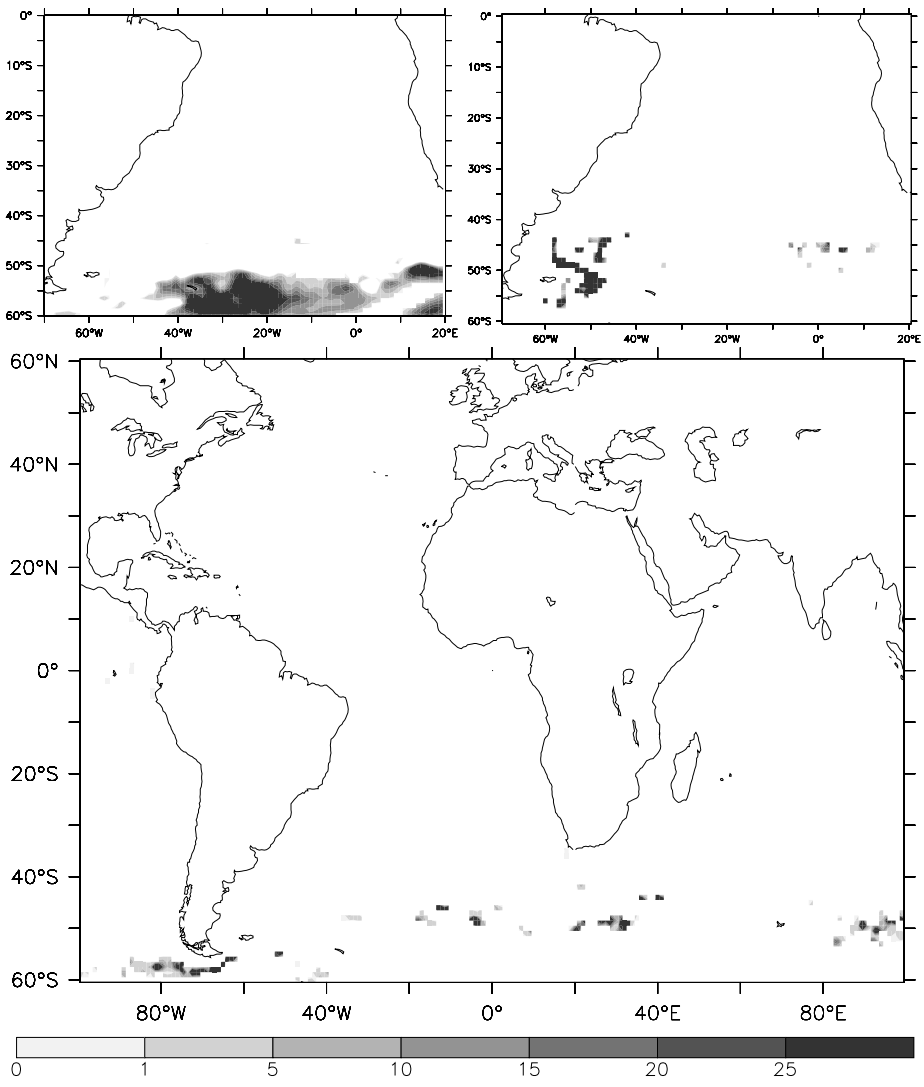

Figure 4.11: *Idem like Fig. 4.7 for the AAIW.*

	Formation	S_{Lag}	Trop. Atl.	N. Atl.	other	Median time	O_{Lag}
SW	7.3	6.2	5.4	0.1	0.7	2.2	12.8
lSACW	14.7	12.0	4.1	0.7	7.2	3.9	8.0
SASTMW	13.0	2.8	0.4	0.2	2.2	1.9	2.2
SAMW	12.8	8.5	0.1	0.2	8.2	2.6	1.7
AAIW	9.0	13.4	0.0	0.0	13.4	4.1	5.0
DW	0.7	15.5	0.0	0.0	15.5	3.0	13.4

Table 4.3: *Table with formation, subduction and reemergence rates for different water masses (in Sv). The reemergence of subducted water particles is divided into three different regions: Tropical Atlantic (15°S to 15°N), North Atlantic, and other parts of the world ocean. The forelast column indicates the median time between subduction and reemergence (in years). The last column shows the obduction rates within the South Atlantic basin (in Sv).*

plotted, as the drift of the OCCAM model for this heavy water mass could seriously hamper the Lagrangian analysis of the subduction (Lee et al., 2001), and the subduction rate of this water mass is small in the South Atlantic. There is a good, quantitative agreement with Blanke et al. (2002b). The subtropical gyre and the ACC act as the main subduction zones. The eastern equatorial upwelling regions, a strip along the western boundary, and the ACC, are the main obduction zones. The median time between subduction and reemergence is less than 5 years for all watermasses. Although there is no well-defined timescale for subduction, the bulk of the particles return within 7 years.

Figure 4.7 shows that SW is mainly formed by air-sea interaction in the Brazil-Malvinas Confluence, Agulhas region and the South Atlantic Current. The subduction of SW, however, takes place in the western tropical Atlantic. This coincides with the subduction of Salinity Maximum Water (Blanke et al., 2002a). The subduction rate of SW (6.2 Sv) in OCCAM is lower than model estimes (7.2 Sv, Blanke et al., 2002a) and observational estimates (9.0 Sv, Blanke et al., 2002a). The water mass lSACW (Fig. 4.8) is formed along the STF and in the Cape Basin and subducts in the subtropical gyre of the South Atlantic. To reach its subduction area in the South Atlantic, a large part of the newly formed SW and lSACW has to cross the region where the curl of the wind stress vanishes, located around 30°S, and where the Ekman transport changes sign becoming southward. To overcome the Ekman drift, a strong mean flow is needed to advect the SW and lSACW northward. This could be provided by the Benguela Current which draws water from the South Atlantic Current. The connection between the two currents, however, is weak in OCCAM (Drijfhout et al., 2003a). Most of the SW and lSACW formed in the South Atlantic is exported to the Indian Ocean where it recirculates and is replaced by Agulhas leakage, whereafter it subducts.

Some SASTMW is formed by cooling of lSACW, but most is formed by warming of SAMW. Formation of SAMW occurs along the SAF in the ACC

(Fig. 4.10); 12.4 Sv of AAIW is converted by surface heating into SAMW. Of the newly formed SAMW, 8.5 Sv subducts within the South Atlantic. The subducted SAMW stays within the ACC and re-emerges further downstream. Only a tiny part enters the Atlantic basin and re-emerges in the Atlantic eastern equatorial region or the northern North Atlantic.

Figure 4.11 shows the formation areas of AAIW, which is mainly formed by buoyancy gain of cold waters south of the ACC (8.2 Sv). However, the strong transformation of light AAIW into SAMW results in a net comsumption of AAIW (4.2 Sv, Fig. 4.6). Because of the eastward flow of the ACC, AAIW, that is subducted in the Malvinas Current and the Brazil-Malvinas confluence region, must originate from the Pacific ocean. Newly formed AAIW partially subducts in the South Atlantic ocean east of 20°W (0.9 Sv), but most of this AAIW is exported toward the Indian Ocean. Only a negligible part of the subducted particles reaches the northern North Atlantic. Most AAIW re-emerges in the ACC downstream of the Kerguelen plateau and in the northern part of Drake Passage. The South Atlantic mixed layer is a large net sink of AAIW, fed by AAIW from the Pacific ocean.

4.7 Discussion

4.7.1 Comparison to observations

The transformation of SAMW in the South Atlantic in OCCAM is in reasonable agreement with observations. Sloyan and Rintoul (2001a) combined observations of air-sea fluxes and hydrographic sections with an inverse model to infer the ocean circulation of the southern hemisphere. They calculated a formation of SAMW of 8.4 Sv due to buoyancy gain of Antarctic Surface Water, compared to an air-sea transformation of 12.4 Sv from AAIW to SAMW for the OCCAM model. The OCCAM model transforms 10.9 Sv of SAMW further into lighter SASTMW along the northern edge of the ACC. This is not in agreement with inverse model calculations, based on the DaSilva dataset, that show an opposite transformation of 6 Sv due to enhanced heat and freshwater loss of thermocline water in the Brazil-Malvinas Confluence (Sloyan and Rintoul, 2001a). However, Karstensen and Quadfasel (2002a) used the NCEP dataset and calculated similar transformation rates as the OCCAM model at this density. This can also be seen in Fig. 4.3, with comparable WMT rates for OCCAM, ECCO and NCEP, whereas the DaSilva and ERA40 datasets show almost no WMT at the $\sigma = 26.6$ isopycnal. This shows the need to improve datasets for air-sea fluxes.

The transformation rate at the isopycnal $\sigma = 26.2$ has an even larger uncertainty (Fig. 4.3). Ocean-only models (OCCAM and ECCO) transform SASTMW to lSACW, while for all other datasets the reverse transformation takes place. The STF in the OCCAM model is northward biased during summer, which leads to more heat input. This results in a negative bias of the WMT rate in OCCAM. The high variability of SW and lSACW formation rates (see Table 4.2) indicates that a longer period is needed for a meaningful estimate of

average formation rates at these densities.

Poole and Tomczak (1999) separated SACW into Eastern SACW (ESACW) and Western SACW (WSACW). The ESACW represents thermocline waters transferred into the Atlantic Ocean at the Agulhas Retroflection, WSACW is locally subducted in the subtropical convergence. Poole and Tomczak (1999) showed that the WSACW dominated the South Atlantic at shallow depths (300 m). Of the total SACW formation of 20.6 Sv by air-sea interaction and mixing in the OCCAM model, 75% subducts. In agreement with Poole and Tomczak (1999), the subducted lSACW resides mostly within the Atlantic basin (10.5 Sv), while subducted SAMW does not penetrate the Atlantic basin further northward. Furthermore, Donners and Drijfhout (2004) showed that, in the OCCAM model, all ESACW is (9.5 Sv) directly transported toward the North Atlantic, dominating the tropical Atlantic SACW at deeper depths.

The AAIW layer of the South Atlantic has been extensively described by Talley (1996) and Sloyan and Rintoul (2001a). There are two distinct formation regions for AAIW: the southwestern Atlantic and the southeastern Pacific. A large volume of Pacific AAIW is formed by strong cooling of SAMW in the southeastern Pacific. This formation region serves the northward AAIW transport in the Pacific and feeds the South Atlantic with AAIW that enters through Drake Passage. This AAIW subducts as South Atlantic AAIW along the Malvinas Current. In OCCAM, over 12.6 Sv of AAIW subducts in the Malvinas Current. This AAIW must be drawn from Drake Passage, in accordance with observations, because AAIW formation in the South Atlantic is located further downstream.

Karstensen and Quadfasel (2002a) estimated the water mass formation due to air sea fluxes and the subduction rate for the southern hemisphere from observational data. Their conclusions are radically different from the ones we obtain from OCCAM. Karstensen and Quadfasel (2002a) added all water masses with densities between $\sigma = 25.2$ and $\sigma = 27.0$ together. The subduction rate calculated by Karstensen and Quadfasel (2002a) is 21 Sv, which is stronger than the subduction rate in the OCCAM model (13.8 Sv). Also the formation rate calculated by Karstensen and Quadfasel (2002a) is much larger than calculated for the OCCAM model (29 Sv versus 9.7 Sv). One of the causes for this large discrepancy could be the surface relaxation used by the OCCAM model, which underestimates the water mass transformation rates. Also, Karstensen and Quadfasel (2002a) used the NCEP air-sea flux dataset, which has the strongest formation rate for this density range (see Figure 4.3). There is, however, some agreement on the interocean exchange between the South Atlantic and Indian Oceans. Karstensen and Quadfasel (2002a) estimated 13 Sv of water to be exported, while the OCCAM model shows an export of 8.2 Sv. To accommodate this export, 12.3 Sv is provided by diffusive processes in the OCCAM model. This shows that, at least for the OCCAM model, diffusive processes can not be ignored to estimate the interocean exchange. However, the water mass transformation F can be used to qualitatively estimate the sum of interocean exchange and Eulerian subduction ($M_{\mathrm{Eul}} + A_{\mathrm{bnd}}$); the error is on average 80%.

4.7.2 Impact of the South Atlantic on the properties of the upper branch of the THC

So far, we have analyzed the water mass transformation and exchange in the South Atlantic mixed layer. With Lagrangian trajectory analysis the fate of subducted water masses has been calculated. The impact of these water mass transformations in the South Atlantic ocean on the thermohaline overturning circulation, however, is not directly apparent from these calculations. With the same Lagrangian methodology we can also calculate the impact of South Atlantic mixed layer processes on the upper branch of the thermohaline circulation. To this end, we follow particles at the Atlantic equator below the mixed layer backward in time to the point where they enter the Indo-Atlantic basin from the Pacific (Speich et al., 2001). This enables us to single out the transformations of the water that is part of the meridional overturning circulation.

14.4 Sv enters the Indo-Atlantic basin from the Pacific ocean and crosses the Atlantic equator northwards. These water masses are modified within the Indo-Atlantic basin, both in the mixed layer and below the mixed layer. A large part subducts for the last time in the South Atlantic basin (6.9 Sv, not shown) before crossing the equator. Water mass transformations and mixing in the South Atlantic thus have a significant impact on the upper branch of the THC. In Fig. 4.12 we show the transformation in the South Atlantic of the transport crossing the Atlantic equator. The upper branch of the THC is transformed at all density levels in the South Atlantic Ocean. The water masses with a density $\sigma < 26.0$ lose buoyancy due to strong surface cooling in the Agulhas region. Surface warming along the ACC increases the buoyancy of Antarctic intermediate and mode waters ($\sigma > 26.0$). The THC gains buoyancy below the mixed layer for $\sigma = 25.5$ in the eastern tropical Atlantic.

The subducted transport from the South Atlantic into the North Atlantic, does not necessarily influence directly the deep water formation in the northern North Atlantic. A large part (3.0 Sv) of the subducted water particles re-emerge within the tropical Atlantic (15°S-15°N), where the water mass properties can again be modified by mixed layer processes. Only 1.1 Sv of the water subducted in the South Atlantic connects directly to re-emergence areas in the northern north Atlantic. All other transport recirculates back into the South Atlantic, to re-emerge somewhere else.

The following picture emerges from these calculations: there is a strong teleconnection between the South and Tropical Atlantic, and this also applies to the upper branch of the THC. A majority of the water involved in NADW formation is also ventilated in the tropical and subtropical North Atlantic. A direct teleconnection between the subpolar North Atlantic and areas remote from the Tropical Atlantic applies to no more than 50% of the NADW return flow. A direct teleconnection between the northern North Atlantic and the South Atlantic applies to only 1 Sv of the THC.

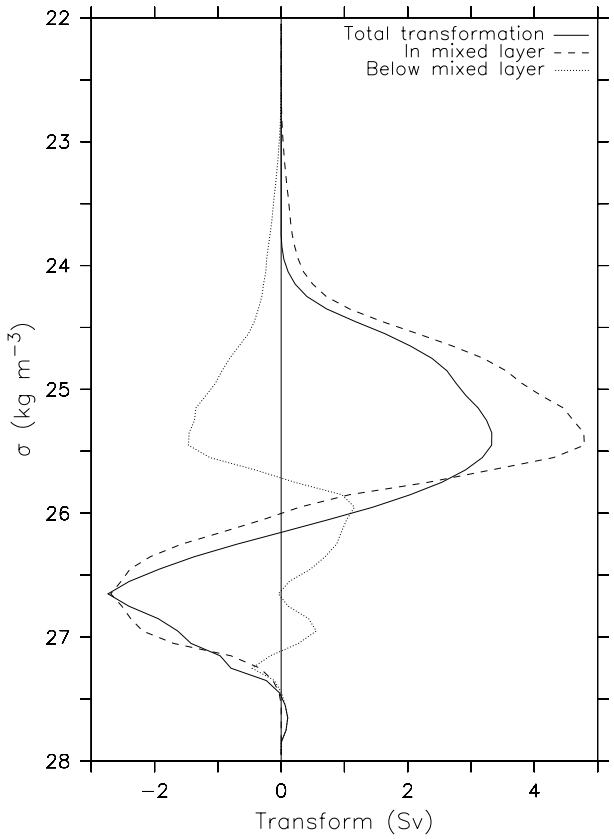

Figure 4.12: *Water mass transformation curves of the upper branch of the THC in the South Atlantic (in Sv). The total transformation is plotted with the solid line. The total transformation is split into two components: the transformation in the mixed layer (dashed) and the transformation below the mixed layer (dotted). A positive transformation denotes densification.*

4.8 Conclusions

We calculated WMT rates for the South Atlantic due to air-sea fluxes for different datasets, ranging from observation-only datasets to model-only datasets. The datasets are in qualitative agreement, although the deviations of the transformation rates for the different datasets are 10 Sv. The air-sea interaction in the OCCAM model supplies buoyancy to the South Atlantic at all density levels. Heavy water masses (AAIW and DW) are transformed into lighter water masses (SASTMW and SAMW). Diffusion generally counteracts the air-sea interaction, by extracting buoyancy from the mixed layer. Due to diffusion, water mass formation rates calculated from air-sea heat and freshwater fluxes are ineffective to estimate of the sum of Eulerian subduction rates and interocean exchange.

The subduction of water masses within the South Atlantic has been analyzed with Lagrangian trajectory analysis. The subducted water masses re-emerge at remote locations, and this generates teleconnections by pathways through the interior ocean. Most of the subducted water in the South Atlantic flows further eastward along the ACC, where it finally re-emerges and is further modified. Most of the subducted water masses that do not enter the ACC, mostly of subtropical origin, re-emerge in the eastern tropical Atlantic. This indicates that there is a teleconnection through the interior ocean between the South Atlantic subtropics and tropics. Only 1.2 Sv of subducted water in the South Atlantic reaches the subtropical or northern North Atlantic. This indicates that there is only a weak teleconnection between the extratropical regions of the North and South Atlantic. The direct influence of subducted water masses from the South Atlantic on the THC is therefore small. On the other hand, part of the NADW return flow is significantly transformed when crossing the South Atlantic.

Chapter 5

Impact of cooling on the water mass exchange of Agulhas rings in a high resolution ocean model

The leakage of water from three Agulhas rings has been studied in a high resolution global ocean model using a Lagrangian particle following technique. A bowl shaped ring boundary that reaches a radius of 140 km and a depth of 800 m separates regions of fast and slow leakage. The dilution of Agulhas ring water generally increases with depth, but a shallow secondary circulation enhances leakage in the upper 150 m. Strong surface cooling upsets the horizonal pressure gradient which is balanced by subinertial motions that act to form this shallow overturning cell.

5.1 Introduction

The Agulhas Current is the strongest western boundary current of the southern hemisphere. It retroflects to the south of South Africa and flows back into the Indian Ocean as the Agulhas Return Current. Agulhas rings are shed off the retroflection loop irregularly and move into the South Atlantic Ocean in a northwesterly direction. These rings form an important link between the subtropical gyres of the South Atlantic Ocean and the Indian Ocean (de Ruijter et al., 1999). This link is thought to play an important role in the upper branch of the global thermohaline circulation (Weijer et al., 1999). Schouten et al. (2000) followed these rings with satellite measurements of sea surface height (SSH). During the first five months after the shedding of Agulhas rings the decay of

Published as Donners et al. (2004a)

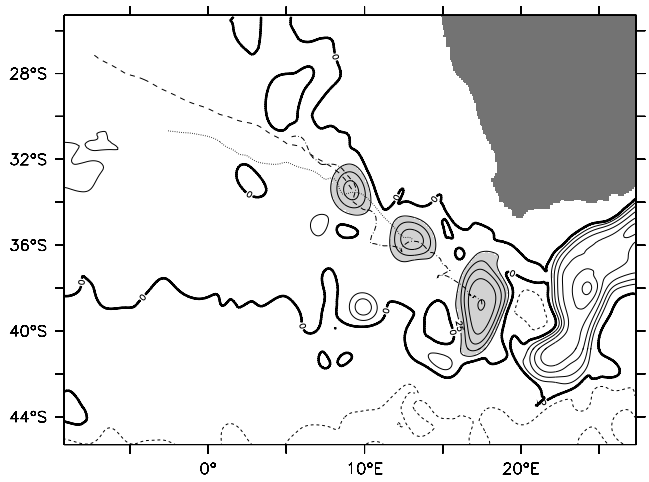

Figure 5.1: *The initial position of the three Agulhas rings and their path in the following year. The contours at every 25 cm indicate the SSH, the light shaded area shows where the Lagrangian trajectories have been initialized. Dark shading indicates the African continent.*

the SSH is strongest. Drijfhout et al. (2003b) showed that the strong decay is associated with a mixed barotropic/baroclinic instability. In most cases this instability leads to split-up of the ring.

From theoretical considerations, Flierl (1981) concluded that, when the rotational speed is larger than the translational speed of the eddy, water is trapped inside eddies. This suggests that leakage across a ring boundary above a certain critical depth is weak, while it will be strong below this depth. Indeed, van Aken et al. (2003) discussing observations of a young Agulhas ring, found no systematic differences of water mass properties between the ring and its surroundings below the 12° C isotherm, located at a depth of 650 m in this ring. The leakage of water from Agulhas rings below this depth has also been found in a numerical model of an Agulhas ring (de Steur et al., 2004).

Agulhas rings are strongly cooled, especially in winter. Dewar (1987) calculated the restructuring of an idealized warm ring using a two-layer model. Estimates of energy release during adjustment suggest that a significant amount of energy is converted into internal wave energy. Drijfhout et al. (2003b), however, found that the effect of cooling is weak; the instability process develops marginally slower. An alternative theory was developed by Young (1994). In his subinertial mixed layer (SML) theory, a balance arises between vertical mixing and "unmixing" by differential advection. The latter is associated with a sheared horizontal pressure gradient that may arise, for instance, from cooling.

In this chapter we analyze the water mass exchange of three Agulhas rings in a high-resolution global ocean model. This enables us to look at the decay processes of Agulhas rings in a realistic setting. The model allows for a detailed

vertical structure within the mixed layer, which has not been studied before. Water mass exchange between the ring and the surroundings is calculated with Lagrangian diagnostics.

5.2 Model and methods

The general circulation model OCCAM (Webb et al., 1997) was used for a detailed study of Agulhas rings. The model uses an eddy-resolving resolution of $1/12^\circ$ and employs 66 depth levels, with 20 layers in the top 200 m. The mixed layer is described by the KPP scheme (Large et al., 1994). The initial potential temperature and salinity fields were interpolated from the WOCE SAC climatology (Gouretski and Jancke, 1996) for most of the World's oceans together with World Ocean Atlas data (Antonov et al., 1998; Boyer et al., 1998). During the run analyzed here, the ocean surface was forced by a monthly average ECMWF wind stress climatology (Gibson et al., 1997) calculated from the years 1986 to 1989 inclusive (Siefridt and Barnier, 1993). Surface relaxation of temperature and salinity toward monthly climatologies (Levitus and Boyer, 1994; Levitus et al., 1994) was also applied. The model was run for two years, of which the second year was used for the analysis. We used instantaneous model fields at three day intervals for all calculations.

For the Lagrangian analysis of leakage from Agulhas rings we used an offline approach (Döös, 1995), extended by de Vries and Döös (2001) for the use with time-dependent flows. Every particle represents a specified volume of water ($10^9\,\mathrm{m}^3$). More than twenty thousand particles were used for the smallest Agulhas ring. Each trajectory was followed for the full second year of the model run. Particles were seeded in the top 2000 m of the Agulhas ring wherever the SSH was above 25 cm. The center of the Agulhas ring was defined as the interpolated location of the SSH maximum. The Agulhas rings were also analyzed in a two-dimensional, Eulerian framework. To this end, the data was azimuthally averaged around the ring center and plotted as a function of radial distance and depth.

5.3 Water mass exchange

Figure 5.1 shows the SSH at the beginning of the year that has been used for the following analysis. The Agulhas Current is centered at 24° E. The light shading indicates the regions within the three Agulhas rings where Lagrangian particles were seeded. Also the path of the three rings has been indicated. The youngest (and largest) Agulhas ring is two weeks old. The ring properties agree very well with Agulhas ring "Astrid" (van Aken et al., 2003) (see Table 5.1), so we conclude that the modeled rings are realistic. The ring breaks up after two months, and sheds some small rings in the following two months. The split-up can be attributed to the mechanism described by Drijfhout et al. (2003b). The middle ring was shed off mid-November, at the end of spring. The oldest ring

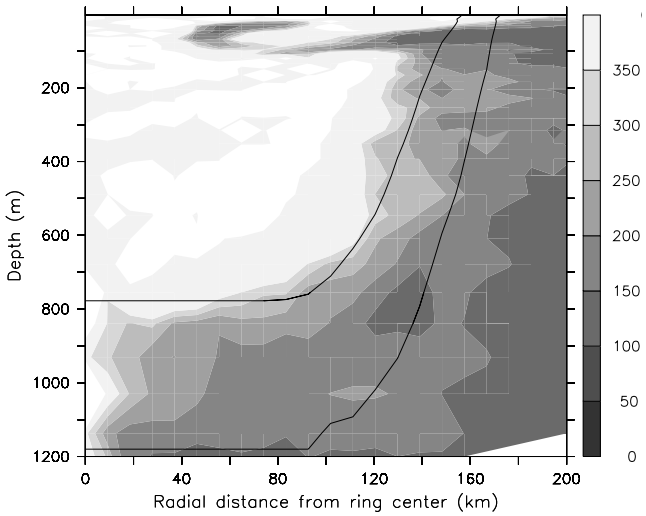

Figure 5.2: *The figure denotes the average residence time (in days) of Lagrangian trajectories within an Agulhas ring. The upper contour indicates the location where the azimuthal velocity is at least twice the translational velocity of the ring. The lower contour indicates the location where the azimuthal velocity is equal or larger than the translational velocity of the ring. The contours define two different ring edges.*

Property	Agulhas ring "Astrid"	OCCAM 1/12°
SSH	82 cm	113 cm
SST	21 °C	20.9 °C
SSS	35.55 psu	35.37 psu
MLD	90 m	110 m
Ring size	220 km	240 km
12 ∘C depth anomaly	460 m	460 m

Table 5.1: *Comparison between observations of a young Agulhas ring "Astrid" (van Aken et al., 2003) and a young Agulhas ring in the OCCAM 1/12° ocean model.*

was formed in mid-winter of the first year. The two oldest rings are stable and do not break up.

The Agulhas rings have been traced with the Lagrangian particle technique for one year to investigate the leakage of water into the environment. Only the results of the middle ring (located at 36° S, 13° E) are shown here. All results are equally applicable to the other Agulhas rings, unless otherwise stated. Figure 5.2 shows the average residence time (or e-folding time scale) of particles within the ring as a function of distance from the ring center and depth. For each azimuthally averaged gridcell an exponential function was fitted to the concentration of particles as a function of time. A clear, bowl shaped division can be seen between particles that reside in the ring (white) and particles that leak into the environment (dark gray). The bowl shape reaches to a distance of 140 km and a depth of 800 m. The decay of the anomalous heat and salt within the bowl is estimated with a linear extrapolation between 2 to 6 years.

Figure 5.2 also shows the contour where the rotational velocity is at least twice the translational speed of the Agulhas ring. Note that the contour shallows at approximately 80 km distance from the ring center, where the maximum azimuthal velocity is largest. At radii larger than 80 km the criterion is a good indicator of the bowl shaped ring boundary. This criterion is also valid for the oldest ring, although for the largest ring it only holds for the period when no instabilities develop. The average residence time along the ring boundary is 250 days. The criterion of Flierl (1981) for the ring boundary, namely where the rotational speed equals the translational speed, is also shown on Figure 5.2 (lower contour). This reaches down to 1200 m and 20 km further outward. This criterion defines a less sharp boundary in terms of the average residence time, which can be attributed to the unsteadiness of both the ring boundary and its self advection (de Steur et al., 2004).

In the upper 150 m of the Agulhas ring a significantly stronger water mass exchange can be seen, in the form of a curl of water with a lower residence time. This suggests that the surrounding water is drawn into the ring at 100 m depth, upwells within the ring and flows radially outward near the surface. The streamfunction of the circulation causing the enhanced leakage near the surface is shown in Fig. 5.3. The shallow overturning cell is the strongest circulation feature within the bowl shaped ring boundary and is confined to the mixed layer. The cell is present in all Agulhas rings during winter and spring, when heat loss is strong. The overturning circulation in the mixed layer is independent of the azimuth angle (not shown).

5.4 Mixed layer processes

For a better understanding of the mechanism behind the secondary circulation described in the previous section, we calculated the different terms of the density balance:

$$\frac{\partial \rho}{\partial t} + u\frac{\partial \rho}{\partial r} + w\frac{\partial \rho}{\partial z} - \frac{\alpha Q}{c_w} - \beta S(P-E) - \Gamma = 0 \tag{5.1}$$

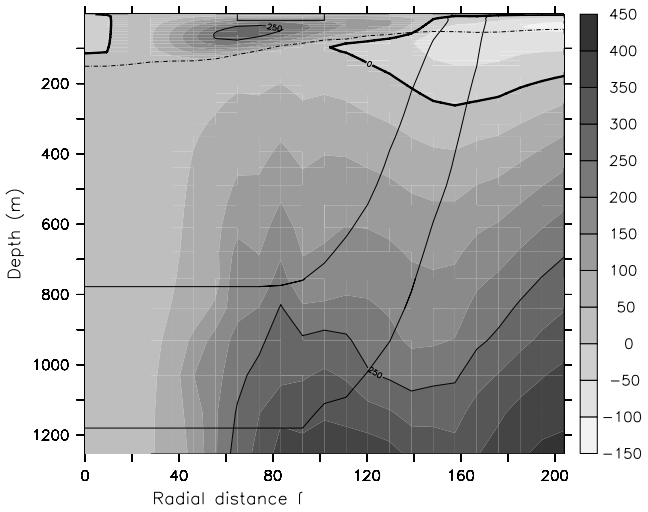

Figure 5.3: *Streamfunction of the shallow overturning cell (in mSv) at the end of winter. Positive values indicate clockwise rotation. The MLD is indicated with the dash-dotted line.*

All variables were azimuthally averaged. The mixing term Γ, which includes all cross-correlational terms, was not calculated explicitly but equalled to the residual.

The different terms of the density balance were calculated as a function of time in the top 11 m (upper two grid boxes), where the overturning cell and the atmospheric interaction are both strong. The density balance is plotted in Figure 5.4. There is a clear balance between the strong surface forcing and horizontal advection. The freshwater forcing is weak and constant ($5.7{\cdot}10^3\,\mathrm{kg\,s^{-1}}$). Atmospheric cooling of the Agulhas ring in winter causes the strong surface forcing. The surface cooling of Agulhas rings increases in autumn and winter and diminishes during spring. The horizontal advection is directed radially outward at the surface. Dense (cold) water flowing radially outward is replaced by light (warm) water from the ring center. This balance also holds for the other two Agulhas rings. For the largest ring this balance is only established when no more instabilities develop.

The surface cooling is strongest close to the ring center, but this heat loss is effectively distributed over the depth of the mixed layer by convection. Near the ring center the mixed layer is deeper, so the effective cooling of the mixed layer is largest near the ring boundary where the mixed layer shallows. The maximum effective forcing coincides with maximum horizontal advection.

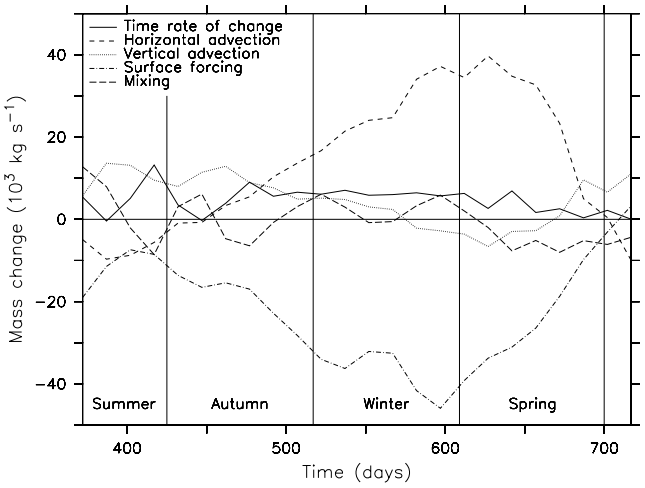

Figure 5.4: *The mass budget as a function of time for the ring volume in the top 11 m of the Agulhas ring between 65 km and 102 km from the ring center (indicated in figure 5.3).*

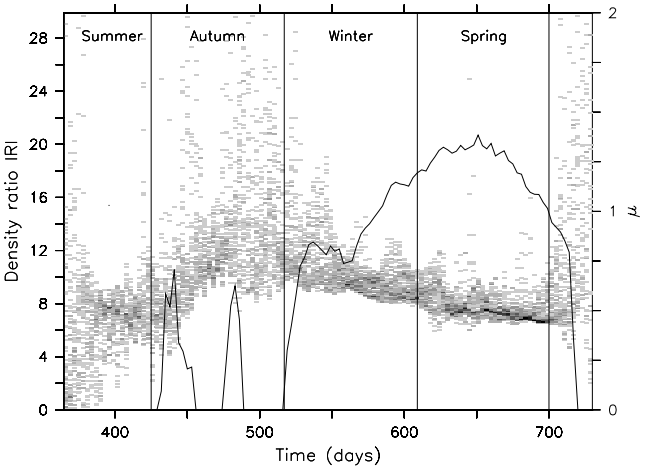

Figure 5.5: *The distribution of the density ratio $|R|$ in the shallow overturning cell of an Agulhas ring as a function of time. The thick line is the parameter μ. The SML theory is applicable if $\mu \approx 1$.*

5.5 Discussion

The SML theory (Young, 1994) may explain how the overturning circulation arises. The buoyancy flux upsets the preexisting geostrophic equilibrium and the system moves towards a new geostrophically adjusted state. The resulting horizontal pressure gradient features strong vertical shear and subinertial motions balance this pressure gradient with vertically sheared advection. Shear-driven restratification operates most efficiently when the timescale of vertical mixing of momentum τ_U is on the order of the inertial timescale f^{-1}, when the parameter $\mu \equiv (f\tau_U)^{-1} \approx 1$. The parameter μ can be estimated from a relation between the Brunt-Väisälä frequency N^2 and buoyancy B in combination with the Richardson number Ri (Young, 1994, Eq. 4.9):

$$N^2 = \frac{\tau}{\tau_U}(1+\mu^2)^{-1} f^{-2} \nabla B \cdot \nabla B \tag{5.2}$$

$$Ri \equiv \frac{N^2}{u_z^2 + v_z^2} = \frac{\tau}{\tau_U} \tag{5.3}$$

The variable τ is the timescale of vertical mixing of temperature and salinity. During the cooling phase the parameter μ is close to 1 for all rings, in agreement with the SML theory (Fig. 5.5). At the onset and ending of the cooling phase μ tends towards 0, indicating that momentum mixing weakens and the ageostrophic velocity decreases. For $\mu \ll 1$, the validity of Eq. 5.2 breaks down. The Richardson number Ri is lower than 0.25, which indicates that vertical mixing of temperature and salinity is more rapid than vertical mixing of momentum.

The combined action of unbalanced motions and vertical mixing in the SML theory rapidly removes density gradients but leaves behind compensated temperature and salinity gradients. To test whether this process also applies here, we calculated the complex density ratio R according to Ferrari and Paparella (2003):

$$R \equiv \frac{\alpha}{\beta} \frac{T_x + iT_y}{S_x + iS_y} \tag{5.4}$$

with α and β the thermal expansion and the haline contraction coefficients, respectively. When gradients of temperature and salinity are compensated, $|R|$ is equal to 1, while $|R|$ is larger than 1 when temperature gradients determine the density gradients. Fig. 5.5 shows the occurrence of $|R|$ within the overturning cell. There is a preferred density ratio $|R|$ of 8 and the alignment of temperature and salinity gradients is enhanced during the strong cooling phase (not shown). The Agulhas ring maintains the large scale radial temperature and salinity gradients, but the overturning circulation removes temperature and salinity gradients with other density ratios.

5.6 Conclusions

We have analyzed the water exchange of three Agulhas rings during one year in an eddy-resolving global ocean model. There is a sharp boundary between particles that stay within the Agulhas ring and particles that mix into the environment. The ring boundary is well predicted by a criterion, based on Flierl (1981), that the azimuthal velocity is at least twice the translational velocity at any time. The original criterion of Flierl (1981) is less suited to indicate the ring boundary due to unsteadiness of the ring boundary and its self advection (de Steur et al., 2004). The bowl shaped ring boundary reaches 140 km from the Agulhas ring center and down to 800 m. Below 800 m the Agulhas ring quickly loses its original water mass, in agreement with observations (van Aken et al., 2003). The criterion for the ring boundary is not applicable to Agulhas rings that split due to a mixed barotropic-baroclinic instability (Drijfhout et al., 2003b).

Strong surface cooling generates a shallow overturning cell with radially outward flow near the surface and a compensating inward flow at depth. The circulation is limited to the mixed layer. The cell can be explained by the SML theory of Young (1994): cooling creates vertically sheared pressure gradients which induce vertically sheared subinertial motions. Vertical mixing is balanced by restratification due to the sheared flow. The overturning cell forms an effective pathway between the edge and the inside of the Agulhas ring and it amplifies the dilution of anomalous water properties of Agulhas rings near the surface. The surface water is not trapped in the core, but connected with the outside: the overturning cell amplifies this water mass exchange by constantly bringing new water to the edge where it is mixed with the environment.

Chapter 6

Intermediate Waters crossing the Atlantic equator; where do they come from?

The origin of the intermediate waters that cross the equatorial Atlantic as part of the return flow for North Atlantic Deep Water was studied in the OCCAM model using a Lagrangian particle following technique. Most of these waters were subducted in the southeast Indian Ocean. Less than twenty percent comes directly from Drake Passage without looping into the Indian Ocean; the majority being provided by Agulhas leakage. Most of the intermediate waters that form in the South Atlantic do not follow the South Atlantic/Indian Ocean supergyre, but remain within the Antarctic Circumpolar Current, and gradually transform into Circumpolar Deep Water by diapycnal mixing

6.1 Introduction

Extending northward from the SAF a layer of low salinity is found in the Atlantic, Pacific and Indian Oceans, lying at about 800 to 1000 meters. In the Atlantic this layer can be traced up to 30° N (Talley, 1996). The origin and northward spread of the inherent watermass was first described by Wüst (1935). He concluded that the Antarctic Intermediate Water (AAIW) was mainly transported in a northwestward boundary current off the shelf break of South America. This view was challenged when further observations suggested that the anticyclonic subtropical gyre extends to intermediate depths. Taft (1963) deduced from salinity maps that AAIW was formed in the southeast Pacific and

Submitted as Drijfhout et al. (2004)

South Atlantic. In the South Atlantic, most AAIW would spread from the southwest corner around the subtropical gyre, which was consistent with the notion of non-unidirectional flow along the western boundary. Until recently (Larqué et al., 1997; Reid, 1989), the possibility of direct northward flow along the western boundary was still left open. Boebel et al. (1997) addressed this issue by analyzing direct observations of moored current meters and neutrally buoyant floats, concluding that no evidence existed for direct northward flow between 40° S and 30° S. The emerging picture was, that AAIW, either entering the South Atlantic via Drake Passage or formed at the Brazil-Malvinas Confluence (Piola and Gordon, 1989) from its primary precursor SAMW (McCartney, 1977), was advected within the South Atlantic with the wind-driven gyre (Schmid et al., 2000) until it reached the Santos bifurcation, where part of it returned southward to recirculate within the subtropical gyre, and another part followed the northern route to cross the Atlantic equator.

Such a picture was consistent with the view of Rintoul (1991) that AAIW entering the South Atlantic via Drake Passage is the major contributor to the NADW return flow, challenging the warm water route described by Gordon (1986). In an update, Gordon et al. (1992) stressed the role of AAIW, but argued that most AAIW would flow downstream in the Indian-Atlantic supergyre (de Ruijter, 1982) across the South Atlantic into the Indian Ocean sector of the Southern Ocean, looping into the subtropical gyre from the south-central and southeast Indian Ocean. Feeding the Agulhas Current it could return to the South Atlantic by Agulhas leakage. This was supported by several model studies (Donners and Drijfhout, 2004; Speich et al., 2001). Corroborating the theory of McCartney (1977), it was found that SAMW and AAIW feature rather close origins, follow rather similar flow patterns, and seem to be governed by rather similar dynamics. Typically, about 1 Sv of SAMW and AAIW flows from Drake Passage to the Atlantic equator by directly folding from the South Atlantic Current into the Benguela Current, while some 5-6 Sv of these water masses are provided by Agulhas leakage; the rest being made up by warmer water coming from the Indian Ocean.

These model results themselves do not discard the picture sketched above of a gradual northward spread of the intermediate waters (SAMW and AAIW) that are formed in the South Atlantic. Two other model studies, however, do question this view. Firstly, Donners et al. (2004b) show that the amount of intermediate water (IW) that crosses the Atlantic equator is only a fraction of what is formed in the South Atlantic. Presumably, the majority of IW would be gradually consumed and transformed into Circumpolar Deep Water (CDW) by mixing with denser water masses. Secondly, Speich et al. (2002) demonstrated in the model that the NADW return flow enters the Indian/Atlantic basin not only via Drake Passage, but also via the Pacific Indonesian Throughflow (PIT) and via Tasman Leakage. While transfer of IW through the PIT is small, Tasman leakage is dominated by IW. These two model results seriously question whether IW that is formed in the South Atlantic and subsequently advected downstream to the Indian and Pacific sectors of the Southern Ocean is the same IW that is brought back to the South Atlantic by Agulhas leakage.

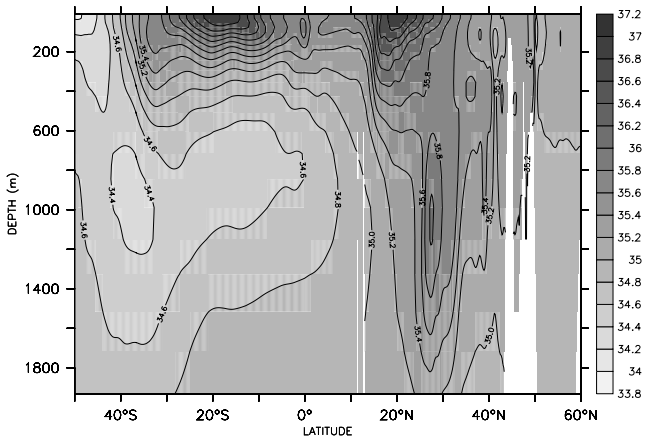

Figure 6.1: *salinity of the OCCAM model in the upper 2000 m along approximately 25° W, showing the northward spread of low salinity, intermediate water in the Atlantic. The topography is denoted in white.*

This prompts the question where the IW that crosses the Atlantic equator comes from. We intend to answer this question by a Lagrangian analysis of a high-resolution, global ocean model. Observational data are too sparse and non-synoptic to give an unequivocal answer to the origin of a water mass. In the ocean model the origin of water masses can be traced exactly, but the model may be biased in some respects. Therefore, we regard the model results as a hypothesis for the real world, that can be further tested within an observational program.

6.2 Results

Figure 6.1 shows a vertical section of salinity along 25° W in the South Atlantic. North of the equator, the section follows a curve that ends east of Iceland. The exact course of the section is not relevant here. It almost coincides with the sections discussed by Tsuchiya et al. (1992, 1994) and Talley (1996). As we use the climatology of a three-year average, the model field is somewhat smoother than the fields derived from a quasi-synoptic hydrographic section. The main characteristics, however, are strikingly similar. There is a minimum salinity layer which subducts poleward of the Subantarctic Front at 45° S. Surface values fall below 34.0 psu. A salinity layer with minimum values of 34.36 psu extends to 1000 m depth and as far north as the the Brazil Current Front at 32° S. Equatorward from 32° S the salinity minimum is found at about 800 m depth and gradually becomes more saline; at the equator the salinity minimum has become 34.6 psu. Northward of the equator the salinity minimum can be traced till about 20° N. At about 30° N a salinity maximum of 36.0 psu is found at 1000 m depth, associated with the Mediterranean outflow. The salty

Mediterranean outflow prohibits further northward propagation of the salinity minimum layer. Apparently, in the model, propagation of the AAIW core layer in the Atlantic is still very close to the observations and the same holds for its T-S characteristics and the large-scale density field. The numerical model also suggests a 'classical' picture of northward propagation of the South Atlantic, low salinity IW.

The origin of the IW that crosses the Atlantic equator was traced with the Lagrangian trajectory technique described above. The IW was defined with density values in between $\sigma_0 = 26.5$ and $\sigma_0 = 27.3$. There is 6.1 Sv of IW that crosses the equator northward; about 40% of the upper branch of the Atlantic meridional overturning circulation (MOC). Of this 6.1 Sv, 1.0 Sv was subducted in the South Atlantic, the remainder coming from elsewhere. Figure 6.2 shows the subduction sites of the IW that crosses the Atlantic equator. The majority, 3.9 Sv originates from the southeast Indian Ocean. McCarthy and Talley (1999) showed that the dominant mode of ventilation for the Indian Ocean is Southeast Indian SAMW (SEISAMW). It appears that in the model this mode water is the main contributor to the cross-equatorial intermediate flow in the Atlantic. This can be understood, as the major part of the intermediate water (re)enters the South Atlantic by Agulhas leakage, while the direct connection between Drake Passage and the Atlantic equator, with the South Atlantic Current folding into the Benguela Current, is small, of the order of 1 Sv (Donners and Drijfhout, 2004). With the majority of the IW that is formed in the South Atlantic looping into the Indian Ocean, the South Atlantic subduction sites are effectively further remote from the Atlantic equator than the subduction sites in the southeast Indian Ocean.

The spread of SEISAMW in the Indian Ocean was suggested by the map of potential vorticity at its core layer (McCarthy and Talley, 1999). South of Australia there is westward spread of SEISAMW. Beyond the west cape it follows a more northerly route, where after it seems to become entrained into the South Indian subtropical gyre, heading toward Madagascar. This pathway almost exactly coincides with the main route of Tasman leakage, described in Speich et al. (2002), which was found with the same Lagrangian trajectory technique as has been used here. It was also found that it is mainly IW that follows this route. So, IW at the Atlantic equator is mainly ventilated as SEISAMW following the pathways of Tasman leakage. It should be noted that along this route the waters gradually densify through diapycnal mixing. As a result, part of this water is subducted as thermocline water (TW). From Fig. 6.2 we see, however, that most of the subduction sites of TW are very close to the SEISAMW subduction sites and that they can be taken as the same variety.

If the source regions of IW that crosses the equator are mainly in the southeast Indian Ocean, the question arises what the fate is of the IW that subducts in the South Atlantic. It appears that 11.6 Sv of IW subducts in the South Atlantic. Of this 11.6 Sv, only 3.7 Sv ultimately crosses the Atlantic equator as part of the northward upper branch of the MOC. The remaining 7.9 Sv is advected downstream with the Antarctic Circumpolar Current and gradually mixes with denser waters to form deep water, mainly CDW. Of the 3.7 Sv that

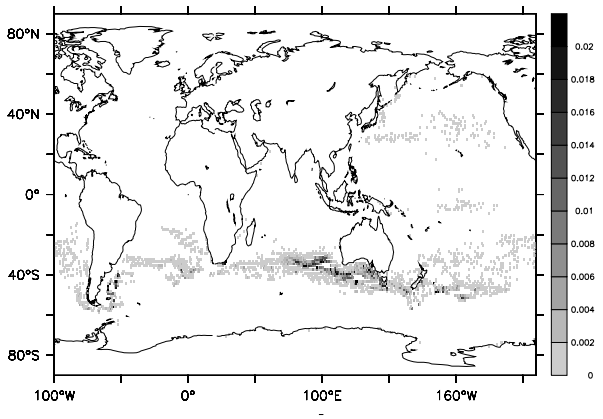

Figure 6.2: *Subduction sites of the intermediate waters that cross the Atlantic equator northward. Lagrangian particles were followed backward from the Atlantic equator. Mass fluxes are denoted in Sv per* $1^\circ \times 1^\circ$ *gridbox.*

crosses the Atlantic equator, 1.5 Sv re-emerges and re-subducts as TW and 2.2 Sv crosses the Atlantic equator as IW. Of this 2.2 Sv, 1.6 Sv re-emerged and was re-subducted outside the Atlantic basin. This implies that of the South Atlantic IW 68% transforms to deep water; 13% transforms to TW which crosses the Atlantic equator; 14 transforms to other varieties of IW, mainly Southeast Indian SAMW (SEISAMW), which thereafter cross the Atlantic equator; 5% directly feeds the NADW return flow as South Atlantic IW. Figures 6.3 and 6.4 summarize these transformations by showing, after re-emergence in the mixed layer, the last subduction site before the South Atlantic IW is either transformed to deep water (Fig. 6.3), or, crosses the Atlantic equator within the upper branch of the MOC (Fig. 6.4). Figure 6.3 shows that most transformation to deep water takes place in the Southern Ocean forming CDW, but that some transformation also occurs in the tropical and North Pacific. 4.7 Sv IW re-emerges and re-subducts before it transforms to deep water, while 3.2 Sv directly mixes with denser water after being subducted in the South Atlantic. Figure 6.4 shows the equatorward subduction sites in the South Atlantic where IW is re-subducted as TW, together with the subduction sites further downstream in the Southern Ocean where South Atlantic IW is re-subducted as other varieties of IW, mostly SEISAMW. From these figures it is seen that the different fates of South Atlantic IW are associated with similar subduction regions in the Southern Ocean into which the subduction is clustered. Apparently the Antarctic Circumpolar Current is a region of chaotic mixing where nearby initial positions may lead to completely different trajectories.

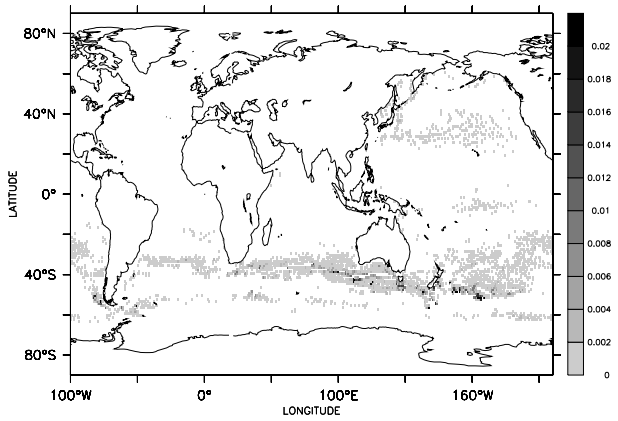

Figure 6.3: *Final subduction sites of South Atlantic intermediate waters that are ultimately transformed into deep water. Lagrangian particles were followed forward from their South Atlantic subduction location.*

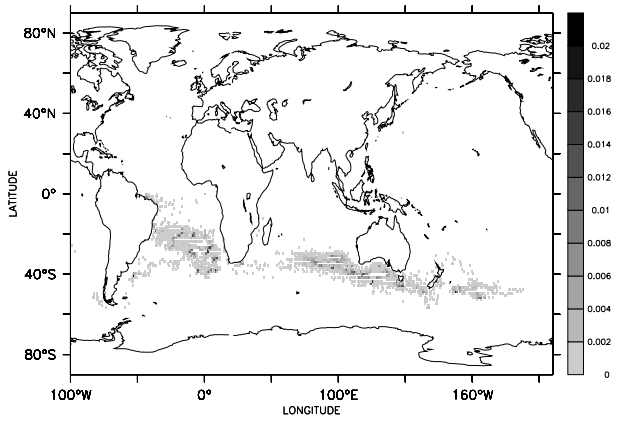

Figure 6.4: *Final subduction sites of South Atlantic intermediate waters that reach the North Atlantic either as thermocline water, or as other varieties of intermediate water. Lagrangian particles were followed forward from their South Atlantic subduction location.*

6.3 Discussion and Conclusions

Two model deficiencies could severely impact the picture that is sketched above. Firstly, the model is not yet in steady state, and model drift may affect subduction rates and subduction pathways. Donners and Drijfhout (2004) tested transport timeseries of IW and TW in the South Atlantic, but found no significant trend. Drift might spuriously increase the apparent diapycnal mixing of water masses in the model. This could bias the fate of South Atlantic IW toward a transformation into more CDW. But the excess of IW subduction in the South Atlantic with respect to IW crossing the Atlantic equator necessitates a large fraction of it to transform into CDW. For instance, Sloyan and Rintoul (2001a) estimate a total IW to CDW conversion of 31.7 Sv for the World Ocean. This suggests that our finding that the main fraction of South Atlantic IW is transformed into CDW is not caused by a too large diapycnal mixing that is associated with model drift.

A second model deficiency is a too weak water mass transformation due to relaxing to surface climatologies of temperature and salinity (Fox and Haines, 2003). This model error will tend to produce too weak subduction rates. Karstensen and Quadfasel (2002a), for instance, estimate larger subduction rates in the South Atlantic as we find with our model, but they also find a larger export of these subducted water masses to the other ocean basins. As the MOC in OCCAM is of realistic strength, a larger subduction rate of South Atlantic IW would necessitate a larger fraction of it to be converted into CDW, opposing a possible bias due to drift. By and large, we may conclude that these model deficiencies are likely to underestimate the total subduction rates of IW all over the World Ocean, but that there are no simple arguments which suggest that the qualitative picture that emerges from these model results is biased. In our opinion, the transformation of South Atlantic IW into CDW might even be larger in reality.

In summary, our main conclusions are that most IW crossing the Atlantic equator is formed in the southeast Indian Ocean, being dominantly SEISAMW. The fate of South Atlantic IW is mainly a transformation into CDW. The largest fraction that crosses the Atlantic equator as IW has re-emerged elsewhere, and was re-subducted, mainly in the southeast Indian Ocean. Most of the South Atlantic IW that directly flows to the Atlantic equator without being re-subducted in other basins is transformed and re-subducted in the South Atlantic as TW.

Bibliography

Antonov, J. I., Levitus, S., Boyer, T. P., Conkright, M. E., O'Brien, T. D., and Stephens, C. (1998). *World Ocean Atlas 1998 Volume 1: Temperature of the Atlantic Ocean*. NOAA ATLAS NESDIS 27. U.S. Government Printing Office.

Blanke, B., Arhan, M., Lazar, A., and Prévost, G. (2002a). A lagrangian numerical investigation of the origings and fates of the Salinity Maximum Water in the Atlantic. *J. Geophys. Res.*, 107(C10).

Blanke, B. and Raynaud, S. (1997). Kinematics of the Pacific Equatorial Undercurrent: An Eulerian and Lagrangian approach from GCM results. *J. Phys. Oceanogr.*, 27:1038–1053.

Blanke, B., Speich, S., Madec, G., and Maugé, R. (2002b). A global diagnostic of interior ocean ventilation. *Geophys. Res. Lett.*, 29.

Boebel, O., Lutjeharms, J., Schmid, C., Zenk, W., Rossby, T., and Barron, C. (2003). The Cape cauldron: a regime of turbulent inter-ocean exchange. *Deep-Sea Res. II*, 50:57–86.

Boebel, O., Schmid, C., and Zenk, W. (1997). Flow and recirculation of Antarctic Intermediate Water across the Rio Grande Rise. *J. Geophys. Res.*, 102:20967–20986.

Boyer, T. P., Levitus, S., Antoniv, J. I., Conkright, M. E., O'Brien, T. D., and Stephens, C. (1998). *World Ocean Atlas 1998 Volume 4: Salinity of the Atlantic Ocean*. NOAA ATLAS NESDIS 30. U.S. Government Printing Office.

Broecker, W. S. (1991). The great ocean conveyor. *Oceanogr.*, 4(2):79–89.

Cushman-Roisin, B. (1987). Subduction. In Müller, P. and Henderson, D., editors, *'Aha Huliko'a Proceedings of the University of Hawai'i*, pages 181–196.

Da Silva, A. M. and Young, C. C. Levitus, S. (1994). *Atlas of surface marine data. Vol. 1, Algorithms and procedures*. NOAA ATLAS Series. NOAA.

de Ruijter, W. (1982). Asymptotic analysis of the Agulhas and Brazil current systems. *J. Phys. Oceanogr.*, 12:361–373.

de Ruijter, W. P. M., Biastoch, A., Drijfhout, S. S., Lutjeharms, J. R. E., Matano, R. P., Pichevin, T., van Leeuwen, P. J., and Weijer, W. (1999). Indian-Atlantic interocean exchange: Dynamics, estimation and impact. *J. Geophys. Res.*, 104(C9):20885–20910.

de Steur, L., van Leeuwen, P. J., and Drijfhout, S. S. (2004). Tracer leakage from modeled Agulhas rings. *J. Phys. Oceanogr.*, 34(6):1387–1399.

de Vries, P. and Döös, K. (2001). Calculating Lagrangian trajectories using time-dependent velocity fields. *J. Atmos. Ocean. Tech.*, 18:1092–1101.

Dewar, W. K. (1987). Ventilating warm rings: Theory and energetics. *J. Phys. Oceanogr.*, 17:2219–2231.

Donners, J. and Drijfhout, S. (2004). The Lagrangian view of South Atlantic interocean exchange in a global ocean model compared with inverse model results. *J. Phys. Oceanogr.*, 34:1019–1035.

Donners, J., Drijfhout, S. S., and Coward, A. C. (2004a). Impact of cooling on the water mass exchange of Agulhas rings in a high-resolution ocean model. *Geophys. Res. Lett.*, 31.

Donners, J., Drijfhout, S. S., and Hazeleger, W. (2004b). Water mass transformation and subduction in the South Atlantic. *J. Phys. Oceanogr. (accepted).*

Döös, K. (1995). Interocean exchange of water masses. *J. Geophys. Res.*, 100:13499–13514.

Döös, K. and Coward, A. (1997). The Southern Ocean as the major upwelling zone of North Atlantic Deep Water. *Int. WOCE Newsl.*, (27):3–4.

Drijfhout, S. S., de Vries, P., Döös, K., and Coward, A. C. (2003a). Impact of eddy-induced transport on the Lagrangian structure of the upper branch of the thermohaline circulation. *J. Phys. Oceanogr.*, 33:2141–2155.

Drijfhout, S. S., Donners, J., and de Ruijter, W. P. M. (2004). Impact of cooling on the water mass exchange of Agulhas rings in a high resolution ocean model. *Geophys. Res. Lett. (submitted).*

Drijfhout, S. S., Katsman, C. A., de Steur, L., van der Vaart, P. C. F., van Leeuwen, P. J., and Veth, C. (2003b). Modeling the intial, fast sea-surface height decay of Agulhas ring "Astrid". *Deep-Sea Res. II*, 50:299–319.

Drijfhout, S. S., Maier-Reimer, E., and Mikolajewicz, U. (1996). Tracing the conveyor belt in the Hamburg large-scale geostrophic ocean general circulation model. *J. Geophys. Res.*, pages 22563–22575.

Ferrari, R. and Paparella, F. (2003). Compensation and alignment of thermohaline gradients in the ocean mixed layer. *J. Phys. Oceanogr.*, 33:2214–2223.

Flierl, G. R. (1981). Particle motions in large-amplitude wave fields. *Geophys. Astro. Fluid Dyn.*, 18:39–74.

Fox, A. D. and Haines, K. (2003). Interpretation of water mass transformations diagnosed from data assimilation. *J. Phys. Oceanogr.*, 33:485–498.

Fox, A. D., Haines, K., de Cuevas, B. A., and Webb, D. J. (2000). Altimeter assimilation in the OCCAM global model part II: TOPEX/POSEIDON and ERS-1 assimilation. *Journal of Marine Systems*, 26:323–347.

Ganachaud, A. (2000). *Large Scale Oceanic Circulation and Fluxes of Freshwater, Heat, Nutrients and Oxygen.* PhD thesis, Massachusetts Institute of Technology and Woods Hole Oceanographic Institution.

Ganachaud, A. (2003). Large-scale mass transports, water mass formation and diffusivities estimated from World Ocean Circulation Experiment WOCE hydrographic data. *J. Geophys. Res.*, 108:3213.

Garzoli, S. L. and Gordon, A. L. (1996). Origins and variability of the Benguela current. *J. Geophys. Res.*, 101(C1):897–906.

Gibson, R., Kållberg, P., Uppala, S., Hernandez, A., Nomura, A., and Serrano, E. (1997). 1997: The ERA description, the ECMWF re-analysis project report series. Technical report, ECMWF.

Gnanadesikan, A. and Hallberg, H. W. (2000). On the relationship of the circumpolar current to southern hemisphere winds in coarse-resolution ocean models. *J. Phys. Oceanogr.*, 30:2013–2034.

Gordon, A. L. (1986). Interocean exchange of thermocline water. *J. Geophys. Res.*, 91:5037–5046.

Gordon, A. L. (1997). Which is it: Warm or cold route, or maybe both? *Int. WOCE Newsl.*, (28):37–38.

Gordon, A. L., Weiss, R. F., Smethie Jr., W. M., and Warner, M. J. (1992). Thermocline and intermediate water communication between the South Atlantic and Indian Oceans. *J. Geophys. Res.*, 97(C5):7223–7240.

Gouretski, V. V. and Jancke, K. (1996). A new hydrographic data set for the South Pacific: Synthesis of WOCE and historical data. Technical Report 2, WHP SAC.

Griffies, S. M., Pacanowski, R. C., and Hallberg, R. W. (2000). Spurious diapycnal mixing associated with advection in a z-coordinate ocean model. *Mon. Weather Rev.*, 128:538–564.

Gu, D. and Philander, G. S. (1997). Interdecadal climate fluctuations that depend on exchanges between the tropics and extratropics. *Science*, 275:805–807.

Hazeleger, W., de Vries, P., and Friocourt, Y. (2003). Sources of the Equatorial Undercurrent in the Atlantic in a high-resolution ocean model. *J. Phys. Oceanogr.*, 33(4):677–693.

Jackett, D. and McDougall, T. (1997). A neutral density variable for the world's oceans. *J. Phys. Oceanogr.*, 27(2):237–263.

Kalnay, E. et al. (1996). The NMC/NCAR 40-year reanalysis project. *Bull. Am. Meteorol. Soc.*, 77:437–471.

Karstensen, J. and Quadfasel, D. (2002a). Formation of southern hemisphere thermocline waters: Water mass conversion and subduction. *J. Phys. Oceanogr.*, 32:3020–3038.

Karstensen, J. and Quadfasel, D. (2002b). Water subducted into the Indian Ocean subtropical gyre. *Deep-Sea Res. II*, 49:1441–1457.

Killworth, P. D. (1996). Time interpolation of forcing fields in ocean models. *J. Phys. Oceanogr.*, 26:136–143.

Kunze, E. and Toole, J. M. (1997). Tidally driven vorticity, diurnal shear, and turbulence atop Fieberling seamount. *J. Phys. Oceanogr.*, 27:2663–2693.

Large, W. G., McWilliams, J. C., and Doney, S. C. (1994). Oceanic vertical mixing: A review and a model with a nonlocal boundary layer parameterization. *Rev. Geophys.*, 32(4):363–403.

Larqué, L., Maamaatuaiahutapu, K., and Garçon, V. (1997). On the Intermediate and Deep Water flows in the South Atlantic ocean. *J. Geophys. Res.*, 102:12425–12440.

Laurent, L. C. S., Simmons, H. L., and Jayne, S. R. (2002). Estimating tidally driven mixing in the deep ocean. *Geophys. Res. Lett.*, 29(23).

Ledwell, J. R., Watson, A. J., and Law, C. S. (1998). Mixing of a tracer in the pycnocline. *J. Geophys. Res.*, 103(C10):21499–21529.

Lee, M.-M., Coward, A. C., and Nurser, A. G. (2001). Spurious diapycnal mixing of the deep waters in an eddy-permitting global ocean model. *J. Phys. Oceanogr.*, 32.

Levitus, S. and Boyer, T. P. (1994). *World Ocean Atlas 1994 Volume 4: Temperature*. NOAA ATLAS NESDIS 4. U.S. Government Printing Office.

Levitus, S., Burgett, R., and Boyer, T. P. (1994). *World Ocean Atlas 1994 Volume 3: Nutrients*. NOAA ATLAS NESDIS 3. U.S. Government Printing Office.

Lutjeharms, J. R. E. and Ballegooyen, R. C. v. (1988). The retroflection of the Agulhas Current. *J. Phys. Oceanogr.*, 18:1570–1583.

Macdonald, A. M. (1998). The global ocean circulation: a hydrographic estimate and regional analysis. *Prog. Oceanogr.*, 41:281–382.

Macdonald, A. M. and Wunsch, C. (1996). An estimate of global ocean circulation and heat fluxes. *Nature*, 382:436–439.

Marshall, J. C., Jamous, D., and Nilsson, J. (1999). Reconciling thermodynamic and dynamic methods of computation of water-mass transformation rates. *Deep-Sea Res. I*, 46:545–572.

Marshall, J. C., Olbers, D., Ross, H., and Wolf-Gladrow, D. (1993). Potential vorticity contraints on the dynamics and hydrography of the Southern Ocean. *J. Phys. Oceanogr.*, 23:465–487.

Matano, R. P. and Beier, E. J. (2003). A kinematic analysis of the Indian/Atlantic interocean exchange. *Deep-Sea Res. II*, 50:229–249.

McCarthy, M. C. and Talley, L. D. (1999). Three-dimensional isoneutral potential vorticity structure in the indian ocean. *J. Geophys. Res.*, 104(C6):13251–13267.

McCartney, M. S. (1977). Subantarctic Mode Water. In Angel, M., editor, *A Voyage of DISCOVERY, George Deacon 70th Anniversary Volume*, pages 103–119. *Deep-Sea Res.*, (Suppl).

McDougall, T. (1987). Neutral surfaces. *J. Phys. Oceanogr.*, 17:1950–1964.

McDougall, T. J. (1998). *Three-Dimensional Residual Mean Theory*, pages 269–302. Kluwer.

McIntosh, P. C. and Rintoul, S. R. (1997). Do box inverse models work? *J. Phys. Oceanogr.*, 27:291–308.

Model, F. (1950). Warmwasserheizung europas. *Ber. Deut. Wetterdienstes*, 57:213–244.

Niiler, P. and Stevenson, J. (1982). The heat budget of tropical ocean warm-water pools. *J. Mar. Res.*, 40 (suppl.):465–480.

Nurser, A. J. G., Marsh, R., and Williams, R. G. (1999). Diagnosing water mass formation from air-sea fluxes and surface mixing. *J. Phys. Oceanogr.*, 29:1468–1487.

Pacanowski, R. C. and Philander, S. G. H. (1981). Parameterization of vertical mixing in numerical models of tropical oceans. *J. Phys. Oceanogr.*, 11:1443–1451.

Peterson, R. G. and Stramma, L. (1991). Upper-level circulation in the South Atlantic Ocean. *Prog. Oceanogr.*, 26:1–73.

Piola, A. R. and Gordon, A. L. (1989). Intermediate Waters in the southwest South Atlantic. *Deep-Sea Res.*, 36:1–16.

Polzin, K. L., Toole, J. M., Ledwell, J. R., and Schmitt, R. W. (1997). Spatial variability of turbulent mixing in the abyssal ocean. *Science*, 276:93–96.

Poole, R. and Tomczak, M. (1999). Optimum multiparameter analysis of the water mass structure in the Atlantic Ocean thermocline. *Deep-Sea Res. I*, 46:1895–1921.

Provost, C., Escoffier, C., Maamaatuaiahutapu, K., Kartavtseff, A., and Garçon, V. (1999). Subtropical mode waters in the South Atlantic Ocean. *J. Geophys. Res.*, 104(C9):21033–21049.

Qiu, B. and Huang, R. X. (1995). Ventilation of the North Atlantic and North Pacific: Subduction versus obduction. *J. Phys. Oceanogr.*, 25:2374–2390.

Reason, C. J. C., Lutjeharms, J. R. E., Hermes, J., Biastoch, A., and Roman, R. E. (2003). Inter-ocean fluxes south of africa in an eddy-permitting model. *Deep-Sea Res. II*, 50:281–298.

Reid, J. R. (1989). On the total geostrophic circulation of the South Atlantic Ocean: Flow patterns, tracers, and transports. *Prog. Oceanogr.*, 23:149–244.

Reynolds, R. W. and Smith, T. M. (1994). Improved global sea surface temperature analyses using optimal interpolation. *J. Climate*, 7:929–948.

Rintoul, S. R. (1991). South Atlantic interbasin exchange. *J. Geophys. Res.*, 96(C2):2675–2692.

Roberts, M. and Marshall, D. (1998). Do we require adiabatic dissipation schemes in eddy-resolving ocean models? *J. Phys. Oceanogr.*, 104:2050–2063.

Schmid, C., Boebel, O., Zenk, W., Lutjeharms, J., Garzoli, S., Richardson, P., and Barron, C. (2003). Early evolution of an agulhas ring. *Deep-Sea Res. II*, 50:141–166.

Schmid, C., Siedler, G., and Zenk, W. (2000). Dynamics of Intermediate Water circulation in the subtropical South Atlantic. *J. Phys. Oceanogr.*, 30:3191–3211.

Schmitz, W. J. J. (1995). On the interbasin scale thermohaline circulation. *Rev. Geophys.*, 33(2):151–173.

Schouten, M. W., de Ruijter, W. P. M., van Leeuwen, P. J., and Lutjeharms, J. R. E. (2000). Translation, decay and splitting of Agulhas rings in the southeastern Atlantic Ocean. *J. Geophys. Res.*, 105(C9):21913–21925.

Siefridt, L. and Barnier, B. (1993). Banques de données AVISO vent/flux: Climatologie des analyses de surface du CEPMMT. Technical Report 91 1430 025.

Simmons, A. J. and Gibson, J. K. (2000). The ERA-40 project plan: ERA-40 project report series. Technical report, ECMWF.

Sloyan, B. M. and Rintoul, S. R. (2000). Estimates of area-averaged diapycnal fluxes from basin-scale budgets. *J. Phys. Oceanogr.*, 30:2320–2341.

Sloyan, B. M. and Rintoul, S. R. (2001a). Circulation, renewal and modification of Antarctic mode and intermediate water. *J. Phys. Oceanogr.*, 31:1005–1030.

Sloyan, B. M. and Rintoul, S. R. (2001b). The Southern Ocean limb of the global deep overturning circulation. *J. Phys. Oceanogr.*, 31:143–173.

Speer, K., Isemer, H.-J., and Biastoch, A. (1995). Water mass formation from revised COADS data. *J. Phys. Oceanogr.*, 25:2444–2457.

Speer, K. and Tziperman, E. (1992). Rates of water mass formation in the North Atlantic Ocean. *J. Phys. Oceanogr.*, 22:93–104.

Speer, K. G., Holfort, J., Reynaud, T., and Siedler, G. (1996). *South Atlantic Heat Transport at 11° S*, pages 105–120. In Wefer et al. (1996).

Speich, S., Blanke, B., de Vries, P., Döös, K., Drijfhout, S., Ganachaud, A., and Marsh, R. (2002). Tasman leakage: a new route in the global ocean conveyor belt. *Geophys. Res. Lett.*, 29(10):55–1–55–4. doi:10.1029/2001GL014586.

Speich, S., Blanke, B., and Madec, G. (2001). Warm and cold water routes of an O.G.C.M. thermohaline conveyor belt. *Geophys. Res. Lett.*, 28(2):311–314.

Stammer, D., Wunsch, C., Giering, R., Eckert, C., Heimbach, P., Marotzke, J., Adcroft, A., Hill, C. N., and Marshall, J. (2000). The global ocean state during 1992–1997, estimated from ocean observations and a global circulation model. part i: Methodology and estimated state. Technical Report 4, Scripps Institution of Oceanography.

Sterl, A. (2001). On the impact of gap-filling algorithms on variability patterns of reconstructed oceanic surface fields. *Geophys. Res. Lett.*, 28:2473–2476.

Sterl, A. and Hazeleger, W. (2002). Coupled variability and air-sea interaction in the South Atlantic ocean. *Clim. Dyn.*, 21:559–571.

Stramma, L. and England, M. (1999). On the water masses and mean circulation of the South Atlantic Ocean. *J. Geophys. Res.*, 104(C9):20863–20883.

Sutton, R. and Allen, M. (1997). Decadal predictability of North-Atlantic sea surface temperature and climate. *Nature*, 388:563–567.

Taft, B. A. (1963). Distribution of salinity and dissolved oxygen on surfaces of uniform potenial specific volume in the south atlantic, south pacific, and south indian oceans. *J. Mar. Res.*, 21:129–146.

Talley, L. D. (1996). Antarctic intermediate water in the South Atlantic. In Wefer et al. (1996), pages 219–238.

Talley, L. D. (1999). Some aspects of ocean heat transport by the shallow, intermediate and deep overturning circulations. In Clark, Webb, and Keigwin, editors, *Mechanisms of Global Climate Change at Millennial Time Scales*, pages 1–22. American Geophysical Union.

Thompson, S. R., Stevens, D. P., and Döös, K. (1997). The importance of interocean exchange south of Africa in a numerical model. *J. Geophys. Res.*, 102(C2):3303–3315.

Tomczak, M. and Godfrey, J. S. (1994). *Regional Oceanography: An Introduction*. Pergamon.

Toole, J. M., Polzin, K. L., and Schmitt, R. W. (1994). Estimates of diapycnal mixing in the abyssal ocean. *Science*, 264:1120–1123.

Treguier, A. M., Boebel, O., Barnier, B., and Madec, G. (2003). Agulhas eddy fluxes in a 1/6° Atlantic model. *Deep-Sea Res. II*, 50:251–280.

Tsuchiya, M., Talley, L. D., and McCartney, M. S. (1992). An eastern Atlantic section from Iceland southward across the equator. *Deep-Sea Res.*, 39:1885–1917.

Tsuchiya, M., Talley, L. D., and McCartney, M. S. (1994). A western Atlantic section from South Georgia Island (54°S) northward across the equator. *J. Mar. Res.*, 52:55–81.

Tziperman, E. (1986). On the role of interior mixing and air-sea fluxes in determining the stratification and circulation of the oceans. *J. Phys. Oceanogr.*, 16:680–693.

van Aken, H. M., van Veldhoven, A. K., Veth, C., de Ruijter, W. P. M., van Leeuwen, P. J., Drijfhout, S. S., Whittle, C. P., and Roualt, M. (2003). Observations of a young Agulhas ring, Astrid, during MARE in March 2000. *Deep-Sea Res. II*, 50:167–195.

Walin, G. (1982). On the relation between sea-surface heat flow and thermal circulation in the ocean. *Tellus*, 34:187–195.

Webb, D. J., Coward, A. C., de Cuevas, B., and Gwilliam, C. S. (1997). A multiprocessor ocean general circulation model using message passing. *J. Atmos. Ocean. Tech.*, 14:175–183.

Webb, D. J., Cuevas, B. A. d., and Coward, A. C. (1998). The first main run of the OCCAM global ocean model. Technical report, Southampton Oceanography Centre.

Wefer, G., Berger, W. H., Siedler, G., and Webb, D. J., editors (1996). *The South Atlantic: Present and Past Circulation*. Springer-Verlag.

Weijer, W., de Ruijter, W. P. M., Dijkstra, H. A., and van Leeuwen, P. J. (1999). Impact of interbasin exchange on the Atlantic overturning circulation. *J. Phys. Oceanogr.*, 29:2266–2284.

Weijer, W., de Ruijter, W. P. M., Sterl, A., and Drijfhout, S. S. (2002). Response of the Atlantic overturning circulation to South Atlantic sources of buoyancy. *Global Planet. Change*, 34:292–311.

Wunsch, C. (1978). The North Atlantic general circulation west of 50° W determined by inverse methods. *Rev. Geophys. Space Phys.*, 16(4):583–620.

Wüst, G. (1935). *The Stratosphere of the Atlantic Ocean*. Amerind.

Young, W. R. (1994). The subinertial mixed layer approximation. *J. Phys. Oceanogr.*, 24:1812–1826.

List of abbreviations

SACW	South Atlantic Central Water
lSACW	light South Atlantic Central Water
NADW	North Atlantic Deep Water
AAIW	Antarctic Intermediate Water
SASTMW	South Atlantic Subtropical Mode Water
SAMW	Subantarctic Mode Water
SEISAMW	Southeast Indian SAMW
T-S	temperature-salinity
SSS	sea surface salinity
SST	sea surface temperature
ACC	Antarctic Circumpolar Current
SAC	South Atlantic Current
AC	Agulhas Current
THC	thermohaline circulation
MOC	meridional overturning circulation
BMC	Brazil-Malvinas Confluence
SA	South Atlantic
WOCE	World Ocean Circulation Experiment
NCEP	National Center for Environmental Prediction
ECCO	Estimating the circulation and climate of the ocean
ERA40	ECMWF Reanalysis project
ECMWF	European Centre for Medium-Range Weather Forecasts
OCCAM	Ocean Circulation and Climate Advanced Modelling
SML	subinertial mixed layer

Samenvatting

Het klimaat van de aarde wordt voor een groot deel bepaald door warmte en licht van de zon. De hoeveelheid zonnestraling op aarde is nagenoeg onveranderlijk in de periode van een mensenleven. Toch zien we dat het klimaat en het weer zeer grillig zijn. Deze grilligheid (ook wel 'variabiliteit' genoemd) van het klimaat moet daarom veroorzaakt worden door processen die zich op aarde afspelen: stromingen in de atmosfeer en de oceaan, ijskappen en land. Een ander belangrijk effect van de stromingen in de atmosfeer en de oceaan is dat zij het klimaat op aarde minder extreem maken. De zonnestraling op de evenaar is het sterkst en wordt minder dichter bij de polen. Dicht bij de noord- en zuidpool is het zelfs een half jaar nacht. Dit zorgt voor een tropisch klimaat op de evenaar en een veel kouder klimaat bij de polen. De atmosfeer en de oceaan transporteren warmte van de evenaar richting de polen, waardoor het temperatuurcontrast wordt verkleind.

Maar de Zuid-Atlantische Oceaan, gelegen tussen Zuid-Amerika en Afrika, transporteert als enige oceaan warmte richting de evenaar, in tegenspraak met het globale idee van poolwaarts warmtetransport. Metingen uit 1935 tonen dit voor de eerste keer aan. Maar de duitse oceanograaf Wüst vond dit zo tegen-intuïtief dat hij het niet heeft vermeld in zijn discussie van de observaties. De eerste studie die het abnormale warmtetransport in de Zuid-Atlantische Oceaan benoemde, werd pas 15 jaar later gepubliceerd. Dat de Noord- en Zuid-Atlantische Oceaan allebei warmte noordwaarts transporteren, is een resultaat van de thermohaliene circulatie. Voor deze circulatie kan de oceaan ruwweg in twee lagen van elk 2 km dik worden opgedeeld: in de bovenste laag stroomt warm water vanuit alle oceanen richting de Noord-Atlantische Oceaan. De noordwaartse oppervlakte-stroming koelt steeds verder af, zodat rond 70 °N het warmtetransport in de oceaan nog maar klein is vergeleken met dat van de atmosfeer. De afgestane warmte wordt over West-Europa gevoerd en zorgt voor haar zachte winters. In de onderste laag van de thermohaliene circulatie verspreidt koud water uit de Noord-Atlantische Oceaan (Noord-Atlantisch Diep Water, of 'NADW') zich over de gehele wereld. De verbinding tussen beide lagen wordt tot stand gebracht door de sterke afkoeling in de Noord-Atlantische Oceaan; het koude water in de onderste laag wordt heel langzaam buiten de Atlantische Oceaan opgewarmd door het bovenliggende warmere water. De complete cyclus duurt ongeveer 1000 jaar.

Een belangrijk schakel van de stroming in de bovenste laag van de thermo-

haliene circulatie ligt rond Zuid-Afrika: hier wisselt de Indische Oceaan zijn warme en zoute zeewater uit tegen Atlantisch kouder en zoeter zeewater. De sterke Agulhas stroom ('AC') in de Indische Oceaan transporteert veel warm en zout water poolwaarts. Een aantal keren per jaar ontstaan er grote ringen in dit gebied, die een klein gedeelte van het warme en zoute water uit de Indische Oceaan verplaatsen naar de Zuid-Atlantische Oceaan. Deze 'Agulhasringen' hebben een doorsnee van ongeveer 300 km, en zijn vergelijkbaar met een hogedrukgebied in de atmosfeer. Satellieten kunnen de hoogte van het zeeoppervlak meten, en een Agulhas ring steekt ongeveer een meter boven zijn omgeving uit. Agulhas-ringen kunnen jaren blijven bestaan, maar ze verliezen veel energie en warmte in de eerste maanden. Dit verval vindt plaats in de Benguela stroom en deze transporteert het water richting de Noord-Atlantische Oceaan. Agulhas-ringen vormen zo een belangrijk onderdeel van de thermohaliene circulatie.

Maar de Benguela stroom bestaat niet alleen uit water van Agulhas ringen; een deel is koud en minder zout water van de Zuid-Atlantische stroom ('SAC') en de Antarctische Circumpolaire stroom ('ACC'). In Fig. 1.4 is de Zuid-Atlantische oceaan met de belangrijkstre stromingen getekend. De verdeling van de watermassa's uit de AC, de ASC en de ACC bepaalt de eigenschappen van de Benguela stroom, en daarmee van een deel van de thermohaliene circulatie.

De verdeling van watermassa's in de Benguela stroom is geschat met behulp van verschillende metingen, maar de antwoorden lijken geen eenduidig beeld te geven: sommige studies laten zien dat Agulhas ringen van belang zijn voor de thermohaliene circulatie, terwijl andere studies dat lijken te weerleggen. In dit proefschrift zijn de resultaten van verschillende studies vergeleken met de resultaten van een computermodel van de oceaan.

In het oceaanmodel kan het water in de oceaan 'gevolgd' worden. Hierdoor kunnen we direkt bepalen waar het water uit de Benguela stroom vandaan komt en waar het naartoe gaat, en daarmee zien we wat de route is die de thermohaliene circulatie volgt. Metingen moeten uitwijzen of de echte oceaan zich op dezelfde manier gedraagt. Maar vanuit een satelliet is aleen het oppervlak zichtbaar, en observaties vanaf een schip zijn duur en langzaam. Deze metingen zijn erg omslachtig: voor oceanografisch onderzoek wordt met een schip de oceaan overgestoken, waarbij elke 20 tot 30 kilometer het schip een paar uur stilligt om de watersamenstelling tot 4 kilometer diepte te meten. De gegevens van zo een meetcampagne kunnen gebruikt worden om de oceaancirculatie in het gebied te berekenen. Door de resultaten van meetcampagnes samen te voegen in een *inverse box model*, onstaat een wereldwijd beeld van de circulatie.

Maar het circulatiepatroon rond Zuid-Afrika is vooralsnog te ingewikkeld om goed in kaart te brengen met een inverse box model. Verschillende stromingen komen samen en beïnvloeden elkaar, en Agulhas ringen worden gevormd, bewegen en veranderen. Een inverse box model is daardoor niet in staat om een consistent beeld te geven waar het water van de Benguela stroom vandaan komt, of waar het water van de Agulhas stroom naartoe gaat.

De oceaan beïnvloedt de atmosfeer door de uitwisseling van vooral warmte

en water. In de winter koelt het zee-oppervlak sterk af. Het koude water aan het oppervlak mengt onder invloed van de wind en de golven met het water eronder, waardoor er een dikke laag water met een homogene temperatuur en saliniteit, een 'watermassa', ontstaat. In de lente wordt de menglaag ondieper en blijft het homogene water onder het zee-oppervlak. Dit proces heet 'subductie'. Deze watermassa kan vele jaren circuleren, vervolgens weer aan het zeeoppervlak verschijnen en zo klimaatschommelingen veroorzaken door zijn interactie met de atmosfeer.

In dit proefschrift is onderzocht hoe de uitwisseling van warmte, verdamping en regen de eigenschappen van het water aan het zee-oppervlak verandert. Er zijn verschillende datasets die deze uitwisseling beschrijven. De temperatuur en saliniteit van de bovenste laag van de thermohaliene circulatie wordt flink veranderd in de Zuid-Atlantische Oceaan. Helaas zijn de foutenmarges in deze datasets nog erg groot. Het oceaanmodel laat zien dat de eigenschappen van de thermohaliene circulatie voortdurend aan verandering onderhevig zijn: warmte en regen in het gebied rond de evenaar spelen hierbij ook een belangrijke rol. Subductie-processen en oppervlakte-veranderingen in de Zuid-Atlantische Oceaan zullen daarom geen direkte invloed op de thermohaliene circulatie verder stroomopwaarts in de Noord-Atlantische Oceaan hebben.

Agulhas ringen verliezen veel energie en warmte in de Benguela stroom gedurende de eerste maanden van hun bestaan. Er is nog veel onduidelijk hoe een Agulhas-ring precies 'vervalt' door een gebrek aan voldoende metingen. Tegenwoordig zijn oceaanmodellen in staat om de details het verval van Agulhas ringen te berekenen. In hoofdstuk vijf bestuderen we de verandering van een Agulhas ring door afkoeling in de winter in een oceaanmodel. Het water in een Agulhas-ring blijkt niet alleen als een tol rond te draaien: de afkoeling veroorzaakt een drie-dimensionaal stromingspatroon, dat de uitwisseling tussen de Agulhas-ring en zijn omgeving versterkt.

In hoofdstuk zes wordt ingegaan op een specifieke watermassa: intermediair water ('IW'). IW wordt gevormd in de winter in verschillende gebieden in de Zuidelijke Oceaan, gelegen rond Antarctica. Metingen in de Atlantische oceaan laten zien dat de bovenste laag van de thermohaliene circulatie voor een groot deel uit intermediair water bestaat. Het intermediaire water in de Atlantische Oceaan blijkt voornamelijk ten zuidwesten van Australië gevormd te worden, waarna het via de Agulhas stroom en Agulhas ringen in de Atlantische Oceaan terechtkomt. Observaties laten zien dat de karakteristieken van het intermediaire water in Agulhas ringen inderdaad grote gelijkenis vertoont met metingen in dit gebied.

Mijn dank is groot!

Er staat slechts één naam op de omslag van dit proefschrift, maar zonder de hulp van vele anderen had dit nooit tot een goed einde gebracht.

Sybren, jij bent zonder twijfel de grootste bijdrage geweest aan dit proefschrift. Ik vond je heel prettig om mee samen te werken: je had altijd tijd als ik vragen had of met problemen zat, maar je kon mij ook rustig laten werken zonder over mijn schouder mee te hoeven kijken. Veel van jou ideëen zijn in dit proefschrift verwerkt. Ook Wilco bedankt voor de vele keren dat ik met plaatjes kwam binnenvallen om te vragen naar jou interpretatie ervan. Je werk als co-auteur en als lezer van mijn artikelen heeft zeker bijgedragen aan de kwaliteit van dit proefschrift.

Will de Ruijter bedankt voor de wekelijkse begeleiding op het IMAU en als mijn promoter. De tafelgesprekken op vrijdag waren altijd gezellig en de discussies over onze resultaten hebben geleid tot een betere interpretatie van mijn resultaten.

Ook de mensen bedankt, waarmee ik vier jaar lang (oceanografisch) lief en leed heb mogen delen. Caroline, bedankt voor alle keren tijdens jouw laatste maanden dat je tijd hebt vrijgemaakt om mijn vervelende vragen ('Hoe zit dat met die geostrofe balans?') te beantwoorden. Hein en Gerrian hebben het drie jaar lang met mij, en mijn muziek, uit kunnen houden. Iedereen bij OO en VO bedankt voor de goede sfeer en de interessante discussies tijdens de koffiepauzes.

Andrew, thank you very much for all your help during my one week stay in February 2004 and for answering all my questions about the peculiarities of the ocean model. The resulting paper would not have been published so fast without it.

En iedereen bedankt die belangstelling heeft getoond naar mijn werk. Zonder jullie interesse zou dit alles slechts nutteloze bezigheidstherapie zijn geweest.

Curriculum vitae

Op 15 februari 1977 werd ik geboren in Ransdaal. Daar ben ik opgegroeid en tussen 1989 en 1995 heb ik het Coriovallum College in Heerlen bezocht. In 1995 ben ik naar Nijmegen verhuisd, om de opleiding natuurkunde te volgen. Mijn oorspronkelijke doelstelling was, om na een jaar de richting milieukunde op te gaan. Tijdens de propaedeuse heb ik mijn plan bijgesteld, en in 2000 heb ik mijn doctoraal natuurkunde gehaald. Tot dan toe had ik nog geen weet van de geofysische stromingsleer die van belang is voor de studie van de oceaan. Maar mijn interesse voor klimaat en geofysica was wel gewekt tijdens een bezoek met de studievereniging aan het Koninklijk Nederlands Meteorologisch Instituut (KNMI). Vanaf april 2000 ben ik werkzaam geweest als promovendus bij de oceanografische afdeling van het KNMI. Dit boekje geldt als eindresultaat van mijn periode als promovendus. Momenteel werk ik aan modellen van het gehele klimaatsysteem voor het Centre for Global Atmospheric Modelling als onderdeel van de University of Reading.